Western Graduate&PostdoctoralStudies

Western University
Scholarship@Western

Electronic Thesis and Dissertation Repository

12-13-2019 2:30 PM

The Co-Delivery of Syngeneic Adipose-Derived Stromal Cells and Macrophages on Decellularized Adipose Tissue Bioscaffolds for In Vivo Soft Tissue Regeneration

Hisham A. Kamoun
The University of Western Ontario

Supervisor
Flynn, Lauren E.
The University of Western Ontario

Graduate Program in Biomedical Engineering
A thesis submitted in partial fulfillment of the requirements for the degree in Master of Engineering Science
© Hisham A. Kamoun 2019

Follow this and additional works at: https://ir.lib.uwo.ca/etd

Part of the Biomaterials Commons, and the Molecular, Cellular, and Tissue Engineering Commons

Recommended Citation
Kamoun, Hisham A., "The Co-Delivery of Syngeneic Adipose-Derived Stromal Cells and Macrophages on Decellularized Adipose Tissue Bioscaffolds for In Vivo Soft Tissue Regeneration" (2019). *Electronic Thesis and Dissertation Repository*. 6727.
https://ir.lib.uwo.ca/etd/6727

This Dissertation/Thesis is brought to you for free and open access by Scholarship@Western. It has been accepted for inclusion in Electronic Thesis and Dissertation Repository by an authorized administrator of Scholarship@Western. For more information, please contact wlswadmin@uwo.ca.

Abstract

Decellularized adipose tissue (DAT) bioscaffolds are a promising platform for the delivery of pro-regenerative cell populations with the goal of promoting adipose tissue regeneration. The current study investigated the effects of seeding DAT bioscaffolds with syngeneic bone marrow-derived macrophages and/or adipose-derived stromal cells (ASCs) on *in vivo* soft tissue regeneration. Methods were established to derive the macrophages from MacGreen mice, which were dynamically seeded onto the DAT scaffolds alone or in combination with ASCs. Seeded and unseeded scaffolds were implanted subcutaneously into C57Bl/6 mice. At 2 and 4 weeks, cell infiltration, angiogenesis, and adipogenesis were analyzed through histology and immunohistochemistry. Substantial variability was observed, but higher blood vessel densities and greater $CD31^+$ cell recruitment was observed in the implants that were greatly infiltrated with cells. A diverse, infiltrating macrophage population was identified in all implants, with quantitatively higher iNOS expression in the scaffolds that showed greater levels of cell infiltration.

Keywords

adipose tissue engineering, adipose-derived stromal cells, extracellular matrix, decellularized adipose tissue, angiogenesis, cell recruitment, biomaterials, cell therapy, tissue engineering, macrophage.

Summary for Lay Audience

Adipose or fat tissue has a limited ability to repair and regenerate itself following trauma, burns, surgical removal of tumors, or birth defects. The process of fat regeneration is dependent on 1) coordinating multiple types of cells in the body to migrate, 2) forming new blood vessels, 3) and cells achieving a more pro-regenerative state to support new fat cell formation. There is an increasing interest in delivering therapeutic cells, such as adipose-derived stromal cells (ASCs) and immune cells called macrophages, which have been shown to stimulate the biological process of fat tissue regeneration. Also, 3-D porous decellularized adipose tissue (DAT) implants have been previously developed as a promising platform to deliver therapeutic cells into areas of the body with large defects. The present thesis focused on using DAT implants to deliver both ASCs and macrophages into mice. Initially, the DAT implants were found to support macrophage and ASC attachment. After DAT implants were delivered into mice either alone or with macrophages, ASCs, or macrophages + ASCs, different levels of cell migration, as well as blood vessel and fat formation were observed within the implants in all groups after 2 and 4 weeks. In general, the implants that had greater levels of cells migrating into them also had more blood vessels being formed. Also, different types of macrophages were observed within the DAT implants in all groups at both time points, all of which may be playing an active role in regeneration. Overall, this study showcases the intricate and complex relationships between regeneration, cell recruitment, blood vessel formation, and inflammation.

Acknowledgments

I would first like to express from the bottom of my heart, my sincerest gratitude to my master's supervisor, Dr. Lauren Flynn. Her insight, dedication, passion, mentorship, time, and patience were invaluable to me. Thank you so much for seeing something in me and taking me on as a student. I will treasure my time at Western not only because of the invaluable scientific training that I received, but also for the important "life skills" that I gained along the way, and this was in part by your guidance.

I would also like to extend my gratitude towards the members of my advisory committee, Dr. Gregory Dekaban and Dr. Douglas Hamilton. Thank you so much for taking the time to provide me with your insight and feedback. I would also like to thank Christy Barreira from the Dekaban lab for her time and technical assistance with the flow cytometry experiments. Christy you were always generous with your time and always found time to answer my questions.

Of course, I can't forget to thank my friends and colleagues in the Flynn lab. I learned a lot from every single person who I met, including post-docs, graduate students, laboratory technicians, and undergraduate students. You all do superb work and I have the utmost respect for you all! In particular, I'd like to give a special shout out to Dr. Laura Juignet, Kevin Robb, Pascal Morissette Martin, and Cody Brown, who worked alongside me and helped me to hone my laboratory skills. Thank you to all past and present members of the Flynn lab who I've encountered, especially for all of the wonderful memories in and out of the lab!!

Last, but not least, I'd like to thank my parents and my three older sisters for their love and support through this process. It wasn't easy and I truly hope that one day I can pay it all back.

Looking back, this experience was humbling in the best of ways and now I know more myself as a STEM professional and as a human being. I feel blessed to have had this opportunity to learn more about tissue engineering and regenerative medicine alongside other people passionate about these fields.

Table of Contents

Abstract ii

Summary for Lay Audience iii

Acknowledgments iv

Table of Contents v

List of Tables viii

List of Figures ix

List of Appendices xi

List of Abbreviations xii

Chapter 1 1

1 Literature review 1

- 1.1 Introduction 1
- 1.2 Adipose tissue physiology 1
- 1.3 Adipose tissue cellular composition 2
  - 1.3.1 Adipose-derived stromal cells 3
- 1.4 Components of the adipose tissue extracellular matrix 6
- 1.5 Clinical options to restore soft tissue defects 8
- 1.6 Adipose tissue engineering strategies 10
- 1.7 Cell sources for soft tissue regeneration 11
  - 1.7.1 ASC-based strategies for soft tissue regeneration 13
  - 1.7.2 Macrophage-based strategies for soft tissue regeneration 15
- 1.8 Biomaterials for soft tissue regeneration 18
  - 1.8.1 Synthetic biomaterials 18
  - 1.8.2 Naturally-derived biomaterials 19
  - 1.8.3 Decellularized biomaterials 21

1.8.4 Decellularized adipose tissue 22
1.9 Project overview, hypothesis, and specific aims 24
1.9.1 Project overview 24
1.9.2 Hypothesis 26
1.9.3 Objectives 26
Chapter 2 27
2 Materials & Methods 27
2.1 Materials 27
2.2 Animal work 27
2.3 ASC isolation and culture 27
2.4 Macrophage isolation and culture 28
2.5 Immunophenotyping of cultured macrophages 30
2.6 Decellularized adipose tissue bioscaffold fabrication and seeding 32
2.6.1 Adipose tissue procurement and decellularization 32
2.6.2 Decellularized adipose tissue bioscaffold preparation and seeding 32
2.7 *In vitro* characterization of seeded implants 33
2.7.1 DAPI staining and double stranded DNA quantification 33
2.7.2 Metabolic activity quantification 34
2.8 *In vivo* assessment of the bioscaffolds 34
2.9 Masson's trichrome staining and quantification 35
2.10 Immunofluorescence assessment of angiogenic and macrophage markers 36
2.10.1 Detection of CD31$^+$ cells 36
2.10.2 Immunofluorescence assessment of infiltrating macrophages 36
2.11 Statistical analyses 37
Chapter 3 38
3 Results 38

- 3.1 Murine cell isolation and culture 38
- 3.2 Macrophage characterization 39
  - 3.2.1 Cell surface marker expression 39
- 3.3 *In vitro* analysis of cell-seeded decellularized adipose tissue bioscaffolds 42
  - 3.3.1 Assessment of cell distribution 42
- 3.4 *In vivo* analysis of the DAT bioscaffolds 45
  - 3.4.1 Macroscopic evaluation of implants 45
  - 3.4.2 Qualitative assessment of cellular infiltration, angiogenesis, and remodeling of the DAT implants 46
  - 3.4.3 Semi-quantitative analysis of cellular recruitment, blood vessel density, and adipose tissue remodeling 54
- 3.5 Immunofluorescence analysis of CD31$^+$ cell recruitment 57
- 3.6 Immunofluorescence analysis of infiltrating macrophage phenotypes 61

Chapter 4 68

- 4 Discussion 68
- 5 Conclusions and future directions 79
  - 5.1 Summary of findings and conclusions 79
  - 5.2 Future recommendations 81

References……………………………………………………………………………..84

Appendix 1 116

Curriculum Vitae 120

List of Tables

Table 1.1.1. The immunophenotypic profile of human ASCs. 5

Table 3.1. Immunophenotype of the cultured murine bone marrow-derived macrophages isolated from the MacGreen mice.. 40

Table 3.2. Histological scoring of the levels of cellular infiltration in the unseeded, macrophage, ASC, and co-culture seeded DAT implant cross-sections 52

Table 3.3. The average blood vessel density of all seeding conditions after 2 and 4 weeks. . 55

List of Figures

Figure 2.1. Summary of the isolation protocol for bone marrow-derived macrophage progenitor cell population. 30

Figure 3.1. Morphology of bone marrow-derived macrophages differentiated after 7 days in culture. 39

Figure 3.2. Cultured bone marrow-derived macrophages express characteristic macrophage markers. 41

Figure 3.3. Seeded macrophages and ASCs were heterogeneously distributed within the decellularized adipose tissue bioscaffolds after 24 hours in dynamic culture. 43

Figure 3.4. Assessment of dsDNA content and metabolic activity in the macrophage-seeded, ASC-seeded and co-culture-seeded DAT scaffolds after 24 hours in dynamic culture. 45

Figure 3.5. Macroscopic evaluation of the DAT implants 46

Figure 3.6. Adipocytes and blood vessels were localized to the peripheral regions of DAT implant groups at 2 weeks post-implantation in C57BL/6J mice. 48

Figure 3.7. Adipocytes and blood vessels were localized to the peripheral regions of DAT implant groups at 4 weeks post-implantation in C57BL/6J mice. 49

Figure 3.8. Implants within each seeding condition exhibited varying levels of cell infiltration at 2 and 4 weeks post-implantation in C57BL/6J mice 51

Figure 3.9. Infiltrating cell populations were distributed along areas adjacent to the inguinal fat pad either alone, or in addition to areas adjacent to the skin 53

Figure 3.10. Higher levels of cellular infiltration within the implants correlated to higher levels of angiogenesis and adipogenesis. 54

Figure 3.11. Quantification of *in vivo* cellular infiltration, blood vessel density, and adipose tissue remodeling within the DAT implants at 2 and 4 weeks. 56

Figure 3.12. Cell seeding did not influence the erythrocyte-containing blood vessel diameter or infiltration profiles within the DAT implants at 2 and 4 weeks. 57

Figure 3.13. Representative images of CD31$^+$ cells within the implant periphery from all scaffold groups after 2 and 4 weeks *in vivo*. 59

Figure 3.14. Representative images of the different CD31 expression patterns found in implant groups containing different levels of cell infiltration after 2 weeks *in vivo*.. 60

Figure 3.15. Quantification of relative CD31$^+$ expression within the DAT implants at 2 and 4 weeks.. 61

Figure 3.16. Representative images of CD68, Arg-1, and iNOS, co-staining along the apical and basal borders from all seeding conditions after 2 weeks *in vivo*.. 63

Figure 3.17. Representative images of CD68, Arg-1, and iNOS co-staining along the apical and basal borders from all seeding conditions after 4 weeks *in vivo* 64

Figure 3.18. Implants from all seeding conditions contain and abundant subpopulation of CD68$^+$ Arg-1$^+$ iNOS$^-$ Hoechst$^+$ cells and a smaller population of CD68$^+$ Arg-1$^+$ iNOS$^+$ Hoechst$^+$ cells after 4 weeks *in vivo*.. 65

Figure 3.19. Further subpopulations of CD68$^+$Arg-1$^-$ iNOS$^+$ Hoechst$^+$ cells and CD68$^+$Arg-1$^-$ iNOS$^+$ Hoechst$^+$ have been identified in some of the implants in both time points *in vivo*. .. 66

Figure 3.20. Representative images of the CD68, Arg-1, and iNOS co-staining from implants containing different levels of cell infiltration after 2 weeks *in vivo*.. 67

List of Appendices

Appendix 1. Supplementary Figures…………………………………………………………...…83

List of Abbreviations

ADAMs	a disintegrin and metalloprotease
Arg-1	arginase-1
ASCs	adipose-derived stromal cells
ATP	adenosine triphosphate
BAT	brown adipose tissue
bFGF	basic fibroblast growth factor
bmMSCs	bone marrow-derived mesenchymal stromal cells
BSA	bovine serum albumin
CMP	common myeloid progenitor
CSFs	colony-stimulating factors
DAT	decellularized adipose tissue
DCB	decellularized cancellous bone
DMSO	dimethyl sulfoxide
dsDNA	double-stranded DNA
dsRed	Discosoma red fluorescent protein
ECM	extracellular matrix
EDTA	ethylenediaminetetraacetic acid
EGFP	enhanced green fluorescence protein
FBS	fetal bovine serum

FSC	forward scatter
GAGs	glycosaminoglycans
G-CSF	granulocyte colony stimulating factor
GFP	green fluorescence protein
GM-CSF	granulocyte/macrophage colony-stimulating factor
HBSS	Hank’s Balanced Salt Solution
HGF	hepatocyte growth factor
HLA-DR	human leukocyte antigen—DR isotype
IFN-γ	interferon-γ
IGF-1	insulin-like growth factor
IL-6	interleukin-6
iNOS	inducible nitric oxidase synthase
iPSCs	induced pluripotent stem cells
LPS	lipopolysaccharide
M-CSF	macrophage colony-stimulating factor
MMPs	metalloproteinases
MCP-1	monocyte chemoattractant protein-1
NO	nitric oxide
PBS	phosphate-buffered saline (PBS)
PECAM-1	platelet-endothelial cell adhesion molecule 1

PEG	polyethylene glycol
PGLA	poly(lactic-co-glycolic acid)
PDGF-AA	platelet-derived growth factor-AA
PLA	polylactic acid
PLLA	poly-1-lactic acid
PlGF-1	placental growth factor-1
PMMA	polymethylmethacrylate
SCID	severe combined immunodeficiency
SD	standard deviation
SDF-1α	stromal-derived growth factor -1α
SIS	small intestinal submucosa
SSC	side scatter
SVF	stromal vascular faction
TBS	tris-buffered saline
TCP	tissue culture polystyrene
TIMPs	tissue inhibitor metalloproteinases
TNF-α	tumor necrosis factor-α
UCP1	uncoupling protein 1
VEGF-A	vascular endothelial growth factor-A
WAT	white adipose tissue

Chapter 1

1 Literature review

1.1 Introduction

Adipose tissue (fat) is a loose, soft connective tissue with discrete depots distributed throughout the body. Excess adipose tissue is often viewed negatively because its overaccumulation is associated with metabolic diseases such as obesity and diabetes[1]. However, fat is a crucial part of the integumentary system and it plays a myriad of important physiological roles in the body including the maintenance of metabolic homeostasis, and the contribution to the normal human appearance[1,2]. Disruption of the soft tissue structure through trauma, congenital abnormalities, burns, oncologic resection, or other means can lead to scar formation, contracture, and possible loss of function[3,4,5]. Moreover, soft tissue deficits may cause patients to develop emotional distress and body image issues. Progress in the fields of plastic and reconstructive surgery have enabled the correction of soft tissue irregularities that can improve patients' emotional and mental well-being[6,7]. However, these procedures often involve autologous tissue grafts, which can have variable and/or limited long-term success in restoring the missing volume, or synthetic or natural volume fillers, which lack the ability to restore the functionality of the missing tissue[8,9]. The limited capability for adipose tissue to repair and regenerate highlights the growing need for novel regenerative medicine-based therapeutic interventions in order to replace lost or damaged tissue and promote healthy fat formation.

1.2 Adipose tissue physiology

In mammals, there are two main forms of adipose tissue: brown adipose tissue (BAT) and white adipose tissue (WAT). BAT is predominantly found in newborns, located in the interscapular, axillary, and perirenal regions of the body[10], and is responsible for non-shivering heat generation, - or thermogenesis during cold exposure[10,11]. BAT is mainly composed of adipocytes, which are terminally differentiated cells that store energy in the form of triglycerides. Notably, the adipocytes within BAT are 10-25 µm in diameter and are multilocular, or contain multiple, small lipid droplets, as well as numerous mitochondria[12]. Additionally, the adipocytes within BAT are organized into bundles by an extracellular matrix (ECM), and are supported by a large network of blood vessels, as well as innervation from the sympathetic nervous system[12]. The adipocytes in BAT are able to produce heat by oxidizing triglycerides within their mitochondria. This process is carried out with the aid of uncoupling protein 1 (UCP1)[10,12], a mitochondrial protein expressed specifically in the adipocytes within BAT, and is unique in that it produces heat without any adenosine triphosphate (ATP) production. The heat then gets circulated to other parts of the body through the extensive vascular network[13].

As a person matures, the BAT content in the body gradually decreases, while the WAT content increases[2]. In humans, WAT is found subcutaneously throughout the majority of the body, as well as viscerally in the omental, mesenteric, and retroperitoneal areas[14]. WAT performs numerous physiological roles including triglyceride storage, thermal insulation, and the protection of other internal tissues. WAT is primarily composed of mature adipocytes that are 20-150 µm in diameter and are unilocular, or contain a single, large lipid droplet[15]. The adipocytes within WAT are similarly distributed into discrete bundles by the surrounding ECM, but they contain fewer mitochondria than the adipocytes within BAT[2,12]. WAT is supported by sympathetic innervation[2,16] and every adipocyte is in contact with at least one capillary[17], although as a whole it is less vascularized as compared to BAT[12]. WAT also functions as an important endocrine organ by synthesizing numerous cytokines, termed adipokines, which are involved in metabolic homeostasis, food intake, vascular function, and control of blood pressure, and inflammation[13,18]. For example, WAT can secrete adiponectin, which controls glucose and fatty acid breakdown in muscle, as well as leptin, which regulates energy expenditure and appetite[13]. Additional molecules that are produced by WAT include the pro-inflammatory cytokines tumor necrosis factor-α (TNF-α) and interleukin-6 (IL-6)[13,18,19], and the pro-angiogenic protein vascular endothelial growth factor (VEGF)[18].

1.3 Adipose tissue cellular composition

Although historically thought of as an inactive, simple tissue, in actuality adipose tissue incorporates many different cell populations. Adipocytes are the main cell type found in both forms of adipose tissue, making up 20-40% of the cellular content and >90% of its volume[20]. Adipocytes have the ability to increase or decrease in size, depending on the body's energy intake and expenditure[20–22]. New adipocytes are derived from differentiating progenitor cells, termed adipose-derived stromal cells (ASCs), as well as more committed pre-adipocytes (further discussed in Section 1.3.1).

When adipose tissue is extracted, processed through mechanical and enzymatic techniques, and centrifuged, the non-adipocytes form a pellet called the stromal vascular fraction (SVF)[23,24]. The cells in the SVF are a heterogeneous population that includes ASCs, erythrocytes, endothelial cells, pericytes, smooth muscle cells, fibroblasts, and immune cells. Macrophages are the most abundant immune cells found in fat, but other immune cells include monocytes, lymphocytes, neutrophils, and natural killer cells[24–27]. ASCs can be isolated from the SVF based on their adherence to tissue culture plastic using culture medium that supports their growth[24].

Studies have shown that the cellular composition of adipose tissue can vary, depending on factors such as depot location and disease state[27–30]. For example, one study found that subcutaneous fat had greater levels of pre-adipocytes than visceral fat[28]. Increases in the levels of myeloid cell populations, such as macrophages, have been associated with altered metabolic function and decreased insulin sensitivity, which may contribute to pathological states such as obesity and diabetes[27,29,31].

1.3.1 Adipose-derived stromal cells

ASCs are a mesenchymal cell population that can be isolated from the stromal vascular fraction derived from adipose tissue. ASCs have been implicated in adipose tissue repair and homeostasis as they have a great capacity for differentiating along the adipogenic lineage[32–36] and have the demonstrated capability to generate neo-adipocytes *in vivo*[37–39]. As a mesenchymal progenitor cell population, they also exhibit the capacity for multipotent differentiation, most notably towards the osteogenic[40–43] and chondrogenic lineages[44–46].

Clonogenic cell assays have estimated ASC frequency within primary isolates to be between 1:30–1:1000 out of total nucleated cells as compared to bone marrow-derived mesenchymal stromal cell populations (bmMSCs), which range between 1:50,000 and 1:1 million.[47,48]. ASCs are thought to be localized in close proximity to the *in vivo* adipose microvasculature, specifically in the perivascular niche, where they closely interact with endothelial cells and pericytes[49–52]. However, their exact distribution *in vivo* remains unclear due to a lack of unique

ASC markers[53]. Instead, studies have relied on characterizing the immunophenotype of ASCs in culture in conjunction with quantitative analysis of multipotency.

In an effort to standardize ASC characterization criteria, the International Federation for Adipose Therapeutics and Science (IFATS) and the International Society for Cellular Therapy (ISCT) have put together guidelines to evaluate the ASC phenotype[54]. In general, in order to confirm that isolated cells from the SVF are an ASC population, they need to 1) adhere to plastic, 2) express an immunophenotypic profile using multi-color flow cytometry as described in Table 1.1, and 3) exhibit multipotent differentiation potential towards the adipogenic, osteogenic, and chondrogenic lineages. Moreover, the immunophenotype of these cells should contain at least two primary positive (>90 %) and two primary negative markers (<2 %). Additional markers should be included in order to strengthen the characterization.

Table 1.1.1. The immunophenotypic profile of human ASCs[48,54,55].

Marker type	Antigen
Primary positive (>90%)	CD90 (Thy-1) CD105 (endoglin) CD73 (ecto-5'-nucleotidase) CD44 (hyaluronic acid receptor) CD29 (β1-integrin) CD13 (aminopeptidase-N) CD34 (progenitor associated marker) * CD146 (melanoma cell adhesion molecule, MCAM or MUC18)*
Secondary positive	CD10 (neprilysin or neutral endopeptidase) CD26 (dipeptidyl peptidase-4, or DPPIV) CD49d (α4-integrin, or VLA4)* CD49e (α5-integrin, or VLA5) CD36 (fatty acid translocase, or GPIIIb)
Primary negative (<2%)	CD31 (platelet endothelial cell adhesion molecule, PECAM) CD45 (leukocyte-common antigen, LCA) CD235a (glycophorin A)
Secondary negative	CD3 (T-cell co-receptor) CD11b (αM-integrin or Mac-1) CD49f (α6-integrin or VLA6) CD106 (vascular cell adhesion protein-1, VCAM-1) PODXL (podocalyxin-like protein or PODXL)

*Variable levels of expression

ASCs can express similar surface markers to bmMSCs as both cell types express CD13, CD73, CD90, and CD105[54]. However, ASCs can be distinguished through their positive expression of CD34 and their negative expression of CD106[53,54]. It is important to note that isolated ASCs are a heterogenous population, though not as heterogenous as the cells belonging to the SVF[56]. The isolated ASC population is comprised of cells with different levels of commitment including cells with uni-, bi-, or tri-potential[57]. This inherent variability points to the importance of transparency in reporting the methods used for ASC isolation and culture. It has been reported that the isolation techniques, passage number, culture conditions, and the donor/fat depot used can influence ASC yield, proliferation, and differentiation potential[56,58–60].

ASCs isolated from mice have been found to share similarities with their human counterparts in terms of their surface marker profile[61,62] and tri-lineage potential[61–66]. In keeping with the common positive markers used to identify human ASCs, murine ASCs exhibit high expression of CD29[61–65] and CD90[61,62,66,67]. In comparison to human ASCs however, they show relatively low expression of CD105[58,62,65], low expression of CD73 and CD34[61–63,67], and variable expression of CD44[61–64]. Stem cell antigen-1 (SCA-1), also known as Ly6A, a shared marker found in murine hematopoietic stem cells and bmMSCs, was reported to be highly expressed on murine ASCs[62–65]. Similar to human ASCs, the immunophenotype of isolated murine ASCs can vary due to differences in isolation and cell culture, passage number and strains of mice used[62,63].

1.4 Components of the adipose tissue extracellular matrix

The adipose ECM is a complex, fibrous network of cell-secreted proteins and polysaccharides that serves to biochemically and biophysically support the cells residing in the tissue. The ECM regulates a broad range of cellular processes including cell attachment, survival, proliferation, and differentiation[68]. The macromolecules that make up the ECM can be broadly categorized into fibrous proteins (e.g. collagen), glycosaminoglycans (GAGs), proteoglycans, and glycoproteins[69]. The microarchitecture, mechanical properties, and bioactivity of the ECM is determined by the relative abundance and spatial arrangement of these macromolecules.

Collagens are the predominant structural components found in the adipose ECM, with collagen type I being the most abundant and contributing the most to the structural integrity of adipose tissue[15,70]. Collagen type I also contributes to the tensile strength of soft tissues, imparting the ability to resist mechanical loading[71,72]. Collagen types IV, V, and VI[15,71,73–76] have also been identified in adipose tissue, while other types such as collagen types II, IX, and XVIII are notably lower in abundance[71]. Elastin is another fibrous protein found in adipose tissue that serves to provide the tissue with elasticity, or the ability to recoil after expanding and contracting [77,72]. Additional components such as GAGs and proteoglycans also contribute to the adipose ECM structure and mechanical integrity. GAGs are linear chains of repeating disaccharide units, while proteoglycans consist of a core protein covalently linked to one or more sulphated GAGs[69]. GAGs are highly anionic structures, which attract and bind water molecules and have the added benefit of sequestering positively-charged growth factors[69]. In addition to collagen, other glycoproteins such as laminin[15,78] and fibronectin[15,79] further contribute to the bioactivity of the ECM by providing binding sites for cellular attachment, which regulate a range of downstream functions including cell survival, proliferation, and differentiation[78,80].

Through immunohistochemical staining, it was discovered that the adipose ECM components are distributed into a loose, supportive network surrounding the adipocytes[2,79]. Immediately encircling the adipocytes, endothelial cells, and nerves in adipose tissue, the ECM is comprised of a mesh-like structure called the basement membrane. The basement membrane is a thin layer of ECM that is enriched in laminin and collagen type IV[75,78], which provides structural support, binding sites for cell attachment, and has been implicated in adipogenesis[78,81]. Collagen type IV is a heterotrimeric glycoprotein that has six associated α-chain subunits (α1(IV) to α6(IV))[75,80], while laminin is a heterotrimeric glycoprotein made up of an α, β, and γ subunit[78]. Both self-assemble into independent sheet-like networks that link together with the aid of the glycoprotein, nidogen, and the heparan sulfate proteoglycan, perlecan[75,78]. Other proteins connected to the basement membrane, including the microfibrillar protein collagen type VI, further aid in promoting cell-ECM interactions by anchoring adipocytes to the basement membrane[14].

Interfacing with the basement membrane is a network of collagen fibers, composed mainly of collagen type I, which maintain the tissue's integrity[15,70]. Collagen type I fibers are heterotrimeric triple helices, formed by two α1(I) subunits and one α1(I) subunit, which aggregate together to form thicker bundles[82]. Collagen type V, a heterotrimeric microfibrillar protein consisting of two α1(V) subunits and one α2(V) subunit, can crosslink with collagen type I and modify its fibrillation pattern and tensile strength[83]. The abundance of these ECM components can differ based on the depot[70,71] as well as within diseased adipose tissue[74,79,84].

Pre-adipocytes, ASCs, adipocytes, and fibroblasts synthesize the ECM[15,74], while other cells such as macrophages and endothelial cells regulate ECM synthesis and remodeling[1,85]. While the ECM plays an instructive role for cell behavior, cell-ECM interactions are bidirectional; cells themselves can regulate ECM synthesis and remodeling. Cell attachment to the ECM occurs through surface receptors, called integrins[86]. Integrins are mechanosensitive, and when activated, trigger a cascade of intracellular signaling through the microtubule and actin filaments of the cell cytoskeleton[69]. Cells can then respond to their microenvironment by secreting factors that can alter their surroundings. For example, cells can secrete matrix metalloproteinases (MMPs) and disintegrin and metalloprotease (ADAMs) family members, which can enzymatically degrade structural components of the ECM to allow for cellular migration, as well as ECM-bound growth factors and matricellular proteins which can regulate angiogenesis, adipogenesis and adipose tissue homeostasis [74,87,88]. The activity of these enzymes is in turn regulated by the secretion of tissue inhibitors of metalloproteinases (TIMPs) and other inhibitors[89,90]. Thus, the balance between these molecules can shift depending on the tissue state in terms of the need for remodeling and/or expansion.

1.5 Clinical options to restore soft tissue defects

Soft connective tissue, like adipose tissue, has a limited capacity for repair and regeneration following physical trauma, oncologic resections, congenital defects, and burns[91]. There have been several medical advances and surgical techniques utilized in the plastic and reconstructive surgical fields that either mimic or rebuild the afflicted areas[3,92,93]. These developments can be categorized based on the defect volume.

Cosmetic procedures can be performed to correct small volume defects through the injection of 1) autologous fat grafts or 2) dermal fillers made of synthetic or naturally-derived materials[94]. Autologous fat grafting through lipofilling is a surgical procedure whereby fat from another depot in the patient’s body is removed through liposuction and grafted into the recipient site. By transferring a patient’s own fat, this technique fills the defect and promotes a soft and natural aesthetic with a low risk of pathogen transmission and immunological rejection[92]. While fat grafting may result in some permanent volume restoration, the persistence of the fat graft is often unpredictable, with volume retention varying between 30-90%[92]. This variability can be due to the lack of a suitable supply of blood vessels to support the grafted tissue, leading to cell necrosis[93], graft resorption, and complications including fibrosis, calcifications, or oil cysts[95]. The outcomes of this technique are also heavily reliant on the surgeon’s skill, frequently requiring repeated supplementary injections to maintain the correction[96].

As a non-surgical alternative to fill small volume deficits, dermal fillers are a popular, more expedient option that do not require a recovery period. Synthetic materials can be used to fill defect sites, such as calcium hydroxylapatite, polymethylmethacrylate (PMMA) beads, or poly-l-lactic acid (PLLA)[94]. However, the use of natural materials, such as human or bovine sourced collagen, and more commonly, hyaluronic acid, are preferred as they have mechanical properties that are more similar to the native tissues and are associated with fewer complications, such as fibrosis[94]. Fillers can be manufactured to come in an array of options that differ based on their crosslinking density and/or particle size[97]. The range of clinical options allows for the matching of material properties of the filler with that of the injection site in order to promote a more natural feel and contour[98]. In comparison to fat grafting, fillers produce a more predictable and consistent natural contour when filling small volume voids[99–101]. A major drawback, however, is that most dermal fillers are not permanent and are resorbed by the body after 3-6 months[94]. As such, repeated injections are necessary to maintain the volume. Further, the use of these fillers would not be practical for larger deficits (such as during breast reconstruction) as they are expensive.

In the case of larger soft tissue voids, such as in post-mastectomy breast reconstruction surgeries, patients can receive synthetic implants filled with silicone or saline. Additional tissue support in the form of the patient’s own tissue or an acellular cadaveric or porcine dermal matrix may be needed for proper coverage of the implant or positioning against the muscle[102]. These implants provide aesthetic support, but do not hold any functional use and are meant to be temporary devices. Further, these devices carry a risk of fibrous encapsulation that can cause further problems such as pain, asymmetry in the surrounding tissue, implant migration, and implant rupture, resulting in a revisional surgery[103]. An alternative option for large volume reconstruction is to surgically transfer autologous, vascularized flaps of skin, fat, and muscle from either the abdomen or back to the recipient site[8,104]. Reconstruction using the patient’s own tissues can provide a more natural looking contour and allow for the permanent restoration of soft tissue defects in comparison to reconstruction using implants. However, these procedures are often long, costly, risk additional complications, require long recovery periods, and can cause donor site morbidity[3,102,105].

In summary, the current strategies for soft tissue repair or augmentation, especially for large volumes, focus on using materials to temporarily fill defects, but they ultimately fail to regenerate the missing adipose tissue. Alternatively, invasive surgical procedures can be utilized to graft autologous fat tissues, but outcomes depend on patients having sufficient tissue and there is a notable risk of complications and donor site morbidity. The dearth of suitable clinical substitutes to predictably and permanently fill soft tissue defects has highlighted the need for novel tissue-engineering strategies that can promote stable, long-term *in situ* adipose tissue regeneration.

1.6 Adipose tissue engineering strategies

In order to address the issues associated with the currently available soft tissue substitutes, the field of tissue engineering may offer novel, promising strategies. Creating implants that can permanently regenerate fat tissue while maintaining volume over time could reduce the number of revisional surgical procedures needed for soft tissue reconstruction. These approaches could enable a more predictable outcome, improve the well-being of patients, and be more cost-effective overall.

While keeping this goal in mind, it is important to note that the growth and expansion of adipose tissue is coupled with angiogenesis, a process where new blood vessels develop from pre-existing ones within the surrounding tissues[106]. When examining the growth of epididymal fat pads in maturing mice, a dense vascular network at the tip of the fat pad was observed to rapidly expand, with new adipocytes developing from within the network in a spatiotemporal manner[2,107]. In the case of existing adipose tissue, expansion occurs through increases in adipocyte size, as well as in the number of adipocytes[59]. However, it has been shown that the delivery of anti-angiogenic agents in a dose-dependent manner can decrease endothelial cell proliferation, increase apoptosis, and induce a reversible weight reduction in obese mice[2,85]. These examples relate back to the fact that adipocytes within native adipose tissue are found in close contact with the surrounding vasculature[2]. The absence of a functional vascular network can impede the survival of adipocytes, which is seen in autologous fat grafts that resorb over time[92]. Eto *et al.* reported that only peripheral adipocytes located within 300 μm of the graft periphery survived within autologous lipoaspirates implanted in immunocompetent C57BL/6J mice, and that adipocytes located deeper within the graft died soon after implantation[108]. Taken together, employing strategies that can stimulate or facilitate the production of a stable vasculature is a necessary design consideration for adipose tissue regeneration.

A common strategy in the tissue-engineering field is to fabricate implants in the form of 3-D porous foams, sponges, microspheres, fibers, or hydrogels[3,4]. These biomaterial-based strategies often incorporate the delivery of therapeutic drugs and/or growth factors in order to induce angiogenesis and/or adipogenesis *in vivo*[3,4]. Common pro-angiogenic and pro-adipogenic growth factors that have been investigated include hepatocyte growth factor (HGF), basic fibroblast growth factor (bFGF), insulin-like growth factor 1 (IGF-1), and vascular endothelial growth factor-A (VEGF-A)[4,109]. In general, growth factors are limited by their stability and short circulating half-life[110]. Moreover, the scale-up of these therapeutic molecules is associated with poor recombinant yields, issues with protein purification, and high production costs[110]. The implementation of growth factors in a clinical setting may also be hindered by the fact that the effects of the growth factor end once the payload is completely delivered, possibly necessitating the injection of multiple boluses until the desired volume is achieved.

As a result, biomaterial-based delivery of therapeutic cell populations is an alternative strategy that has gained attention. In particular, the delivery of stromal cell populations has been found to be a promising approach to coordinate adipose regeneration by either directly differentiating into neo-adipocytes, or by indirectly producing pro-regenerative factors at the site of implantation[25,109]. The cell sources used for adipose tissue engineering will be further discussed in Section 1.7.

To facilitate the successful delivery of these cell populations *in vivo,* the rational design of a 3-D porous biomaterial scaffold must:

(1) Provide a structural and mechanical framework for new adipose tissue growth, ECM deposition, and blood vessel formation[3].
(2) Permit the diffusion of gases, nutrients, and waste exchange[3].
(3) Facilitate cell-biomaterial and cell-cell interactions by supporting cell adhesion, proliferation, survival, migration, and differentiation[3].
(4) Allow for biodegradation at a rate that matches the rate of neo-adipose formation[3].
(5) Not elicit a chronic inflammatory response or cytotoxicity *in vivo*[3].

1.7 Cell sources for soft tissue regeneration

To date, several options have been used for the sourcing of therapeutic cell populations for soft tissue regeneration. In order for the cell population of interest to be a viable option for clinical use, the cells must be readily accessible, abundant, and they should have the capacity to contribute to soft tissue repair and regeneration when grafted[3,109]. Autologous adipocytes are an abundant source of cells, however, they are terminally-differentiated and have been shown to possess a limited capability to proliferate[111]. Adipocytes have also been shown to be sensitive to ischemic conditions and require a stable blood vessel network in order to survive, limiting their application in soft tissue regeneration[38,108]. Pluripotent stem cells such as induced pluripotent stem cells (iPSCs) are another potential autologous source of cells, as they can be derived by reprogramming a patient's own somatic cells[112]. These cells are promising because they can be expanded and remain undifferentiated in culture, and they possess the ability to differentiate into cells belonging to all three embryonic germ layers[112]. However, these cells carry a risk of stimulating teratoma formation *in vivo*, and the methods of reprogramming the cells to gain pluripotency are limited by safety, efficiency, and cost concerns[112].

Tissue-specific stromal cell populations harvested from adipose tissue represent an attractive alternative, as they are more abundant and accessible as compared to bmMSCs, which are harvested from bone marrow using more invasive procedures that pose greater risks for donor-site morbidity[113]. When compared to bmMSCs, ASCs have been reported to have a greater therapeutic capacity for immunomodulation[114,115] and a similar capacity for stimulating angiogenesis[113]. A donor-matched comparison of the tri-lineage differentiation potential of these cells found that ASCs showed greater adipogenic capacity, while bmMSCs were more pre-disposed towards the osteogenic and chondrogenic lineages[116].

An increasing number of studies have either used the freshly isolated, unprocessed, heterogenous SVF cell population, or the expanded subpopulation of ASCs found within the SVF for adipose tissue-engineering applications. ASCs are a more homogenous population of cells as compared to SVF isolates, however both cell populations exhibit pro-adipogenic, pro-angiogenic, and immunomodulatory properties[4,24,117,118].

Unfortunately, few studies have compared the therapeutic ability of ASC populations versus SVF cells in the context of soft tissue regeneration. Though other studies have compared their use in bone[119], renal[120], myocardial[121], and nerve[122] tissue engineering and have demonstrated that SVF cells have a comparable therapeutic capacity when compared to ASCs[119–122]. However, the heterogeneity of the cell populations in SVF is not conducive for long-term culture and expansion, limiting their clinical use to one-time, same-day intraoperative procedures[119]. ASCs by comparison can be expanded in culture to obtain large yields and be banked for future use[123]. Moreover, ASCs may exhibit immunoprivilege properties, as they have been reported to lack the expression of human leukocyte antigen – DR isotype (HLA-DR) and have demonstrated the ability to inhibit activated lymphocyte proliferation[124]. This may broaden ASC sourcing to include both autologous and allogeneic sources. Therefore, ASCs are an attractive and robust option for use in soft tissue-engineering strategies.

1.7.1 ASC-based strategies for soft tissue regeneration

There has been a substantial amount of evidence supporting the use of ASCs in soft tissue regeneration applications. ASCs are commonly delivered through injections or through seeding onto biomaterial implants or fat grafts and then subcutaneously implanted in various pre-clinical models. Common animal models employed include small rodent models such as immunocompetent or immunodeficient mice and rats[4]. After grafting, tracking studies have employed immunohistochemical techniques, potentially in combination with imaging modalities, to identify labeled ASCs in the surrounding tissues and evaluate their retention over time[125–127]. Additional histological and/or immunohistochemical analyses have been performed to assess implant or fat graft volume retention, neo-adipocyte and blood vessels formation, as well as the phenotype of infiltrating cell populations, with unseeded constructs serving as controls [128–131].

In general, ASCs have the ability to promote the survival and retention of fat grafts *in vivo*, as well as the potential to stimulate blood vessel formation and neo-adipocyte formation in biomaterial implants[3,4,132]. However, limited studies have quantitatively assessed the retention of delivered ASC populations over time. When luciferase$^+$GFP$^+$ ASCs were directly injected into an ischemic adipose tissue mouse model, there was an increase in vascular density and an upregulation of the pro-angiogenic factors HGF and VEGF despite bioluminescence imaging showing an overall decline in luciferase$^+$ cells over time[133]. Other studies have reported fluorescently or nanoparticle-labeled ASC populations incorporated into lipoaspirates[134], vascularized tissue-engineering chambers[135], and ischemic hindlimbs[136] have shown similar limitations in the long term retention of donor ASC populations, despite the presence of new blood vessel networks. Even though the exact mechanisms behind *in vivo* ASC-mediated tissue regeneration remain to be fully elucidated, these studies suggest grafted ASCs indirectly contribute to regeneration through paracrine secretions.

Various studies probing the ASC secretome have found that ASCs can establish a pro-regenerative niche through the secretion of pro-angiogenic growth factors (e.g. VEGF, HGF, bFGF)[4,137], immunomodulatory cytokines (e.g. IL-6, IL-8, IL-10, IL-13)[138] and chemotactic factors (e.g. macrophage colony-stimulating factor (MCSF), granulocyte/macrophage colony-stimulating factor (G-MCSF), monocyte chemotactic protein-1/CCL2)[138]. Of particular interest is the ability for ASCs to stimulate angiogenesis when delivered *in vivo*. ASCs have been reported to survive ischemic environments and upregulate pro-angiogenic and anti-apoptotic factors such as VEGF, bFGF, and HGF[139,140]. ASCs have also been shown to stimulate and stabilize endothelial cell network formation *in vitro*, although this was dependent on the direct contact between these two cell types[141–143].

There is also a growing body of evidence that suggests ASCs can further establish a pro-regenerative microenvironment through the secretion of immunomodulatory factors that regulate immune cells including B and T cells[144], dendritic cells[145], and monocytes/macrophages[146,147]. For example, the addition of ASCs to fat grafts was shown to improve graft volume in athymic mice, and it also caused a decrease in mRNA expression of the pro-inflammatory markers IL-1β and IL-6, along with an increase in the pro-regenerative markers CD163 and CD206[118].

ASC interactions with macrophages are of particular interest as it is now known that macrophages are involved in several wound healing and tissue repair processes[148]. ASCs delivered *in vivo* into a murine ear-punch dermal regeneration model using C57BL/6-Tg mice have shown enhanced macrophage recruitment towards injection sites[149,150]. Additionally, ASCs can promote a shift in macrophage phenotype from a more pro-inflammatory, or “M1-like” phenotype, towards a more pro-regenerative or “M2-like” phenotype, described in more detail in the next section[146,147,151,152]. These interactions are bi-directional, as M2 macrophages were reported to stimulate the proliferation of MSC populations, while M1 macrophages inhibited their proliferation *in vitro*[153]. It is important to note, however, that ASC paracrine factor secretion is highly context dependent, as it is strongly influenced by the cellular microenvironment. For example, after ASCs were serum starved and cultured in media containing TNF-α, there was greater secretion of pro-inflammatory cytokines and chemokines such as IL-6, IL-8, chemokine (C-X-C motif) ligand 6 (CXCL6), and CCL2 than as compared to serum starved ASCs cultured without TNF-α[154]. This conditioned media stimulated the *in vitro* migration of human monocytes[154]. Taken together, this means that the rational design of the ASC microenvironment should be mindful of ASC survival, while also conditioning the secretion of pro-angiogenic and immunomodulatory factors when delivered *in vivo*.

1.7.2 Macrophage-based strategies for soft tissue regeneration

Macrophages are phagocytic cells belonging to the innate immune system that contribute to a range of functions, including pathogen removal, inflammation, tissue homeostasis, wound repair and healing[27,155,156]. Most tissues in the body contain macrophage populations, and genetic lineage tracing studies have revealed that the macrophages in the body exist as either tissue-specific macrophages, originating from cell populations of the embryonic yolk sac and fetal liver, or as macrophages derived from precursor cells called monocytes, which originate from the bone marrow[157].

Tissue-resident macrophages such as microglia, Langerhans cells, and Kupffer cells, have the capacity for proliferation and function to maintain tissue homeostasis in response to cues provided by the local tissue microenvironment[158]. Macrophages originating from the bone marrow instead come from a common myeloid progenitor (CMP), which undergoes differentiation along the myeloid lineage after binding to colony-stimulating factors (CSFs) such as granulocyte macrophage colony stimulating factor (GM-CSF), macrophage colony stimulating factor (M-CSF) and granulocyte colony stimulating factor (G-CSF) [159,160]. Eventually, these cells differentiate into monocytes via the transcription factor PU.1, and exit the bone marrow niche in order to enter into the circulation[159,160]. In response to inflammatory signals, monocytes extravasate into tissues and begin to differentiate into macrophages[161]. In the context of wound healing or biomaterial implantation, it is thought that the tissue-resident macrophages are the first to respond to injuries or implants, and then they facilitate the recruitment of other macrophage populations including monocyte-derived macrophages through various chemotactic factors[148,155,162].

Macrophages are highly plastic cells that can respond to various external microenvironmental signals[163]. Under controlled *in vitro* conditions, macrophages can be stimulated to exhibit a more pro-inflammatory “M1-like” phenotype or a more pro-regenerative “M2-like” phenotype as described below[164]. When considering *in vivo* conditions, there are numerous factors that can serve as stimuli to activate or “polarize” macrophages towards various phenotypes, resulting in a wide spectrum of unique macrophage surface marker expression and secretory profiles[165,166]. Regardless, the M1/M2 paradigm still remains useful for describing the differing functions of macrophages during tissue repair and regeneration[167,168]. This also highlights how macrophage function and phenotype remain highly context-dependent, and emphasizes the importance of clearly reporting the *in vitro* and *in vivo* conditions in which these cells are isolated, cultured, or examined[167].

Pro-inflammatory or “classically-activated” M1 macrophages are activated by pro-inflammatory signals such as interferon-γ (IFN-γ), lipopolysaccharide (LPS), and tumor necrosis factor-α (TNF-α), and upregulate and secrete pro-inflammatory cytokines (e.g. IL-1, IL-6, IL-23, and TNF-α), superoxide anions, and oxygen and nitrogen radicals to aid in pathogen and necrotic tissue clearance[169,155]. M1 macrophages also show an upregulation of inducible nitric oxide synthase (iNOS), an enzyme which metabolizes arginine into nitric oxide (NO) and citrulline[170]. A study by Novak *et al.* showed that the addition of allogeneic pro-inflammatory macrophages improved skeletal muscle regeneration outcomes following injury in mice[171]. While M1 macrophages are a necessary component of wound healing and angiogenesis[168], a prolonged M1 response can lead to chronic inflammation and damage to the surrounding tissues[172].

In contrast, anti-inflammatory or “alternatively-activated” M2 macrophages play an important role in healthy adipose tissue homeostasis and the clearance of apoptotic cells[173]. More broadly, M2 macrophages show increased arginase-1 (Arg-1) expression, an enzyme that hydrolyzes arginine into ornithine and urea, thereby limiting arginine availability to produce NO[170]. Further classifications into M2 subsets have been developed based on cellular function, surface receptor expression, and the exogenous factors that induce polarization[174,175]. The M2a subset, activated by IL-4 and IL-13, is thought to contribute to wound stabilization, extracellular matrix deposition, cell migration and proliferation after the influx of M1 macrophages during the early stages of wound healing[156]. The M2b subset has been shown to be activated by immune complexes and toll-like receptor agonists and play a role in the suppression of the pro-inflammatory response by upregulating immunoregulatory cytokines such as IL-10[176]. In contrast, the M2c subset is activated by IL-10, and is involved in ECM synthesis and tissue remodeling[177].

Macrophages are an attractive cell population to employ in a cell-based soft tissue regeneration strategy because they are involved in blood vessel sprouting[178,179]. Lilja *et al*. found that when Matrigel supplemented with Zymosan to induce sterile inflammation was implanted into C57Bl/6 mice within a tissue engineering chamber system, there was an upregulation in the gene expression of chemotactic proteins including monocyte chemoattractant protein (MCP)-1 at 0.5 and 2 days, as well as the recruitment of myeloid cells originating from the bone marrow at 7 days[180]. This was followed by the development of neovascularization and neo-fat tissue after 14 days[180]. Later studies showed that depleting the infiltrating macrophage population using Clodronate liposomes showed minimal presence of $CD31^+$ cells within the implant, as well as limited expression of adipogenic markers, highlighting the close relationship between inflammation, angiogenesis, and adipogenesis[181]. Additional *in vitro* studies have postulated that different macrophage subsets may play different roles in the context of angiogenesis including the promotion of blood vessel sprouting (M1 subset), increasing vascular remodeling (M2c subset), the promotion of blood vessel fusion (M2a subset), and the recruitment of pericytes (M2a subset)[182].

There is an emerging interest in further implementing macrophage-based therapies for soft tissue regeneration, extending from the current understanding of their roles in wound healing and angiogenesis. There have been a growing number of studies that have observed that *in vivo* adipose regeneration coincides with a shift in macrophage phenotype from an M1-like phenotype to an M2-like phenotype[151,165,183,184]. To date, there have been few animal studies in which exogenously-prepared macrophages were directly delivered *in vivo* to assess their therapeutic efficacy in the context of soft tissue regeneration. One study performed by Phipps *et al.*, utilized *in vitro* prepared macrophages that were harvested through intraperitoneal injection of Brewer's thioglycolate, followed by subsequent stimulation with MCSF and IL-6[185]. The generated cells showed an M2-like phenotype as indicated by an upregulation in *arg1 and il10* mRNA and downregulation of *inos* and *il12* mRNA. Fat grafts supplemented with these M2-like macrophages were delivered *in vivo* into immunocompetent C57Bl/6 mice and showed greater graft retention and blood vessel density, as well as increased levels of infiltrating F4/80$^+$CD11b$^+$ macrophages as compared to phosphate-buffered saline supplemented controls[185]. Thus, there is a need for more studies to assess the delivery of exogenously-prepared macrophage therapies in order support strategic use of these cells.

1.8 Biomaterials for soft tissue regeneration

1.8.1 Synthetic biomaterials

A range of synthetic polymer biomaterial implants have been designed to promote adipose tissue regeneration. Synthetic biomaterials have the advantage of having more readily tailorable mechanical and chemical properties, which is important as numerous studies have shown that matching the scaffold stiffness with that of native adipose tissue (2-4 kPa)[186] can stimulate adipogenesis[187–190].

Polyesters such as such as poly(lactic-co-glycolic acid) (PLGA)[191,192], polyglycolic acid (PGA)[193], and polylactic acid (PLA)[194], have been widely utilized as cell and/or growth factor delivery platforms for adipose regeneration. A common strategy that was employed was to seed pre-adipocytes or ASCs directly onto PLGA scaffolds and then pre-differentiating them towards the adipogenic lineage *in vitro* before delivering them *in vivo* into immunodeficient mice[192,195,196]. This strategy allowed for significantly more adipose tissue formation after 2 months as compared to when the cell populations were injected on their own[197]. Interestingly, Patrick *et al.* delivered male rat pre-adipocytes into the dorsa of immunocompetent Lewis rats by using PLGA foams and histologically evaluated adipose formation within the constructs between 1-12 months[198]. They found that pre-adipocyte-seeded PLGA foams formed significantly more adipose tissue than acellular foams, with peak neo-adipose tissue formation occurring at 2 months[198]. However, the volume of adipose tissue formed decreased dramatically after this time frame due to scaffold resorption[198]. Polyester biomaterial degradation can be modified in a number of ways by changing their method of fabrication, molecular weight, crystallinity, or ratio of copolymers[199–201]. These polymers degrade through hydrolysis and they generate byproducts, such as lactic acid and glycolic acid, which are non-toxic and can be cleared by the body.

However, a build-up of these byproducts can alter the pH of the local tissue microenvironment and cause adverse tissue and inflammatory reactions[202,203].

In addition to solid polymer networks, hydrogel constructs have also been widely explored for adipose tissue engineering. Hydrogels are highly hydrophilic polymer networks that can be physically or chemically cross-linked and can be made into an injectable format. The material properties of hydrogels can be modified with the addition of chemical crosslinkers[204], as adding more crosslinks will create stiffer, denser scaffolds that degrade more slowly. In addition, the properties can be tuned by forming interpenetrating polymer networks or double networks[183,205]. Polyethylene glycol (PEG)-based hydrogels are a common biomaterial employed due to their tunable properties[206]. PEG biomaterials are known to be biologically inert, and like many other synthetic polymer systems, lack innate bioactivity, limiting their capacity to promote tissue regeneration[25]. To address this, strategies have been developed to incorporate ECM proteins, such as collagen, fibronectin, vitronectin and laminin, to make hybrid constructs[207]. Alternatively, polymers can be modified with small bioactive peptide ligands, such as the RGD, IKVAV or YIGSR peptide sequences, to promote cell adhesion[208,209]. Brandl *et al* modified PEG hydrogels by adding YIGSR peptide sequences, as well as collagenase-sensitive peptides, allowing the scaffolds to be enzymatically degraded[210]. The group demonstrated that 3T3-L1 preadipocytes cultured in the hydrogels showed higher levels of intracellular triglyceride accumulation and the promotion of a unilocular adipocyte morphology in comparison to non-degradable hydrogel controls[210].

1.8.2 Naturally-derived biomaterials

Unlike synthetic materials, naturally-derived biomaterials are made from components extracted from living organisms. This class of biomaterials offers the advantage of being inherently bioactive and in general do not elicit chronic immune responses *in vivo*[168]. This group of biomaterials includes biopolymers not found in the human body, such as silk[211–213], chitosan[128,214–216], and alginate[217–219], which can be fabricated into 3-D constructs such as sponges, fibers, hydrogels and microspheres. For example, chitosan is a linear, polysaccharide obtained from crustaceans, which is biodegradable, anti-microbial, and supportive of ASC viability and proliferation[195,214–216]. Wang *et al.* fabricated hybrid porous poly(L-glutamic acid)-chitosan scaffolds that supported the proliferation of ASCs *in vitro*[195]. They found that delivering pre-differentiated ASC-seeded constructs into severe combined immunodeficient (SCID) mice enhanced macroscopic vascularization, retention of scaffold volume, and quantitatively greater levels of lipid accumulation after 6 weeks *in vivo,* in comparison to unseeded controls[195]. When pre-adipocytes were seeded onto glutaraldehyde cross-linked collagen/chitosan hydrogels and subsequently implanted into immunocompetent Lewis rats, there was a similar increase in cell infiltration, blood vessel density, and lipid accumulation as compared to acellular scaffolds after 7 days *in vivo*[128]. However, this was followed by a slight decrease in blood vessel density and adiposity after 14 days[128]. The reason for this was unclear, but the authors suggested it was due to a high degree of secreted ECM or due to the slow degradative properties of the scaffold[128].

Naturally-derived biomaterials can also be sourced from extracted ECM components, including collagen[220–222] and hyaluronic acid[223–225]. In particular, collagen and its derivatives have been demonstrated to be supportive of *in vitro* ASC attachment[221,226,227] and *in vivo* blood vessel and fat formation[220,221,228]. Mauney *et al.* compared the ability of collagen, PLA, and silk fibroin scaffolds to support *in vitro* and *in vivo* adipogenesis of bmMSCs and ASCs[229]. While both cell types showed comparable levels of metabolic activity and lipid accumulation when seeded onto collagen scaffolds *in vitro*, the unseeded, bmMSC, and ASC-seeded collagen and PLA scaffolds completely resorbed after 4 weeks *in vivo* in athymic nude rats[229]. The silk fibroin scaffolds in comparison, showed retention of both the scaffold structure and of the ASC and bmMSC populations, and supported *in vivo* adipogenesis, emphasizing the importance of controlling the scaffold degradation rate[229]. Numerous studies have shown that collagen and other naturally-derived materials lack suitable mechanical and degradative properties to sustain implant structural integrity over time[220,230,231]. In order to improve the stability of collagen-based constructs, other studies have employed methods to physically or chemically crosslink collagen[220]. Non-crosslinked collagen has shown extensive contraction and resorption *in vivo*, while crosslinked collagen is notably stiffer, has a slower *in vivo* degradation profile, and has been associated with increased levels of *in vivo* cellular infiltration and angiogenesis[220,232]. Taken together, this highlights the importance of the physical degradative properties of biomaterials, which can affect the retention of delivered cell populations as well as the development of an adequate vascular supply.

1.8.3 Decellularized biomaterials

While the previously mentioned “bottom-up” fabrication strategies have largely focused on developing hybrid biomaterial constructs composed of one or two structural ECM components in combination with a synthetic polymer, these strategies fail to fully recapitulate the unique, tissue-specific composition and material properties found in the native ECM[127]. Tissue decellularization is an alternative option that utilizes a “top-down” fabrication strategy in which tissue or organ samples are processed in order remove the antigenic cellular and nuclear material, while preserving the ECM components as much as possible[233]. Tissue processing often includes a series of chemical, physical, and/or enzymatic treatments in order to disrupt the native tissue structure enough to facilitate the removal of cellular material[233]. Decellularized biomaterials are often used in either their intact form[234–236] or are manipulated in such a way that they can be fabricated into hydrogels[131], foams[237,238], microcarriers[239], or sheets[240,241] depending on the application of interest. Broadly speaking, decellularized biomaterials have biochemical, biophysical, and biomechanical properties that can mimic their native tissue source, and they have the added advantage of being innately bioactive and biodegradable[242]. The method of tissue processing can affect how much of the native tissue composition and ultrastructure is preserved, which in turn can promote or hinder downstream remodeling and regeneration outcomes[242].

Owing to their innate bioactivity and tissue-specific biochemical and biomechanical properties, various types of decellularized biomaterials have been employed as ASC delivery platforms for soft tissue regeneration applications. ASC-seeded decellularized dermis[243–245], small intestinal submucosa (SIS)[191], skin/adipose flaps[246], and placenta[235] have demonstrated *in vivo* ASC retention[191,243–245], neo-vascularization[191,235,243–245], and in a few cases, neo-adipocyte formation[235,246]. Wang, J.Q. *et al.* found that ASCs seeded onto human decellularized adipose tissue microparticles and porcine small intestine submucosa (SIS) microparticles had greater *in vitro* metabolic activity when compared to ASCs cultured on tissue culture polystyrene[247]. However, when implanted into nude mice, the ASC-seeded human adipose tissue extract microparticles showed greater levels of vascularization and neo-adipocyte formation than porcine SIS microparticles[247]. This highlights how strategies utilizing decellularized biomaterials should consider matching the source of ECM used to fabricate the scaffolds with the application in question.

1.8.4 Decellularized adipose tissue

In previous work, the Flynn lab has pioneered the design of the decellularized adipose tissue (DAT) technology[234]. Though human fat is rich in ECM, it is routinely discarded as surgical waste, making it an attractive option to fabricate an off-the-shelf bioscaffold for soft tissue regeneration applications[127,234]. The Flynn lab method of adipose decellularization utilizes a detergent-free protocol that includes mechanical disruption to increase the tissue surface area, freeze-thaw cycles in a hypotonic buffer to initiate cell lysis, multiple rinses in isopropanol to remove lipid content from the tissue, and enzymatic digestion with trypsin-EDTA, DNase, RNase and lipase to enhance the extraction of cells and intracellular components[234]. The ECM that is extracted is then frozen in deionized water and lyophilized, resulting in a 3-D porous bioscaffold that preserves the complex microarchitecture and composition of native adipose tissue[234]. Biochemically, DAT bioscaffolds retain structural ECM proteins such as collagen I and IV, laminin, fibronectin, elastin, GAGs, and proteoglycans[234,248]. High throughput mass spectrometry-based techniques were employed to compare the tissue-specific protein content and abundance between DAT and decellularized cancellous bone (DCB) bioscaffolds[241]. Our study found that in comparison to DCB, DAT contained a diverse array of bioactive ECM components such as soluble growth factors, matrikines, pro-adipogenic proteins, and residual intracellular proteins[241]. This has complemented other studies that have demonstrated that DAT-based bioscaffolds provide a tissue-specific platform to support *in vitro* ASC proliferation and differentiation along the adipogenic lineage[234,237,239,249].

To further recapitulate the native adipose tissue micro-niche, the Flynn lab has investigated the cellular mechanisms underlying the use of DAT bioscaffolds as a cellular delivery system for allogeneic ASCs. We have found that seeding the scaffolds with ASCs augmented remodeling of the DAT bioscaffolds into host-derived fat relative to unseeded controls in an immunocompetent Wistar rat model[165,237]. There was further evidence that the ASC-seeded DAT bioscaffolds had established a pro-regenerative milieu, which included an increase in angiogenesis over time, upregulation of IL-10 expression at early time points, and a shift towards a greater fraction of macrophages with an M2-like, pro-regenerative phenotype[165]. Interestingly, Wang *et al.* seeded ASCs onto DAT microparticles that were processed using a different decellularization protocol, and delivered them along with human fat grafts, subcutaneously into nude Fischer 344 rats[250].

Over time, both the ASC-seeded DAT microparticles and the fat graft showed a decrease in the total number of nucleated cells, with a greater fraction of host cells present within the implants over time[250]. Further immunohistochemical analysis of the infiltrating cell population at 4 weeks found that the cells were negative for macrophage phenotype markers CD68, CD80, and CD163, but a small fraction of cells were positive for T cell markers, CD4 and CD8. After 4 weeks, neo-adipocyte formation was observed in both groups, with some adipocytes having been derived from donor ASC populations[250]. However, the vascularization in the ASC-seeded DAT microparticles was higher in comparison to the fat graft after 2 weeks *in vivo*, but then significantly decreased after 4 weeks, while vascularization of the fat grafts was maintained beyond 4 weeks[250]. While this study demonstrated that ASC-seeded DAT constructs were able to stimulate *in vivo* neovascularization and implant remodeling into neo-fat tissue similar to our previous study[165], the phenotype of the infiltrating cell population lacked any macrophage marker expression[250]. This points to the differences in the mechanisms of ASC-mediated regeneration between immunocompetent and immunodeficient rat models.

In more recent studies performed in the Flynn lab, syngeneic murine ASCs derived from mice from a genetically similar genetic background, were seeded onto DAT bioscaffolds and subcutaneously implanted in the dorsa of immunocompetent MacGreen mice, in which all of the myeloid cells express EGFP[251]. ASC-seeded DAT implants showed significantly higher levels of cell infiltration at 8 weeks post-implantation as compared to unseeded controls[251]. The ASC-seeded implants also showed higher levels of implant remodeling into fat, and immunohistochemical staining confirmed that even though the donor ASCs had been retained after 8 weeks *in vivo*, the new adipocytes were entirely host-derived[251]. Furthermore, Iba-1$^+$ macrophage recruitment was observed to be greater in the ASC-seeded implants, with peak levels observed at 3 weeks[251]. However, the overall levels of Iba-1$^+$ macrophages declined over time[251]. Qualitatively, the infiltrating myeloid cell population also appeared to express high levels of the pro-inflammatory marker, iNOS, relative to the expression of the pro-regenerative marker, Arg-1[251]. However, there were no notable qualitative differences in the levels of iNOS and Arg-1 expression found between ASC-seeded and unseeded implants[251].

1.9 Project overview, hypothesis, and specific aims

1.9.1 Project overview

Adipose is a loose, soft connective tissue distributed throughout the body in different depots that helps to define the natural contours of the body[3,4]. Unfortunately, fat, like many other tissues in the body, has a limited capability for repair and regeneration[3]. The absence of soft tissue can lead to further complications such as scar formation, contracture, and possible loss of function[3,4]. In the case of large soft tissue deficits, the surgical options for repair or reconstruction are limited to grafting autologous soft tissue flaps. However, these procedures are often expensive, require a large amount of soft tissue to create the graft, and they risk additional complications and donor site morbidity[3,102,105].

In order to address these clinical issues, there has been interest in designing tissue-specific constructs to permanently regenerate soft tissue and maintain volume over time. The development of decellularized adipose tissue (DAT) derived from human fat is a promising off-the-shelf bioscaffold that can be used to deliver therapeutic ASC populations[234,237,239,249]. In an *in vivo* immunocompetent Wistar rat model, subcutaneous implantation of allogeneic ASC-seeded DAT was demonstrated to augment the constructive remodeling of the implant into host-derived fat[165]. ASC-seeding is postulated to contribute to the establishment of a pro-regenerative microenvironment, including 1) the development of a supportive vasculature, and 2) a shift towards a pro-regenerative macrophage phenotype[165]. In later studies using an immunocompetent MacGreen murine model, subcutaneous implantation of syngeneic ASC-seeded DAT in the dorsa showed augmented host-derived neo-fat formation, as well as an increase in infiltrating macrophage populations[251].

Other animal studies have revealed a close relationship between adipogenesis, angiogenesis, and inflammation. In a tissue-engineering chamber system implanted in immunocompetent C57Bl/6 mice, Lilja *et al*. found that Matrigel supplemented with Zymosan showed an upregulation in chemotactic factors and the recruitment of bone marrow-derived macrophages at early time points[180]. This was subsequently followed by the development of new blood vessels and fat tissue[180]. Depleting these infiltrating macrophage population using Clodronate liposomes decreased the levels of angiogenesis and adipogenesis in the chamber[181]. These findings are in support of other reports that demonstrate how vascularization[2,107], as well as a shift in recruited macrophages towards a pro-regenerative phenotype[151,165,183,184] are crucial components in order for downstream soft tissue regeneration to occur.

There is evidence that ASC-based therapies indirectly support regenerative processes through the secretion of pro-angiogeneic, pro-chemotactic, and immunomodulatory factors[138]. The injection of ASCs into C57BL/6-Tg mice was observed to stimulate macrophage recruitment towards injection sites[149,150], which complements our studies on ASC-seeded DAT implants promoting the migration of macrophage populations[251]. Further, ASCs in hypoxic culture can express pro-angiogenic and antiapoptotic factors such as VEGF, bFGF, and HGF[139,140], and they have been shown to directly stimulate and stabilize endothelial cell networks[141–143]. Additionally, ASCs have the ability to cause a shift in macrophage phenotype from a pro-inflammatory to a pro-regenerative phenotype[146,147,151,152]. ASC-seeded DAT scaffolds may have provided a similar role in our Wistar rat model, as we found greater levels of blood vessel formation, and the expression of the anti-inflammatory cytokine, IL-10 at early time points[165]. At later time points, we observed a greater fraction of $CD163^+$ pro-regenerative macrophages[165].

Notably, the role of macrophages in the constructive remodeling of ASC-seeded DAT implants into host-derived fat remains to be elucidated. Different macrophage subtypes have been implicated in various roles during wound healing[148] and angiogenesis[178,179]. It is possible that both the ASCs and infiltrating macrophages contributed to the enhanced blood vessel development by producing paracrine factors to support neo-fat formation. Thus, there is strong evidence to support the implementation of an ASC-based therapy alone or in combination with macrophages to augment angiogenesis and promote a shift in macrophage phenotype, which could be particularly advantageous for the reconstruction of larger soft tissue defects.

The present work aims to elucidate the cell-scaffold and cell-cell interactions mediating the remodeling process, with the goal of improving the translation of cell-based therapies for stable and long-term soft tissue replacements. In an effort to gain insight into the role of inflammation in ASC-mediated adipose tissue regeneration, this thesis focuses on investigating the impact of seeding DAT bioscaffolds with syngeneic macrophages and/or syngeneic ASCs, on cellular infiltration, angiogenesis, and macrophage phenotype following implantation in C57Bl/6J mice.

1.9.2 Hypothesis

Hypothesis: Seeding DAT bioscaffolds with syngeneic macrophages and syngeneic ASCs will promote a more pro-regenerative environment that enhances cellular infiltration and angiogenesis in the DAT in an immunocompetent subcutaneous mouse model.

1.9.3 Objectives

Objective 1. Establish methods for isolating and culturing murine monocyte-derived macrophages (M_0) sourced from the bone marrow of MacGreen transgenic mice and characterize their immunophenotype

Objective 2. Develop an *in vitro* culture and seeding protocol for macrophages ± ASCs on the DAT bioscaffolds

Objective 3. Explore the effects of ASC delivery, macrophage delivery, and ASC/macrophage co-delivery in the DAT bioscaffolds relative to unseeded controls in a subcutaneous implant model in C57Bl/6J mice on *in vivo* cellular infiltration, angiogenesis, and macrophage phenotype.

Chapter 2

2 Materials & Methods

2.1 Materials

All chemicals and reagents were purchased from Sigma-Aldrich Ltd. (Oakville, ON) unless otherwise specified.

2.2 Animal work

All animal studies were performed in accordance with the Canadian Council on Animal Care (CCAC) guidelines and were approved by the Animal Care Committee at Western University (Protocol # 2015-049). All mice were housed in clean barrier facilities under humidity and light controlled conditions and had free access to food and water. Murine adipose-derived stromal cells (ASCs) were isolated from 9-12 week old female *Discosoma red fluorescent protein* (dsRed) mice (B6.Cg-Tg(CAG-DsRed*MST)1Nagy/J; C57BL/6J background; Jackson Laboratory, Bar Harbor, ME). Murine bone marrow-derived macrophages were obtained from the hindlimbs of hemizygous 9-12 week old male MacGreen transgenic mice (B6N.Cg-Tg(Csf1r-EGFP)1Hume/J; C57BL/6J background; Jackson Laboratory, Bar Harbor, ME). Implantation studies were performed using a total of twenty-five, 9-12 week old male wild-type C57BL/6J mice (Jackson Laboratory; Bar Harbor, ME, USA).

2.3 ASC isolation and culture

ASCs were isolated using a previously published protocol[252] from the inguinal fat pads of dsRed mice, a transgenic mouse strain in which all cells express the fluorescent protein dsRed. All work was performed within a biological safety cabinet using aseptic technique and sterile reagents. Briefly, fat pads from 3-4 mice were finely minced with surgical scissors and added to 15 mL of a collagenase digest solution consisting of: 0.1% Type I Collagenase (Worthington Biochemical Corp., Lakewood, NJ), 1% bovine serum albumin (BSA; Bioshop, Burlington, ON), and 2 mM calcium chloride in phosphate-buffered saline (PBS). The minced tissue was agitated for 1 hour at 37°C and 75 RPM, and then centrifuged (300 x g, 5 min). The cells were then resuspended in PBS with 1% BSA, and passed through a 100 μm filter (Corning Inc., Corning, NY, USA). Next, the cell suspension was centrifuged (300 x g, 5 min) and then resuspended in 5 mL of complete

ASC media comprised of Dulbecco's Modified Eagle's Medium:Ham's F12 (DMEM:Ham's F12) with 10% fetal bovine serum (FBS; Gibco®, Invitrogen, Burlington, ON) and 1% penicillin-streptomycin (pen-strep; Gibco®, Invitrogen, Burlington, ON), and then plated onto Primaria^{TM} flasks (Corning Inc., Corning, NY) and cultured at 37°C and 5% CO_2.

After 24 hours, the flask was gently rinsed multiple times with sterile PBS until the debris and unattached cells were removed and fresh ASC media was added. The cells were passaged after reaching 80% confluence using 0.25% trypsin/0.1% ethylenediaminetetraacetic acid (trypsin/EDTA; Gibco®, Invitrogen, Burlington, ON) and re-plated at 4000 cells/cm^2 on standard tissue culture polystyrene T-75 flasks (Corning Inc., Corning, NY, USA). Media changes were performed every 2-3 days and fresh P3-P4 cells were used for all experiments.

2.4 Macrophage isolation and culture

Since macrophages had not been previously used in experiments performed in the Flynn lab, new protocols were created in order to harvest, culture, and differentiate macrophages derived from the bone marrow of the hindlimbs of MacGreen mice. MacGreen mice are a strain of transgenic mice in which all myeloid cells express enhanced green fluorescence protein (EGFP) under the control of the *csf1r* promoter[253]. All work was performed within a biological safety cabinet using aseptic technique and sterile reagents. The femurs and tibia of the mice were surgically removed, disinfected using 70% ethanol, and then rinsed in Hank's Balanced Salt Solution (HBSS; Gibco® Invitrogen, Burlington, ON) with 0.1% BSA. The bone marrow was flushed out using HBSS with 0.1% BSA delivered via a 26-gauge needle, and put through a 70 µm filter (Corning Inc., Corning, NY, USA). The bone marrow cells were centrifuged (500 x g, 5 min, 6°C), and then incubated with ammonium chloride solution (STEMCELL Technologies, Vancouver, BC) for 3 minutes in order to remove erythrocytes. Next, the cell suspension was rinsed using HBSS with 0.1% BSA, centrifuged (500 x g, 5 min, 6°C) and incubated with purified mouse I-A^b (Biolegend Inc; San Diego, CA, USA, 114402) and purified rat anti-mouse CD45R/B220 (Becton Dickson (BD); Franklin Lakes, NJ, USA, 553084) antibodies for 30 minutes on ice in order to bind to lymphocytes including B and T cells. Next, the cells were rinsed again using HBSS with 0.1% BSA, centrifuged (500 x g, 5 min, 6°C), and incubated with low tox-m rabbit complement (Cedarlane; Burlington, ON), which is cytotoxic to mouse lymphocytes, especially T cells, for 30 minutes at 37°C. Finally, the cells were washed two more times using HBSS with

0.1% BSA, centrifuged (500 x g, 5 min, 6°C) to remove any dead cells, and resuspended in fresh complete macrophage media consisting of RPMI 1640 (Gibco®, Invitrogen, Burlington, ON) supplemented with 10% FBS, 1% pen-strep, 4 mM l-glutamine (Gibco®, Invitrogen, Burlington, ON), and 20 ng/mL recombinant murine macrophage colony stimulating factor (MCSF; Peprotech, Rocky Hill, NJ, USA). The cells were then seeded onto T75 flasks at 5 million cells/flask and incubated at 37°C and 5% CO_2.

Fresh bone marrow cells were counted using a hemocytometer and centrifuged (500 x g, 5 min, 6°C) and then gently resuspended to obtain a solution containing $5x10^6$ cells/mL in freezing media containing 90% fetal bovine serum (FBS) and 10% dimethyl sulfoxide (DMSO) [254]. The cells and freezing media were placed into cryovials, at 1 mL each[254]. Then the cryovials were placed in a Mr. Frosty™ freezing container and maintained at -80°C freezer for 24 hours, and then transferred to a liquid nitrogen tank[254]. To thaw the cells, a cryovial was quickly transferred to a 37°C water bath until the suspension was completely thawed. The contents were then transferred to a cell culture treated T75 flask filled with 20 mL of complete macrophage media[254].

Fresh complete media was added after 2 days, and a half-media change was performed after 4 and 6 days. At 7 days, the bone marrow-derived macrophage populations were used in subsequent studies.

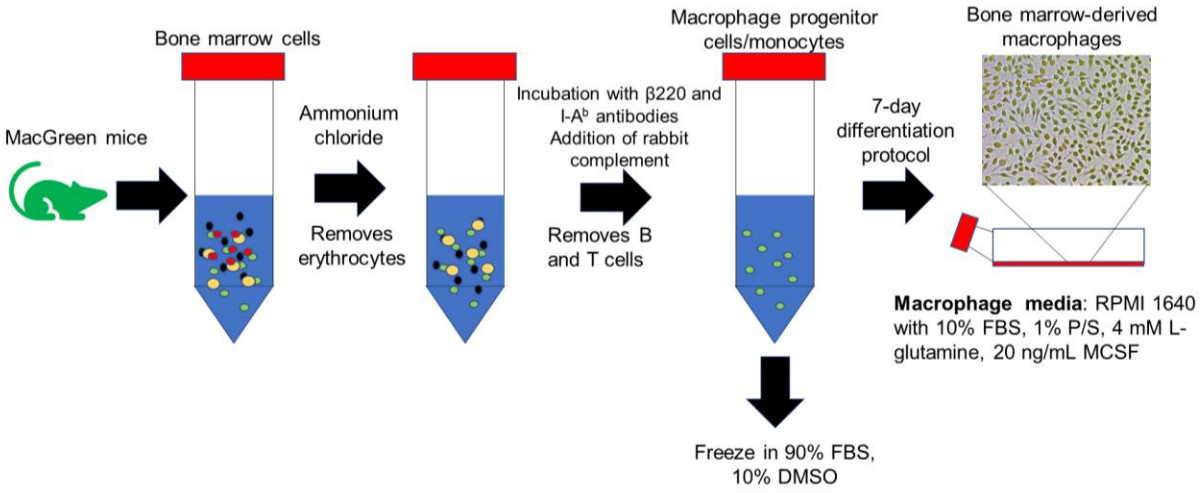
Bone marrow cells
MacGreen mice
Ammonium chloride
Removes erythrocytes
Incubation with β220 and I-A^b antibodies
Addition of rabbit complement
Removes B and T cells
Macrophage progenitor cells/monocytes
7-day differentiation protocol
Bone marrow-derived macrophages
Macrophage media: RPMI 1640 with 10% FBS, 1% P/S, 4 mM L-glutamine, 20 ng/mL MCSF
Freeze in 90% FBS, 10% DMSO

Figure 2.1. Summary of the isolation protocol for bone marrow-derived macrophage progenitor cell population.

2.5 Immunophenotyping of cultured macrophages

With technical support provided by Christy Barreira from the Dekaban lab, flow cytometry was performed to establish a reproducible protocol to assess the immunophenotype of the cultured macrophage populations. Cells were detached from tissue culture flasks through incubation with 0.48 mM Versene Solution (Gibco®, Invitrogen, Burlington, ON) for 15 min at 37°C to preserve cell surface receptors that may be cleaved when enzymatic dissociation methods are applied. The suspended cells were then collected, and the flasks were rinsed using HBSS with 0.1% BSA. If necessary, the flasks were gently scraped using a cell scraper, and the remaining cells were collected. Cells were centrifuged (500 x g, 5 min) and resuspended in 1 mL of sorting buffer, consisting of PBS supplemented with 5 mM EDTA, 25 mM HEPES (pH 7.0), 1% heat inactivated FBS dialyzed against Ca/Mg (Gibco®, Invitrogen, Burlington, ON), and 10 U/ml DNAse II from bovine spleen (Sigma, Oakville, ON). Next, 10 µL of anti-CD16/anti-CD32 (10 µL/mL, Becton Dickenson (BD), Franklin Lakes, NJ) was added, and the cell suspensions were incubated on ice for 10 min to block non-specific Fc-receptor binding. Finally, the cells were washed with PBS, centrifuged (500 x g, 5 min, 6°C), and resuspended in 1 mL of PBS.

To assess cell viability, 2 µL of LIVE/DEAD™ Fixable Aqua Dead Cell Stain (Fisher Scientific, Ottawa, ON) was added and cells were incubated for 20 min at room temperature in the dark. Cells were washed with 6 mL of sorting buffer, centrifuged (500 x g, 5 min, 6°C), resuspended in 0.75 mL of sorting buffer, and then aliquoted into FACS tubes (100 µL of cell suspension/tube). Next, the cells were incubated with a panel of antibodies to assess CD45 (hematopoietic marker), CD11b (macrophage marker), F4/80 (macrophage marker), Ly6G (neutrophil marker), Ly6C (monocyte/macrophage marker) expression. The following monoclonal antibodies were used: Alexa Fluor 700 rat anti-mouse anti-CD45 (1:500; BioLegend Inc., San Diego, CA, cat. 103128), Alexa Fluor 647 rat anti-mouse/human anti-CD11b (1:400; BioLegend, cat. 101218), PE rat anti-mouse anti-F4/80 (1:20; BIO-RAD, Hercules, CA, cat. MCA497PE), Brilliant Violet 421 rat anti-mouse anti-Ly6G (1:40; BioLegend, cat. 127628), and Brilliant Violet 711 rat anti-mouse anti-Ly6C (1:800; BioLegend, cat. 128037). The studies were performed with 5 separate macrophage isolates from wild-type and MacGreen mice to confirm the findings (n=3, N=5).

The cells were incubated with the respective antibodies in the dark (20 min, 4°C), then washed with an additional 2 mL of sorting buffer and centrifuged (500 x g, 5 min, 6°C). Finally, the cells were resuspended in 200 µL of sorting buffer and an additional 100 µL of 4% paraformaldehyde was added to fix the cells, which were then stored at 4°C in the dark. Flow cytometry was performed within 1-2 days after staining using an LSRII digital flow cytometer (BD Biosciences) at the London Regional Flow Cytometry Facility to acquire data for polychromatic analyses. Electronic compensation was performed with UltraComp eBeads antibody capture beads (Invitrogen, Burlington, ON). A minimum of 10,000 events/samples were collected, and forward scatter (FSC), which defines cell size, and side scatter (SSC), which defines cell granularity, gates were set to include only non-debris. Macrophages from wild-type C57BL/6J mice served as a negative control for GFP expression. Data analysis was performed using FlowJo software (Version 10.0.8; Tree Star, Ashland, OR).

2.6 Decellularized adipose tissue bioscaffold fabrication and seeding

2.6.1 Adipose tissue procurement and decellularization

Subcutaneous adipose tissue was collected with informed consent from patients undergoing elective breast reduction or abdominoplasty surgeries at the University Hospital, Cumberland Laser Clinic, and/or St. Joseph's Hospital in London, ON (HREB# 105426). Tissues were transported in sterile PBS supplemented with 20 mg/mL BSA and then subjected to a five-day, detergent-free, decellularization protocol[234]. Briefly, the tissue was treated with three freeze-thaw cycles to promote cell lysis using a hypotonic buffer, multiple lipid extractions using isopropanol, and enzymatic digestion using trypsin-EDTA, RNAse, DNAse, and lipase. The decellularized adipose tissue (DAT) was then frozen in deionized water at -80°C, and then lyophilized to create a porous 3-D bioscaffold.

2.6.2 Decellularized adipose tissue bioscaffold preparation and seeding

The lyophilized DAT bioscaffolds were cut into 6.0 ± 0.5 mg pieces and then rehydrated overnight in deionized water. The bioscaffolds were decontaminated through rinsing in 70% ethanol (3 x 30 min each, 120 RPM), followed by an overnight incubation in 70% ethanol at 120 RPM. Next, the bioscaffolds were transferred under sterile conditions into a new container, and rehydrated with sterile PBS (3 hours, 120 RPM), followed by three rinses in fresh sterile PBS (30 min each, 120 RPM). The PBS was replaced with complete macrophage media and the scaffolds were incubated overnight (37°C and 5% CO_2) prior to seeding.

In order to seed the bioscaffolds, P_2 or P_3 ASCs were trypsinized, and Day 7 macrophages were detached using Versene and cell scraping and counted using a hemocytometer. Each DAT scaffold was transferred into a 15 mL vented cap conical tube containing 3 mL of complete macrophage media and either i) 1×10^6 macrophages, ii)1×10^6 ASCs, or iii) a 1:1 co-culture of macrophages and ASCs (1×10^6 cells total). The scaffolds were dynamically seeded for 24 hours using a BenchWaver^{TM} 3-D rocker (Mandel, Guelph, ON) (95 rpm, 37°C, 5% CO_2) prior to use in *in vitro* culture studies or *in vivo* implantation surgeries.

2.7 *In vitro* characterization of seeded implants

2.7.1 DAPI staining and double stranded DNA quantification

After 24 hours of seeding, the bioscaffolds were rinsed twice in PBS (5 min each, 37°C, 40 RPM) and then fixed in 10% neutral buffered formalin for 2 hours at 100 RPM. Next, the bioscaffolds were rinsed three times in PBS (20 min each, 100 RPM) and then incubated for one hour in a sucrose gradient consisting of 10%, 20%, and then 30% sucrose in PBS. Then the samples were transferred into 70 % ethanol and sent for processing at the Robarts Molecular Pathology Laboratory in London, ON, and then embedded in paraffin. The paraffin-embedded bioscaffolds were sectioned (5 μm) using a Leica RM2235 microtome (Leica Biosystems, Concord, ON, Canada). The sections were deparaffinized by two incubations in xylene (10 min each), followed by rehydration in an ethanol series. To qualitatively assess the cell distribution within the DAT scaffolds, the sections were stained with DAPI mounting medium (Abcam, Toronto, ON) to identify cell nuclei. Non-overlapping images were taken using the EVOS®FL Imaging System (Invitrogen, Ottawa, ON) within 600 µm of the apical and basal borders of the implant periphery as well as within the implant interior.

In addition to the qualitative staining, the amount of double-stranded DNA (dsDNA) content was quantified in a separate set of bioscaffolds using the PicoGreen® dsDNA quantification assay (Invitrogen, Burlington, ON). After seeding for 24 hours, the bioscaffolds were rinsed three times in PBS (5 min each, 37°C, 40 RPM) and then placed in 200 µL of digest solution consisting of 1 x TE buffer with a 1:50 ratio of Proteinase K (Promega, Madison, WI, USA) to the initial dry mass of the scaffolds. The samples were agitated at 60°C and 800 RPM overnight, as well as an additional 15 minutes at 92°C to inactivate the enzyme. Next, the samples were lysed using sonication (6 pulses, 1 second each) and then frozen at -20°C until the assay was performed. The samples were analyzed according to the manufacturer's instructions. Finally, the measured DNA mass was normalized to the initial dry weight of the scaffolds and the average dsDNA content of unseeded scaffold controls was subtracted to account for any background (n = 3 scaffolds per group/trial, N = 3 trials with separate cell isolations).

2.7.2 Metabolic activity quantification

The 3-(4,5-dimethylthiazol-2-yl)-2,5-diphenyltetrazolium bromide (MTT; Life Technologies Inc., Burlington, ON) assay was used to measure the metabolic activity of a separate set of macrophage-, ASC-, and co-culture-seeded DAT bioscaffolds after 24 hours of seeding. A working MTT solution (0.5 mg/mL) was prepared in complete macrophage media. After seeding, the implants were rinsed three times in PBS (5 min each, 37°C, 40 RPM), and then incubated in 3 mL of the working MTT solution (4 hours, 37°C).

Each seeded bioscaffold was transferred into an Eppendorf tube containing 800 µL of dimethyl sulfoxide (DMSO), and then manually minced using surgical scissors. Next, the samples were incubated to extract the water-insoluble formazan product (1 hour, 37°C, 100 RPM) and then centrifuged (15000 x g, 5 min) to collect the supernatant. Finally, the supernatant was further diluted 1:8 in DMSO, and 200 µL of the diluted supernatant was pipetted into a 96-well plate in triplicate. Sample absorbance was measured at 540 nm and corrected for background absorbance at 690 nm using a CLARIOstar® High Performance Monochromator Multimode Microplate Reader (BMG Labtech, Guelph, ON). The measured absorbance was normalized to the dry weight of the scaffolds and the average absorbance of the unseeded scaffold controls was subtracted to account for any background (n = 3 scaffolds per group/trial, N = 3 trials with separate cell isolations).

2.8 *In vivo* assessment of the bioscaffolds

All *in vivo* implantation studies were performed using 9-12 week old male C57BL/6 mice. Surgeries were performed under sterile conditions and using sterile surgical tools. Mice were anesthetized with 1.5% isoflurane in oxygen at 1 L/min throughout the entire surgical procedure, and given pre-operative analgesic doses of meloxicam (2 mg/kg loading dose; 1 mg/kg follow up dose 24 hours post-surgery) and bupivacaine (2 mg/kg) via subcutaneous injection. Each mouse received two small incisions near the upper thigh in the inguinal region to allow for two subcutaneous pockets to be created using blunt-ended forceps. Mice received a total of 2 subcutaneous DAT implants (one on each side in the inguinal region) from the following groups:

(i) unseeded controls
(ii) macrophage-seeded

(iii) ASC-seeded
(iv) 1:1 co-culture

After implantation, the incisions were closed using Monocryl 6-0 absorbable sutures and the mice were closely monitored. At 2 and 4 weeks post-surgery, mice (N = 4-6 mice/treatment group) were euthanized using CO_2 overdose and the scaffolds were excised within their surrounding tissues. The excised scaffolds were processed for paraffin embedding for histological and immunohistochemical analyses.

2.9 Masson's trichrome staining and quantification

Paraffin-embedded samples were sectioned (5 µm) and subjected to deparaffinization in xylene, and then rehydration in an ethanol series. After Masson's trichrome staining, the samples were dehydrated in an ethanol series followed by xylene, and then mounted with Permount® mounting medium (Fisher Scientific, Ottawa, ON). The entire cross-section of each sample was imaged using an EVOS XL CORE light microscope (Life Technologies) under the 10x objective using tissue sections from 3 different depths/implant, spaced 200 µm apart. For analysis, the images were subsequently stitched together using Image Composite Editor (Microsoft) software. In order to generate Masson's trichrome figures for a selected subset of samples, slides were scanned at 20X magnification using an Aperio ImageScope system and software (Vista, CA).

For all implant groups, the ratio of the area infiltrated by cells to the total implant area, the ratio of the number erythrocyte-containing blood vessels to total implant area, and the ratio of remodeled fat within the implant to total implant area, was measured using ImageJ software in order to analyze the percentage of cellular infiltration, blood vessel density, and implant remodeling into fat, respectively. In order to assess angiogenesis, the number, diameter, and distance from the implant periphery of all blood vessels were counted across the entire implant region. All semi-quantitative analyses were conducted in a blinded fashion (n = 3 different depths 200 µm apart/implant (1 section/depth), N = 4 - 6 mice per group).

2.10 Immunofluorescence assessment of angiogenic and macrophage markers

All immunohistochemical staining was performed on 5 µm sections derived from 3 different depths within each implant (200 µm apart). The tissue sections were deparaffinized using xylene and rehydrated in an ethanol series as described above. Unless otherwise stated, all incubation steps were performed at room temperature.

2.10.1 Detection of CD31$^+$ cells

In order to visualize CD31$^+$ endothelial cell recruitment, tissue sections were subjected to heat-mediated antigen retrieval in DAKO target antigen retrieval citrate solution (pH 6.0) (Agilent, Mississauga, ON) at 95°C for 20 min, followed by a 15 min cooling period. Next, the tissue sections were blocked using 10% goat serum + 0.1% Tween-20 in Tris-buffered saline (TBS) for 1 hour at room temperature. Finally, the sections were incubated overnight at 4°C with a rabbit polyclonal anti-CD31 primary antibody (1:100 in TBS + 5% goat serum + 0.1% Tween-20; Abcam, ab28364).

On the following day, the tissue sections were rinsed in TBS and then incubated with a Hoechst counterstain and Dylight®650 conjugated goat anti-rabbit IgG secondary antibody (1:200 in TBS + 5% goat serum + 0.1% Tween-20; Abcam, ab96902) for 1 hour. Sections were rinsed again in TBS and mounted using Fluoroshield^{TM} mounting medium (Abcam, Toronto, ON). Using the 20X objective of an EVOS® FL fluorescence imaging system (Life Technologies), 8-9 non-overlapping images were taken within 600 µm of the implant periphery and automated quantitative analysis of positively stained pixels was performed using ImageJ software. The average counts from images taken along the implant periphery were recorded for each section (n = 3 different depths/implant, 200 µm apart (1 section/depth), N = 4 - 6 mice per group).

2.10.2 Immunofluorescence assessment of infiltrating macrophages

In order to assess the distribution and phenotype of the macrophage populations infiltrating the implants, immunohistochemical staining was performed to triple stain for CD68 as a marker of phagocytic macrophages, arginase-1 (Arg-1) as a marker of a more pro-regenerative M2-like phenotype, and inducible nitric oxide synthase (iNOS) as a marker of a more pro-inflammatory

M1-like phenotype. Sections were subjected to heat-mediated antigen retrieval in 10 mM Tris base, 1 mM EDTA solution, 0.05% Tween 20 (Tris-EDTA solution; pH 9.0) for 25 min at 95°C, followed by a 15 min cooling period. Tissue sections were blocked for one hour using 5% BSA+ 0.1% Tween-20 in PBS, and then incubated overnight at 4°C with the following primary antibodies: rat monoclonal anti-CD68 (1:75; BIO-RAD, MCA1957T), rabbit polyclonal anti-iNOS (1:75; Abcam, ab15323), and chicken polyclonal anti-Arg-1 (1:100; Millipore Sigma, ABS535) diluted in PBS + 1% BSA + 0.1% Tween-20.

On the following day, the tissue sections were rinsed in PBS, and blocked for one hour with 10% goat serum + 0.1% Tween-20 in PBS. Next the sections were incubated with a Hoechst counterstain and the following secondary antibodies for one hour: Alexa Fluor®488 conjugated goat anti-rat IgG (1:100; Invitrogen, A-11006), Alexa Fluor®594 conjugated goat anti-rabbit IgG (1:200; Abcam, ab150080), and Alexa Fluor®680 conjugated goat anti-chicken IgG (1:200; Abcam, ab175779), diluted in PBS + 1% goat serum + 0.1% Tween-20. Sections were rinsed in PBS and mounted using Fluoroshield^{TM} mounting medium (Abcam, Toronto, ON). Using the 20X objective of an EVOS® FL fluorescence imaging system (Life Technologies), 8-9 non-overlapping images were taken within 600 µm of the implant periphery (n = 3 different depths/implant, 200 µm apart (1 section/depth), N = 4 - 6 mice per group).

2.11 Statistical analyses

All numerical data presented were expressed as the mean ± standard deviation (SD) and analyzed using GraphPadPrism 6.0 software (GraphPad Software, San Diego, CA) by one-way or two-way ANOVA with a Tukey’s post-hoc comparison. Differences were considered statistically significant when $p<0.05$.

Chapter 3

3 Results

3.1 Murine cell isolation and culture

As previously mentioned, the methods for the harvesting of murine adipose-derived stromal cells (ASCs) from the inguinal fat pads of dsRed$^+$ mice had been previously developed[251]. After harvesting, the P_0 cells were plated onto Primaria^{TM} flasks to aid in attachment. ASCs were fed every 2-3 days, and after 4-5 days in culture, cells were passaged onto tissue culture treated polystyrene T75 flasks. Each T75 flask yielded between 1 million-1.5 million cells. When growing, the cells showed an elongated, fibroblastic morphology, with multiple spindly-like protrusions (Figure 3.1). After $P_{3 \text{ or } 4}$, the ASCs would proliferate slower, and would adopt a rounded, flattened shape lacking any extensions. When ASCs adopted this morphology, they were unable to be used in experiments as they would lift off the surface of the flask.

While the ASCs could be passaged, the macrophages had to be differentiated from progenitor cell populations. Frozen bone marrow-derived cells were banked due to the abundance of cells harvested and used in future studies. During the differentiation process, the macrophages were less hardy than the ASCs and required new media every other day to maximize overall yield. By day 7, the differentiated cell population would form clusters of cells that had few protrusions as compared to the ASCs and were observed to be either elongated or more rounded (Figure 3.1). In general, the differentiated bone marrow-derived cells were limited by the number of times they could be used. Once they lifted off the T75, they could no longer be passaged.

It is important to note that both ASC and macrophage yield was cell donor dependent, with some batches growing faster or yielding more cells than others. On average, the macrophage yields would be around 3 million – 4 million cells/flask.

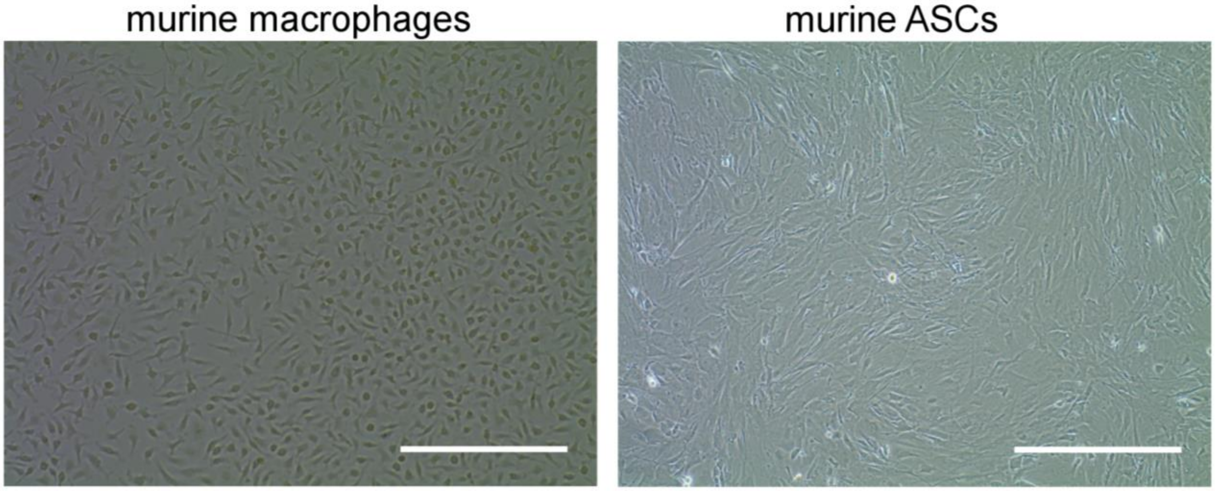

Figure 3.1. Morphology of differentiated murine bone marrow-derived macrophages from MacGreen mice and murine ASCs derived from the inguinal fat pad of dsRed mice. Bright field microscopic images revealed that the differentiated macrophage population (left) were either elongated or rounded with few protrusions, while the cultured ASCs (right) had a fibroblast-like, elongated morphology with multiple protrusions when seeded onto a T75 flask. Scale bar: 500 µm.

3.2 Macrophage characterization

3.2.1 Cell surface marker expression

The immunophenotype of the bone marrow-derived macrophages cultured on tissue culture polystyrene (TCPS) for seven days was assessed by flow cytometry, with the results summarized in Table 3.1 (N=3 biological replicates). Representative flow plots are shown in Figure 3.2. Analysis of the viable cell population demonstrated that the majority of the cells expressed the hematopoietic marker CD45 (94.3% ± 5.3). Moreover, the majority of the $CD45^+$ cell population co-expressed CD11b (99.7% ± 0.3), commonly used as a macrophage marker[162]. Further, the majority of the $CD45^+CD11b^+$ cells co-expressed the pan-macrophage marker, F4/80 (95.9% ± 2.6), while the co-expression of the neutrophil marker Ly6G was negligible (2% ± 2.6). It was also found that only a small fraction of the $CD45^+CD11b^+F4/80^+$ $Ly6G^-$ subset expressed the monocyte/macrophage marker, Ly6C (5.1% ± 2.4). Additional analyses of the $Ly6C^-$ and $Ly6C^+$ cell populations showed subpopulations with varying levels of GFP expression, indicating there was variability in *csf1r* expression within the population.

Table 3.1. Immunophenotype of the cultured murine bone marrow-derived macrophages isolated from the MacGreen mice. Flow cytometric analysis of cell surface marker expression confirmed that the majority of the cultured bone marrow-derived cells were CD45^{+} CD11b $^{+}$F4/80^{+} Ly6G^{-} macrophages. Data represented as mean percentage ± standard deviation displayed from N = 3 separate experiments.

Viability	Viable cells	89.1 ± 3.1%
Myeloid/Macrophage Markers	CD45^{+} (out of total viable cells)	94.3 ± 5.3%
	CD45^{+} CD11b^{+}	99.7 ± 0.3%
	CD45^{+} CD11b^{+} F4/80^{+} Ly6G^{-}	95.9 ± 2.6%
Monocytic/Macrophage Marker	CD45^{+} CD11b^{+} F4/80^{+} Ly6G^{-} Ly6C^{+}	5.1 ± 2.4%
GFP	CD45^{+} CD11b^{+} F4/80^{+} Ly6G^{-} Ly6C^{-} GFP^{+}	69.1 ± 9.5%
	CD45^{+} CD11b^{+} F4/80^{+} Ly6G^{-} Ly6C^{+} GFP^{+}	60.5 ± 10.2%

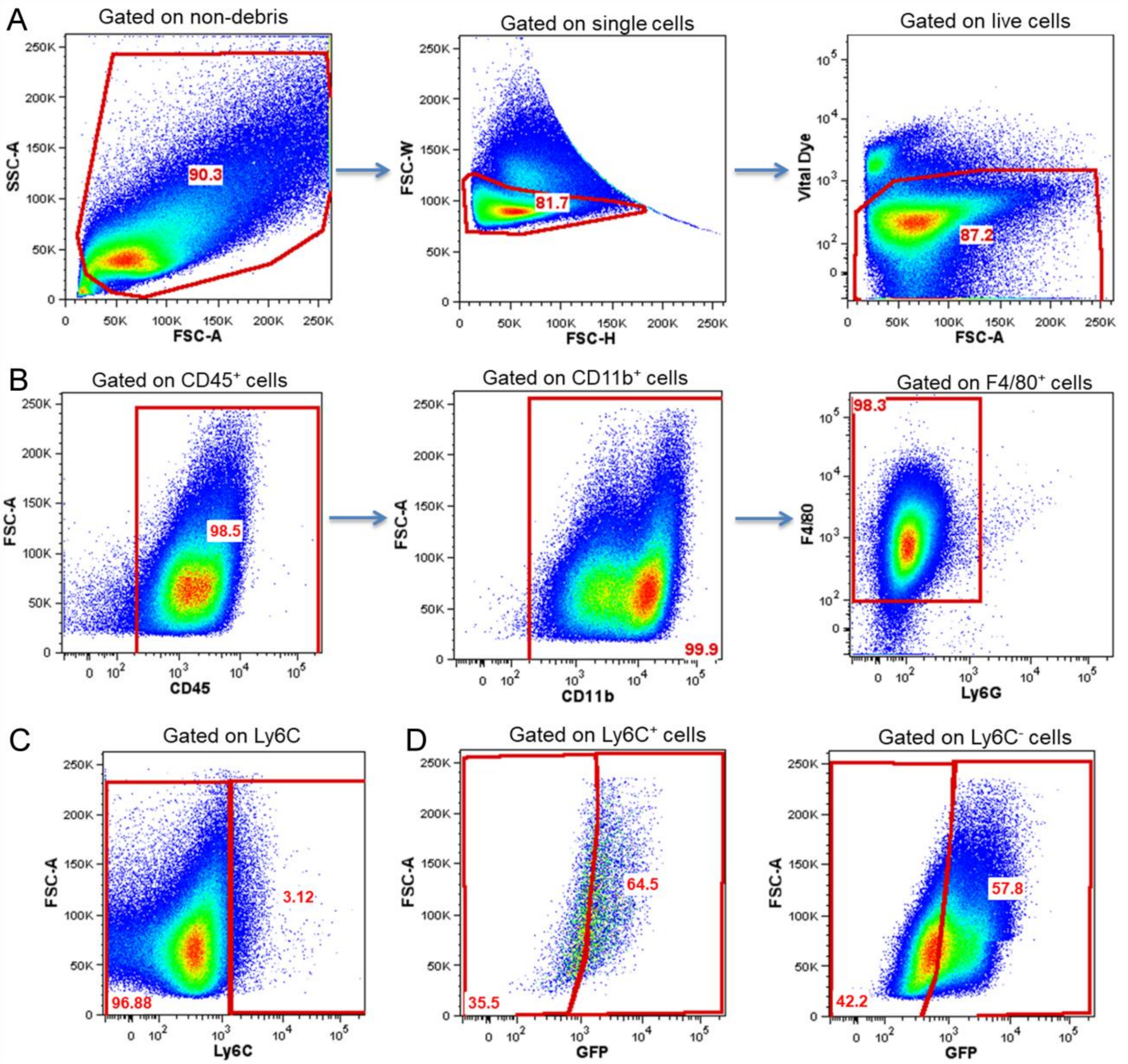

Figure 3.2. Cultured bone marrow-derived macrophages express characteristic macrophage markers. Representative dot plots from one biological replicate demonstrating the gating strategy used to analyze the cultured cells. (A) Cells were gated based on their forward scatter (FSC) and side scatter (SSC) distribution, followed by FSC singlets, and the live cell population (87.2% viable). (B) A large fraction of the CD45$^+$ CD11b$^+$ live cell population was demonstrated to be CD45$^+$ CD11b$^+$ F4/80$^+$ Ly6G$^-$ macrophages (98.3%). There were further subpopulations of CD45$^+$CD11b$^+$ F4/80$^+$ Ly6G$^-$ cells that showed heterogeneous expression of (C) Ly6C (3.09% positive) and (D) GFP (64.5% positive).

3.3 *In vitro* analysis of cell-seeded decellularized adipose tissue bioscaffolds

3.3.1 Assessment of cell distribution

The distribution of macrophages and/or ASCs within the decellularized adipose tissue (DAT) bioscaffolds was qualitatively assessed following dynamic seeding for 24 hours on a 3-D rocker through DAPI nuclear staining of sectioned samples. Non-overlapping images were taken within the implant periphery (<600 µm within the apical and basal borders) and interior (> 600 µm away from the apical and basal borders). The analysis supported that the DAT could be used as a delivery platform for both cell types and showed that there was a heterogeneous distribution of cells throughout the scaffolds (Figure 3.3). In general, a qualitatively higher density of cells was observed within the peripheral regions of the scaffolds in all groups. Although cellular infiltration was observed in the interior of some samples, this was typically limited to regions where the extracellular matrix (ECM) was qualitatively less dense.

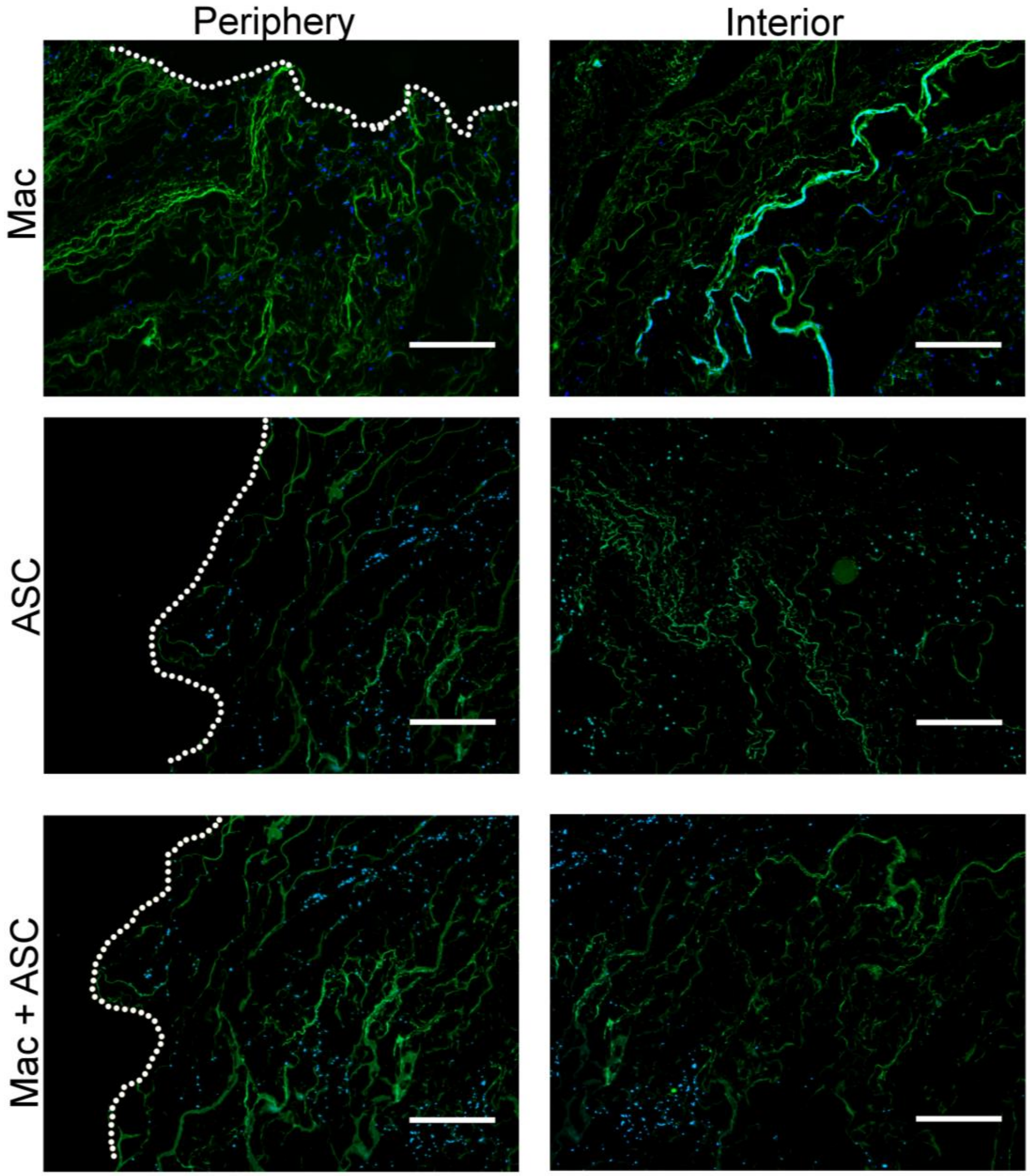

Figure 3.3. Seeded macrophages and ASCs were heterogeneously distributed within the DAT bioscaffolds after 24 hours in dynamic culture. Representative images show the distribution of seeded macrophages and/or ASCs in the peripheral and interior regions of the DAT bioscaffolds. Qualitatively higher cell densities were observed in the scaffold periphery for all seeding conditions (left panels), with limited infiltration observed in the interior regions (right panels). Dotted line: scaffold boundary. Blue: nuclei, green: scaffold autofluorescence. Scale bar: 500 µm. n = 3 technical replicates/group, N = 2 separate cell isolations.

To complement the qualitative assessment of the cellular distribution within the DAT scaffolds, the total double stranded (dsDNA) content was measured in separate sets of samples at 24 h post-seeding using the PicoGreen® assay (Figure 3.4A). Further, in order to probe cellular viability, the metabolic activity was also examined in the various conditions using the MTT assay (Figure 3.4B). In general, there was variability between the biological replicates, particularly in terms of metabolic activity, which resulted in no significant differences between any of the groups. Taken together, the data suggests that while there was variability attributed to different batches of starting cell populations, the total cell density within the DAT scaffolds was similar in the macrophage-seeded, ASC-seeded, and co-culture seeded groups within each trial.

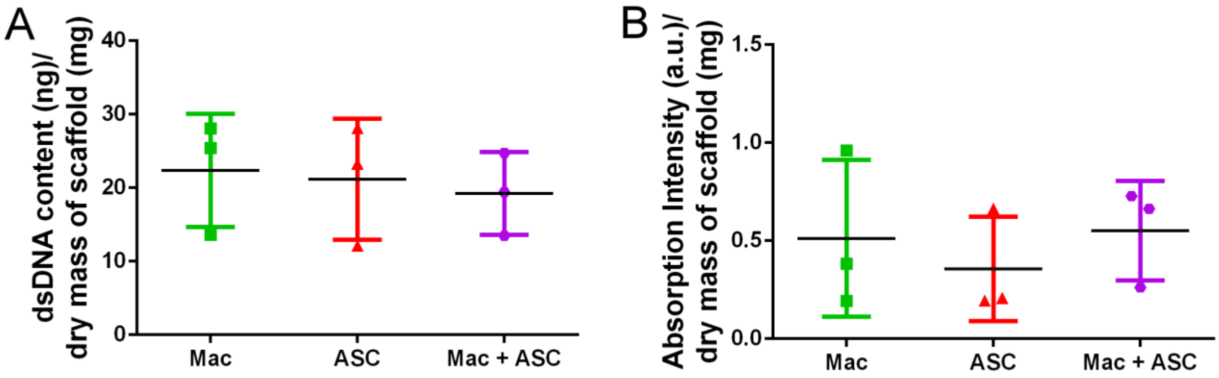

Figure 3.4. Assessment of dsDNA content and metabolic activity in the macrophage-seeded, ASC-seeded and co-culture-seeded DAT scaffolds after 24 hours in dynamic culture. The (A) dsDNA content measured with the PicoGreen Assay and (B) absorption intensity measured with the MTT assay, normalized to the bioscaffold dry weight (mg) to account for minor differences in the size of each individual bioscaffold. No significant differences were observed between the groups for either assay. Data represents mean ± SD. n = 3 technical replicates/group, N = 3 separate cell isolations.

3.4 *In vivo* analysis of the DAT bioscaffolds

3.4.1 Macroscopic evaluation of implants

Macrophage-seeded, ASC-seeded, co-culture-seeded, and unseeded DAT bioscaffolds were subcutaneously implanted within the inguinal region of wild-type C57BL/6J mice. At 1 week post-surgery, the surgical incision sites were fully healed. Cohorts of mice were euthanized at 2 and 4 weeks post-surgery, and the implants were excised within their surrounding tissues. Based on macroscopic evaluation, all implants were found to be well integrated within the inguinal fat pad and/or skin (Figure 3.5). In some mice, visible blood vessels were observed near (Figure 3.5A) or surrounding the implant (Figure 3.5B).

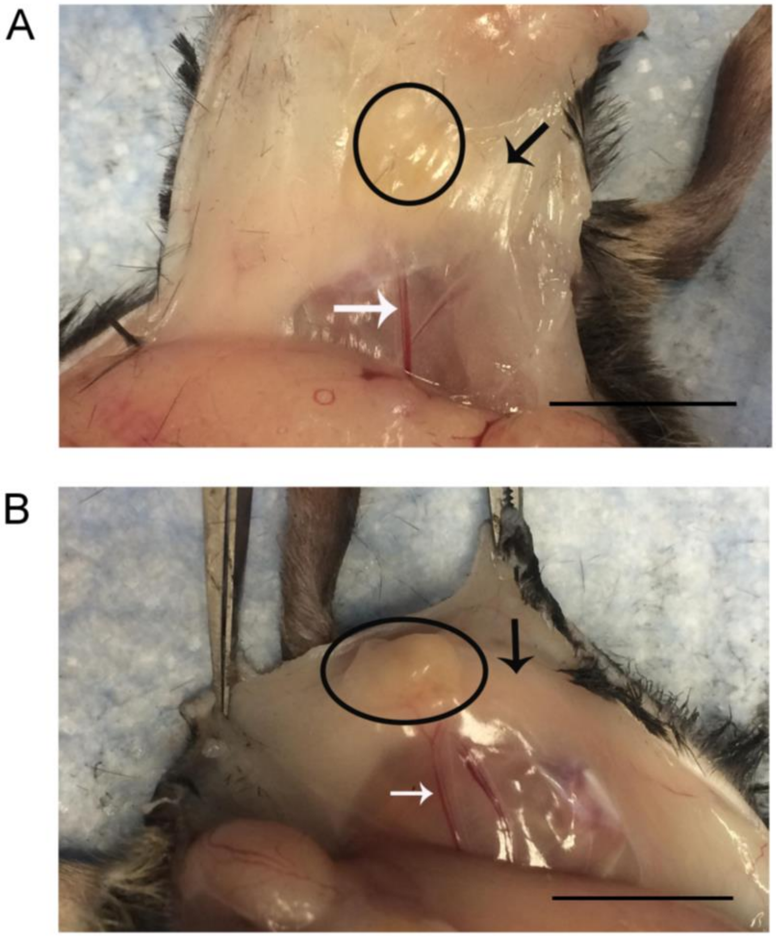

Figure 3.5. Macroscopic evaluation of the DAT implants. Each mouse received two implants, each one from a different seeding condition, inserted in subcutaneous pockets made in the inguinal region of the mouse. Depicted are representative images of (A) unseeded and (B) co-culture seeded implants after 4 weeks *in vivo*. The basal surface of the excised implant (black circle) was situated adjacent to the inguinal fat pad (black arrow). In some mice, blood vessels (white arrow) were observed in close proximity to the fat pad or the implant. Scale bars: 1 cm.

3.4.2 Qualitative assessment of cellular infiltration, angiogenesis, and remodeling of the DAT implants

The Masson’s trichrome staining revealed the presence of a fibrous capsule surrounding the implants in all groups at both time points, located adjacent to the mouse skin and/or inguinal fat pad (Figures 3.6 and 3.7). The fibrous capsule contained cells, and in some instances, erythrocyte-containing blood vessels and adipocytes. Notably, the thickness of the fibrous capsule was more variable in the implants that had direct contact with the inguinal fat pad. More specifically, the fibrous capsule appeared thinner in areas adjacent to the fat pad and integrated well with the fat pad septa, which are the collagen bundles that separate adipocytes into lobules. The regions of the fibrous capsule not in contact with a fat pad, such as the areas in contact with the skin, typically appeared thicker.

At both time points, adipocytes and erythrocyte-containing blood vessels were found to be localized within the boundary of the fibrous capsule, as well as along the peripheral regions of the implants (Figures 3.6 and 3.7).

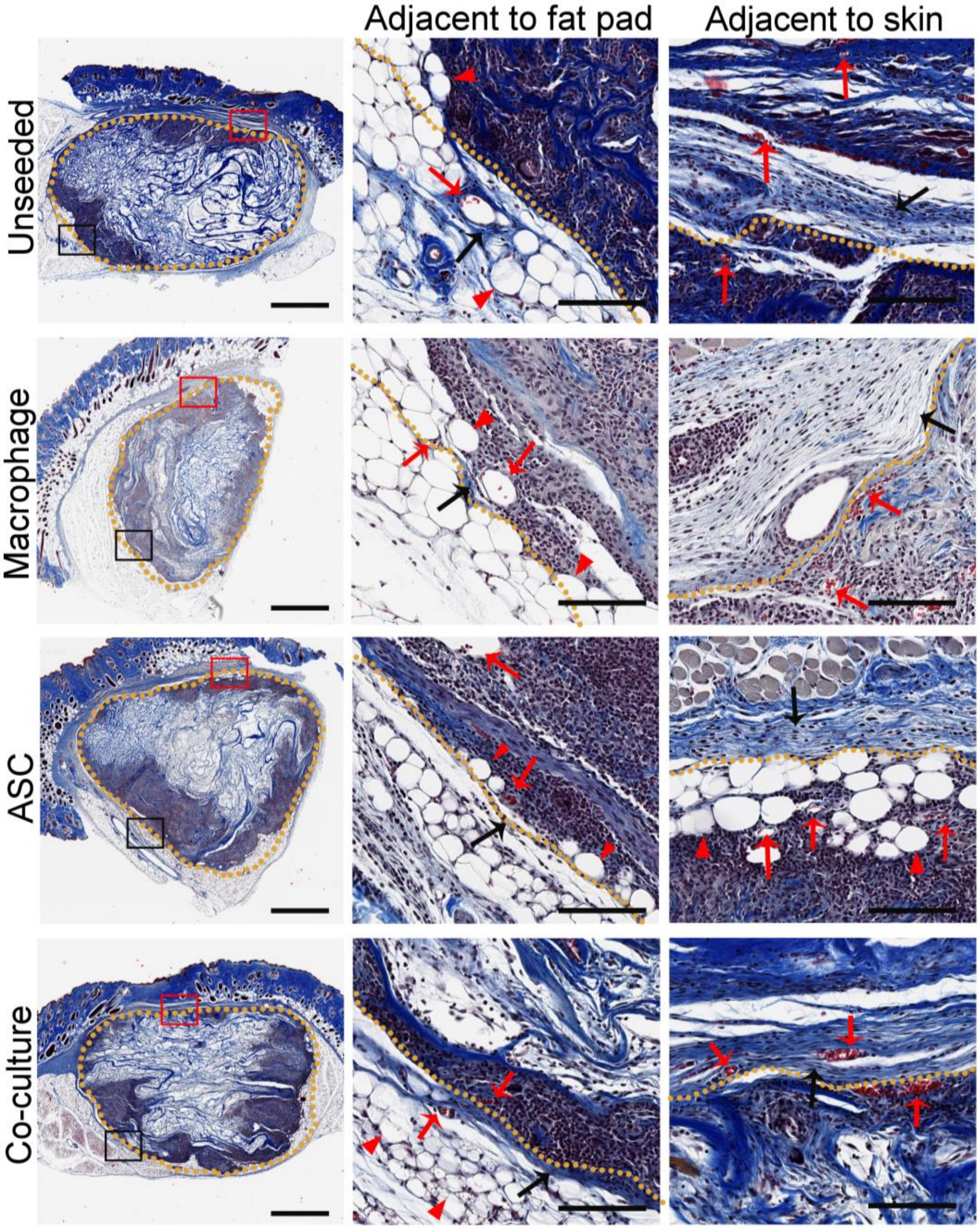

Figure 3.6. **Adipocytes and blood vessels were localized to the peripheral regions of DAT implant groups at 2 weeks post-implantation in C57BL/6J mice.** Representative images from all seeding conditions containing a partial infiltration response after 2 weeks *in vivo* are shown in the left panel. Areas from each group in direct contact with fat pads are boxed in black and magnified in the middle panel, while areas closest to the skin are boxed in red and magnified on the right panel. Dotted line: scaffold periphery; red arrows: erythrocyte-filled blood vessels; red arrow heads: adipocytes; black arrows: fibrous capsule. Left panel scale: 1 mm, middle and right panel scale: 100 µm.

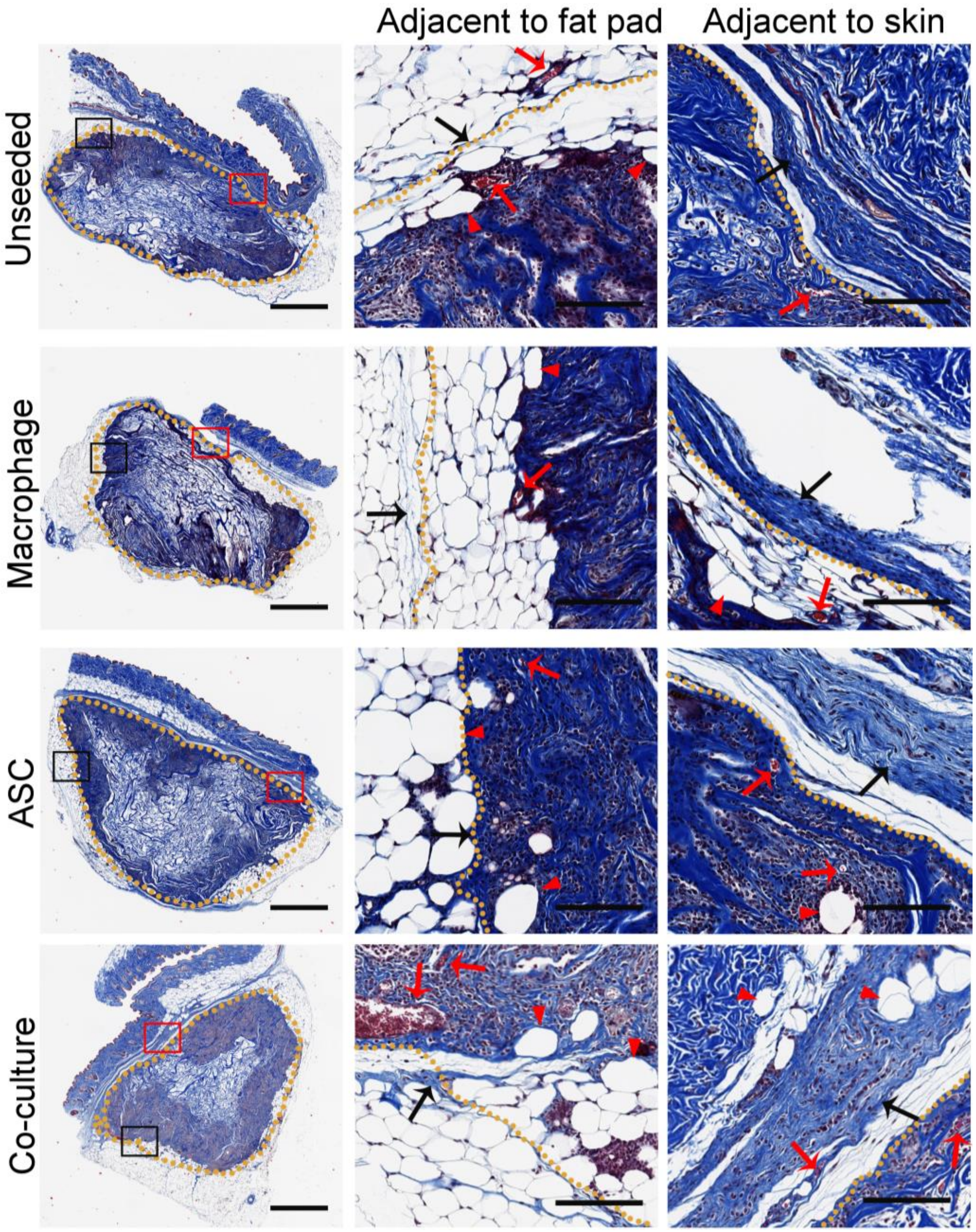

Figure 3.7. Adipocytes and blood vessels were localized to the peripheral regions of DAT implant groups at 4 weeks post-implantation in C57BL/6J mice. Representative images from all seeding conditions containing a mid-to-high infiltration response after 4 weeks *in vivo* are shown in the left panel. Areas from each group in direct contact with fat pads are boxed in black and magnified in the middle panel, while areas closest to the skin are boxed in red and magnified on the right panel. Dotted line: scaffold periphery; red arrows: erythrocyte-filled blood vessels; red arrow heads: adipocytes; black arrows: fibrous capsule. Left panel scale: 1 mm, middle and right panel scale: 100 µm.

Further qualitative analyses of the Masson's trichrome stained cross-sections revealed that the cellular infiltration varied substantially between the implants at both time points, even when comparing samples from the same scaffold group. The seeding conditions included samples that showed (i) low, (ii) low-to-mid, (iii) mid-to-high, or (iv) complete cellular infiltration across the implant cross-sections (Figure 3.8). In general, implants with low levels of infiltration (<10% infiltrated) contained areas with low cell density, which were predominantly localized to the implant periphery. Implants with a low-to-mid profile (10-50% infiltrated) remained largely un-infiltrated but contained areas of higher cell density that were localized to one or more sides of the implant. Mid-to-high infiltrated implants (50-95% infiltrated) showed a dense, infiltrating cell population usually distributed along one or more sides of the implant, while completely infiltrated implants showed a dense infiltrating cell population across the entire implant cross-section (95-100% infiltrated).

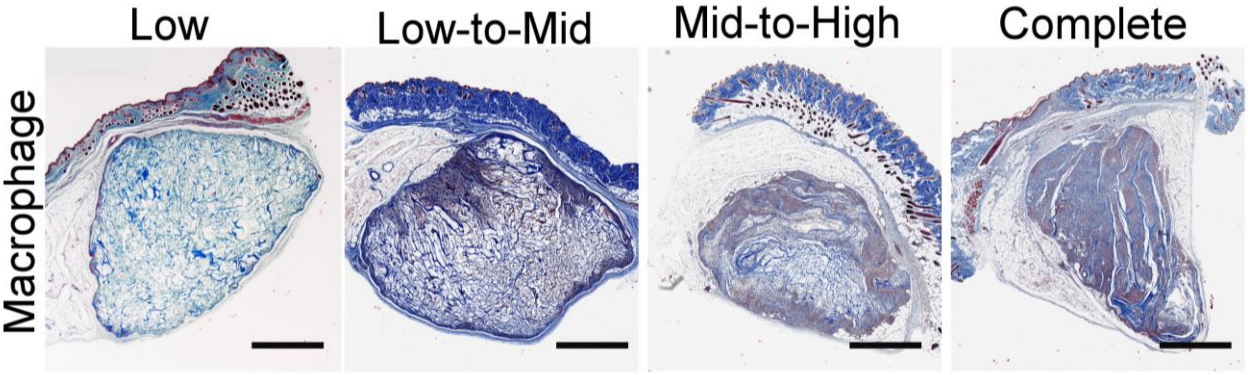

Figure 3.8. Implants within each seeding condition exhibited varying levels of cell infiltration at 2 and 4 weeks post-implantation in C57BL/6J mice. The selected images showing Masson's trichrome stained cross-sections from the macrophage-seeded implant group at 2 weeks post-surgery illustrate the variability in the *in vivo* cellular infiltration response between implants belonging to the same group. The levels of cellular infiltration ranged from low, low-to-mid, mid-to-high, or complete levels of cellular infiltration. Scale bars = 1 mm.

The levels of cellular infiltration in the scaffold cross-sections were scored in a blinded fashion, and each sample was assigned to one of the four previously defined categories. The results are shown in Table 3.2 and are reported as a percentage of the total number of cross-sections analyzed for each group. At 2 weeks, the unseeded group showed a smaller range and overall lower *in vivo* cell infiltration response as compared to the seeded groups, with no samples showing a mid-to-high or complete infiltration response. In contrast, a greater fraction of the macrophage, ASC, and co-culture seeded implants showed higher levels of cell infiltration across the cross-section, with a few of the macrophage and ASC implant cross-sections achieving complete infiltration. At 4 weeks, most of the unseeded implants continued to show relatively low levels of cell infiltration, although a mid-to-high level of infiltration was observed in one implant cross-section. In the seeded groups, substantial sample-to-sample variability in the infiltration levels remained at 4 weeks. Further, a higher fraction of the ASC-seeded and co-culture seeded scaffolds showed a mid-high infiltration response as compared to the unseeded and macrophage-seeded implants at both 2 and 4 weeks. The overall trends suggest that there was not a difference in the overall level of infiltration observed between the two time points investigated in this study for any of the implant groups.

Table 3.2. Histological scoring of the levels of cellular infiltration in the unseeded, macrophage, ASC, and co-culture seeded DAT implant cross-sections. The implant cross-sections from each seeding condition and time point were histologically evaluated and categorized based on their range of *in vivo* infiltration responses. This was displayed as the percentage of implant cross-sections from each seeding condition out of total stained cross-section belonging to each seeding condition. Low cell infiltration = < 10% cell infiltration, low-to-mid infiltration = 10-50%, mid-to-high infiltration = 50-95%, complete infiltration = 95-100%. n = 3 sections/implant, N = 4 – 6 implants/group.

	2 weeks				4 weeks			
	Low	Low-Mid	Mid-High	Complete	Low	Low-Mid	Mid-High	Complete
Unseeded	50%	50%	0%	0%	56%	28%	17%	0%
Macrophage	33%	17%	39%	11%	33%	53%	13%	0%
ASC	33%	0%	61%	6%	17%	33%	50%	0%
Co-culture	20%	13%	67%	0%	0%	56%	44%	0%

When comparing the samples at either time point that showed a low-to-mid cellular infiltration response, there were no obvious trends in terms of the patterns of infiltration, with infiltration observed on the ventral regions adjacent to the inguinal fat pad either alone, or in addition to infiltration observed on the dorsal side adjacent to the skin (Figure 3.9). Samples at both time points with a mid-to-high cellular infiltration response tended to have infiltration coming from areas adjacent to the inguinal fat pad as well as the skin.

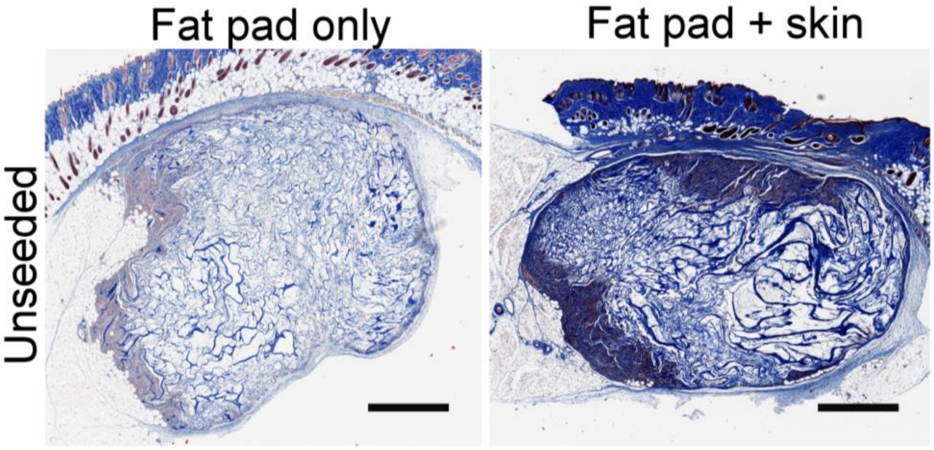

Figure 3.9. Infiltrating cell populations were distributed along areas adjacent to the inguinal fat pad either alone, or in addition to areas adjacent to the skin. The selected images showing Masson's trichrome stained cross-sections from unseeded implants excised after 2 weeks *in vivo* with a low-to-mid infiltration response illustrate the localization of infiltrating cell populations in regions adjacent to the fat pad only (left panel) or both the fat pad and skin (right panel). Scale bars = 1 mm.

Finally, it was found that the implants that contained higher levels of cellular infiltration were observed to have qualitatively higher levels of erythrocyte-containing blood vessels and adipocytes (Figure 3.10).

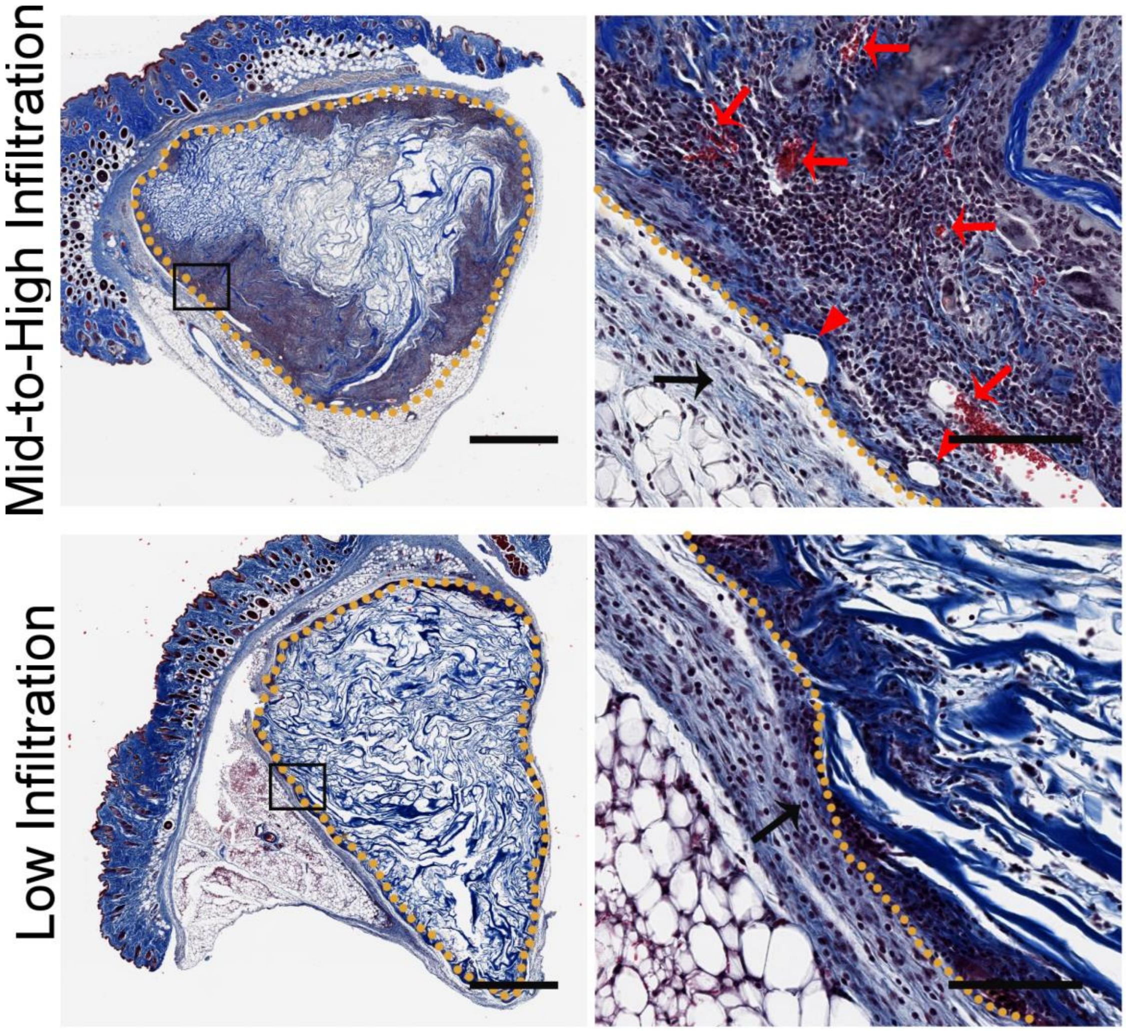

Figure 3.10. Higher levels of cellular infiltration within the implants showed higher levels of angiogenesis and adipogenesis. Representative images from ASC-seeded implants excised 2 weeks post-surgery are shown. Insets from the left panels are magnified in the right panels. Dotted line: scaffold periphery; red arrows: erythrocyte-filled blood vessels; red arrow heads: adipocytes; black arrows: fibrous capsule. Left panel scale: 1 mm, right panel scale: 100 µm.

3.4.3 Semi-quantitative analysis of cellular recruitment, blood vessel density, and adipose tissue remodeling

After two and four weeks, blinded semi-quantitative analyses of the degree of cell infiltration, blood vessel density, and adipose tissue remodeling in unseeded, macrophage-seeded, ASC-seeded, and co-culture-seeded implants was performed on the Masson’s trichrome stained sections. Consistent with the qualitative findings, there was substantial variability observed which led to no differences between the groups in terms of cell infiltration (Figure 3.11A), blood vessel density (Figure 3.11B), and adipose tissue remodeling (Figure 3.11C) responses at either time point. More specifically, at 2 weeks the macrophage-seeded, ASC-seeded, and co-culture-seeded implants exhibited a larger range of *in vivo* cell infiltration responses in comparison to the unseeded implants. Notably, a greater fraction of the cell-seeded implants exhibited higher levels of cell infiltration. In contrast to the response at 2 weeks, the unseeded implants at 4 weeks showed more variability in terms of the range of infiltration responses, with a greater fraction of the samples showing higher levels of overall infiltration. The other implant groups, however, showed less variability in the infiltration response at the later time point.

The average blood vessel density of all seeding conditions after 2 and 4 weeks post-implantation were listed in Table 3.3. In general, while there were low levels of angiogenesis and adipogenesis observed in all implant groups at both time points, the macrophage-, ASC-, and co-culture-seeded implants showed a greater range of blood vessel density responses at 2 weeks in comparison to the unseeded implants. Further, there was a trend towards a decrease in the variability of the blood vessel density responses in all implant groups at 4 weeks in contrast to the variability found in the neo-fat formation response, which increased.

Further analysis of the erythrocyte-containing blood vessels showed that the majority of blood vessels in all groups at both time points were small in diameter (<25 µm) and were localized within 200 µm of the implant periphery (Figure 3.12).

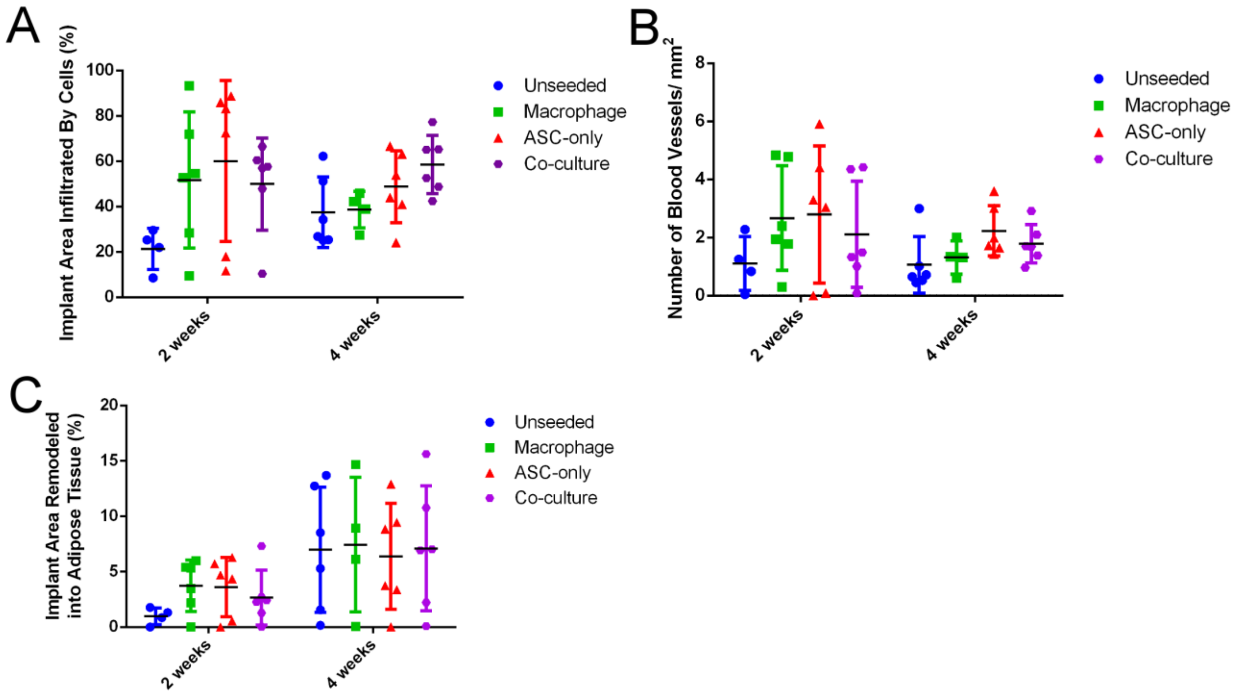

Figure 3.11. Quantification of *in vivo* cellular infiltration, blood vessel density, and adipose tissue remodeling within the DAT implants at 2 and 4 weeks. Within each group, variability was noted in the A) percentage of the DAT implants infiltrated by cells after 2 and 4 weeks *in vivo*. In general, all groups at both time points had B) a low density of erythrocyte-containing blood vessels and C) a low percentage of implant remodeling into fat. Values shown are mean ± SD. N = 4-6 mice per group.

Table 3.3. The average blood vessel density of all seeding conditions after 2 and 4 weeks was found to be relatively low. Since the range of blood vessel density responses varied, this led there to be no detectable differences between any of the groups at either time point.

Average blood vessel density (blood vessels/mm^2)		
	2 weeks	4 weeks
Unseeded	1.1 ± 0.9	0.7 ± 0.2
Macrophage-seeded	2.7 ± 1.8	1.3 ± 0.6
ASC-seeded	2.8 ± 2.4	2.1 ± 0.9
Co-culture seeded	2.1 ± 1.8	1.8 ± 0.7

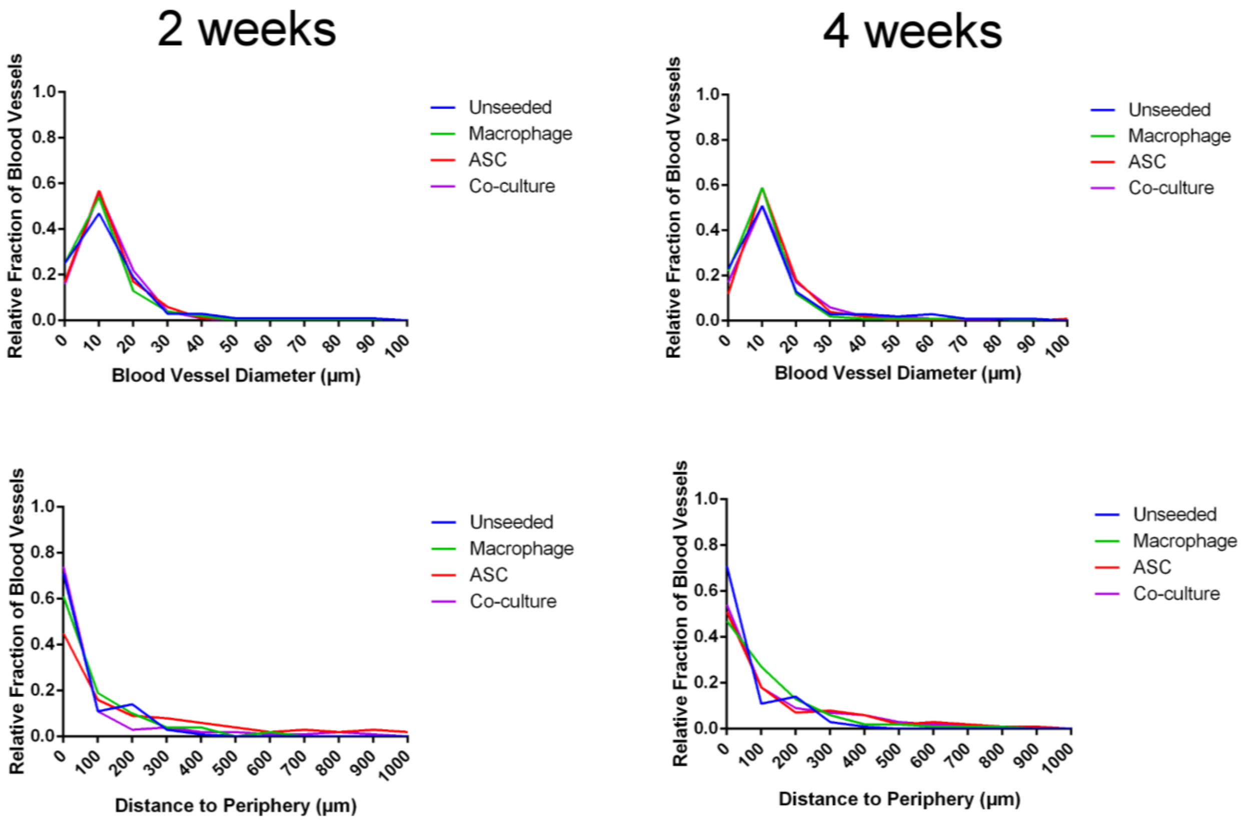

Figure 3.12. **Cell seeding did not influence the erythrocyte-containing blood vessel diameter or infiltration profiles within the DAT implants at 2 and 4 weeks.** Top frequency distribution plots show that the majority of the vessels within the implants were of small diameter (<25 µm) at both time points. Bottom frequency distribution plots showing that the majority of the erythrocyte-containing vessels were localized within 200 µm of the implant periphery in all of the groups at both time points. N = 4-6 mice/group.

3.5 Immunohistochemical analysis of CD31$^+$ cell recruitment

After 2 and 4 weeks, murine endothelial cell recruitment into the peripheral regions of the unseeded, macrophage-seeded, ASC-seeded, and co-culture-seeded implants was assessed through immunostaining for the endothelial marker, CD31. CD31, or platelet-endothelial cell adhesion molecule 1 (PECAM-1), is a transmembrane adhesion protein commonly found on endothelial cells, but can also be found on platelets, monocytes, macrophages, and granulocytes[255]. An assessment of the abundance of CD31 within 600 µm of the apical and basal borders of the implant was performed in all groups at both time points (N = 4-6 implants/group/time point). CD31$^+$ Hoechst$^+$ cells were observed in all conditions, and there were no notable differences in CD31$^+$ Hoechst$^+$ expression when comparing implants from different seeding conditions containing similar levels of cellular infiltration at both time points (Figure 3.13). However, implants with qualitatively higher levels of cellular infiltration tended to have qualitatively more CD31$^+$ Hoechst$^+$ cells visualized within the scaffold periphery (Figure 3.14).

Quantitative analysis of the CD31 staining was performed by automated positive pixel counting (Figure 3.15; n = 8-9 20X frames within 600 µm of the apical and basal borders from 3 depths per implant, 200 µm apart, N = 4-6 implants/treatment group/ time point). Similar to the histological analyses, there was substantial variability observed in the relative levels of CD31$^+$ expression at both time points, with no obvious differences between the groups.

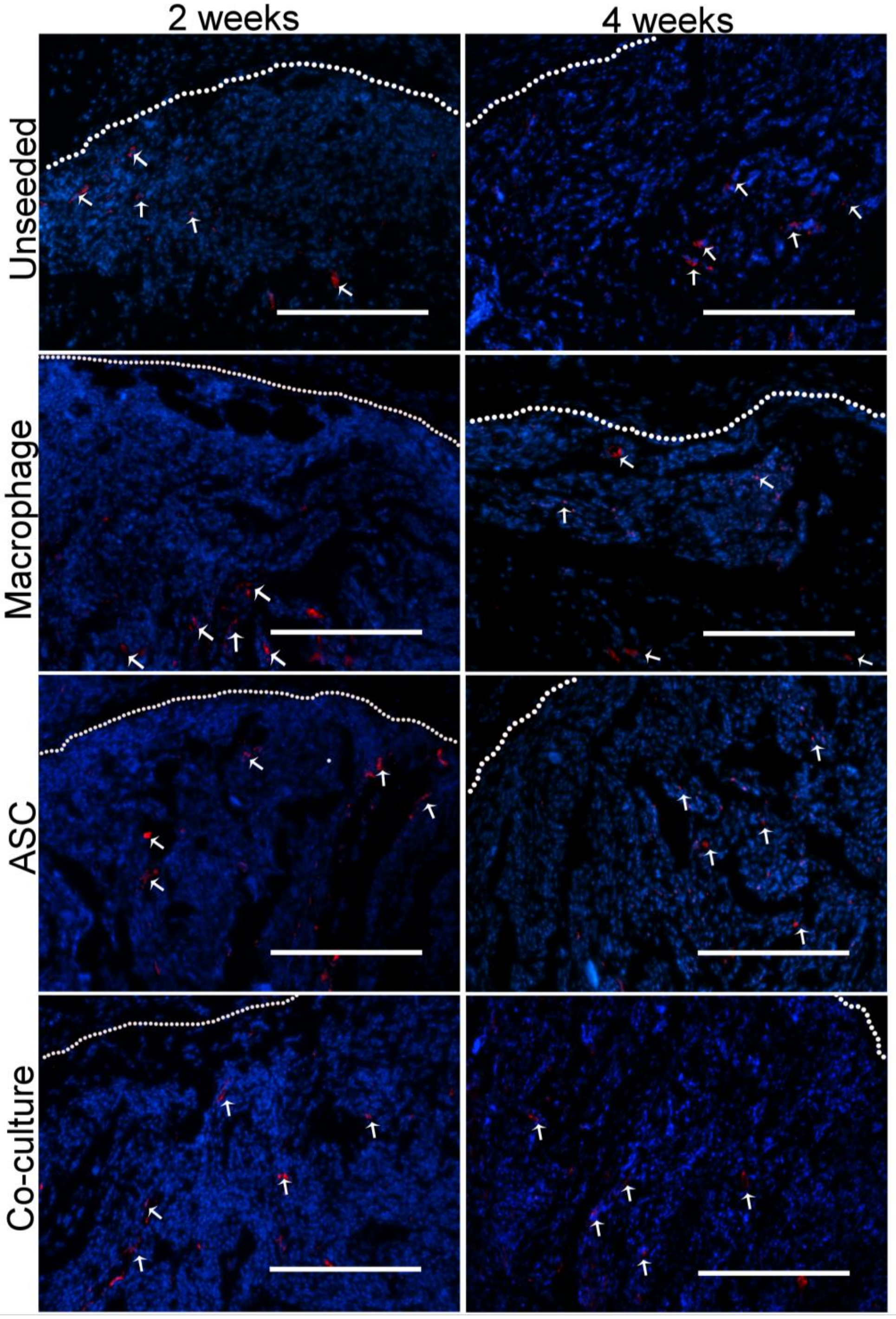
2 weeks
4 weeks
Unseeded
Macrophage
ASC
Co-culture

Figure 3.13. Representative images of CD31$^+$ cells within the implant periphery from all scaffold groups after 2 and 4 weeks *in vivo*. When the overall levels of cellular infiltration were similar, CD31$^+$ Hoechst$^+$ expression was found to be qualitatively comparable across all implant conditions at both 2 (left panel) and 4 weeks (right panel). Dotted line: scaffold periphery. White arrows: CD31$^+$ Hoechst$^+$ cells. Blue: cell nuclei, red: CD31. Scale bar: 200 µm.

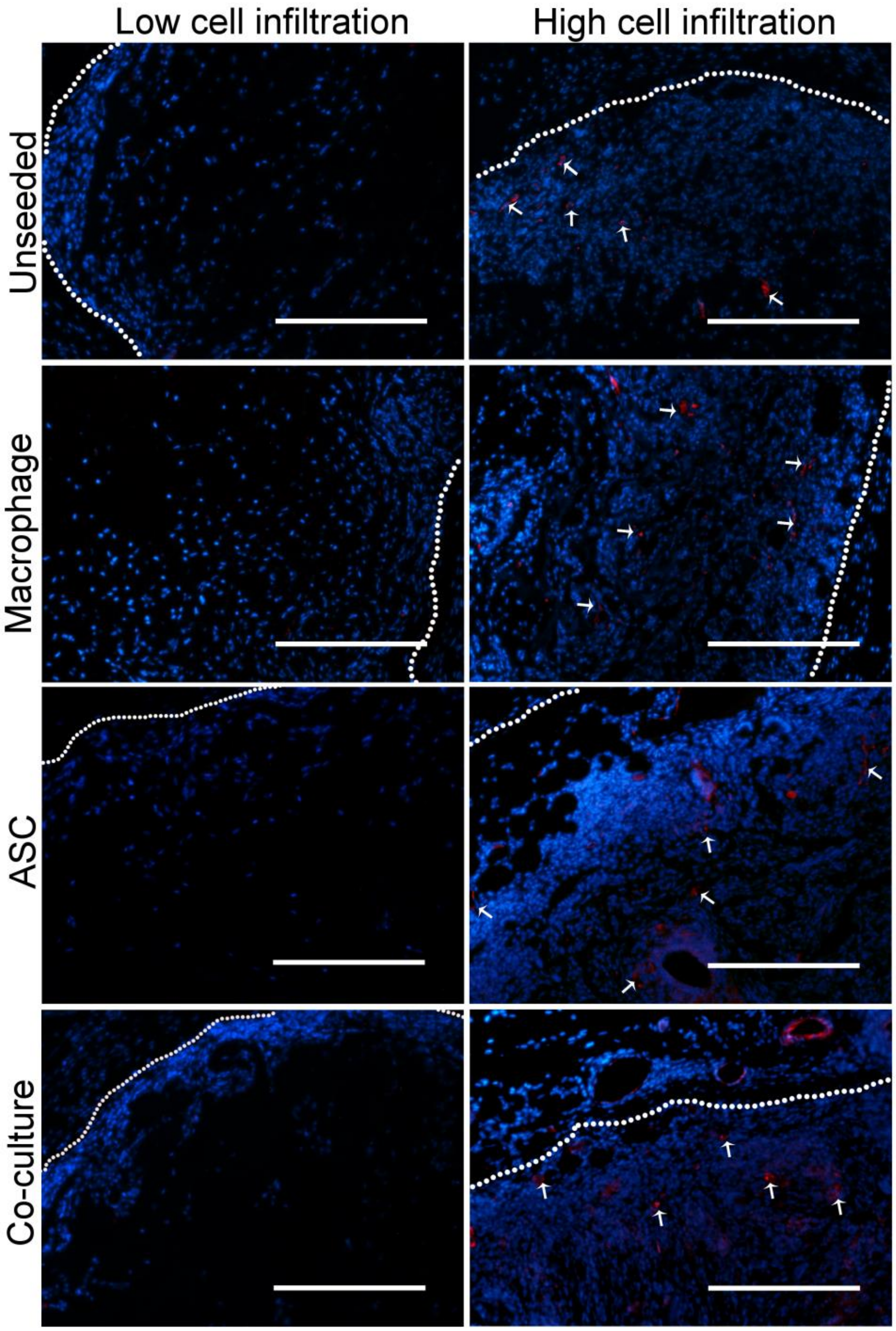
Low cell infiltration
High cell infiltration
Unseeded
Macrophage
ASC
Co-culture

Figure 3.14. Representative images of the different CD31 expression patterns found in implant groups containing different levels of cell infiltration after 2 weeks *in vivo*. Implants with higher levels of total cellular infiltration (right panel) showed qualitatively more CD31$^+$ Hoechst$^+$ cells than implants with low total cell infiltration (left panel). Dotted line: scaffold periphery. White arrows: CD31$^+$ Hoechst$^+$ cells. Blue: cell nuclei, red: CD31. Scale bar: 200 µm.

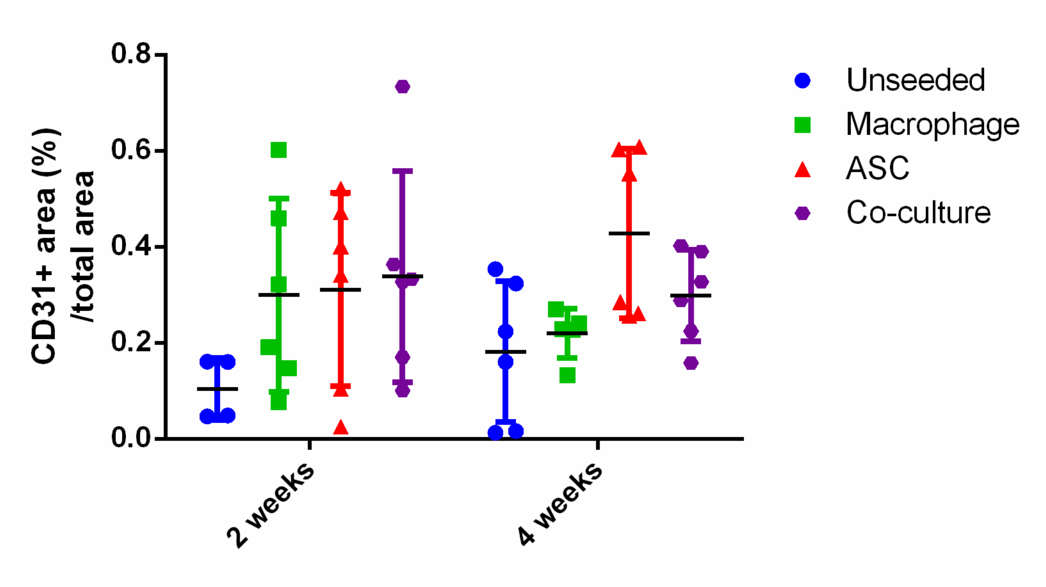

Figure 3.15. Quantification of relative CD31$^+$ expression within the DAT implants at 2 and 4 weeks. No significant differences were observed in the relative CD31$^+$ expression levels between the groups at either time point. Values shown are mean ± SD. 8-9 20X frames were imaged along the apical and basal borders from 3 different depths per implant, 200 µm apart, N = 4-6 implants/group.

3.6 Immunofluorescence analysis of infiltrating macrophage phenotypes

In order to probe the effects of delivering syngeneic macrophages and/or ASCs on host macrophage recruitment and the modulation of macrophage phenotype within the DAT implants, qualitative immunohistochemical analysis of the macrophage phenotype markers, inducible nitric oxide synthase (iNOS) and arginase-1 (Arg-1), were examined in combination with CD68, commonly used as a pan-macrophage marker associated with phagocytosis[256,257]. In general, a high density of cells expressing CD68 and Arg-1 was observed within 600 µm of the apical and basal borders of all implant groups at both time points (Figures 3.16 and 3.17, n = 8-9 20X frames from 3 depths/implant, 200 µm apart, N = 4-6 implants/group/time point). When comparing groups with similar overall levels of cellular infiltration, there were no obvious differences between implant groups at either time point (Figure 3.16 and 3.17). All groups showed a greater proportion of cells that expressed CD68 and Arg-1, with a lower proportion expressing iNOS. Merged images visualizing the co-localization of the three markers revealed an abundant CD68$^+$ Arg-1$^+$ iNOS$^-$ Hoechst$^+$ cell population and a smaller subpopulation of CD68$^+$ Arg-1$^+$ iNOS$^+$ Hoechst$^+$ (Figure 3.18). Some implants also contained subpopulations identified as CD68$^+$ Arg-1$^-$ iNOS$^-$ Hoechst$^+$ cells and CD68$^-$ Arg-1$^+$ iNOS$^-$ Hoechst$^+$ cells (Figure 3.19). Further analysis revealed that samples with higher levels of cellular infiltration qualitatively showed more iNOS$^+$ expression and a larger number of CD68$^+$ Arg-1$^+$ iNOS$^+$ Hoechst$^+$ cells as compared to implants with low cell infiltration (Figure 3.20).

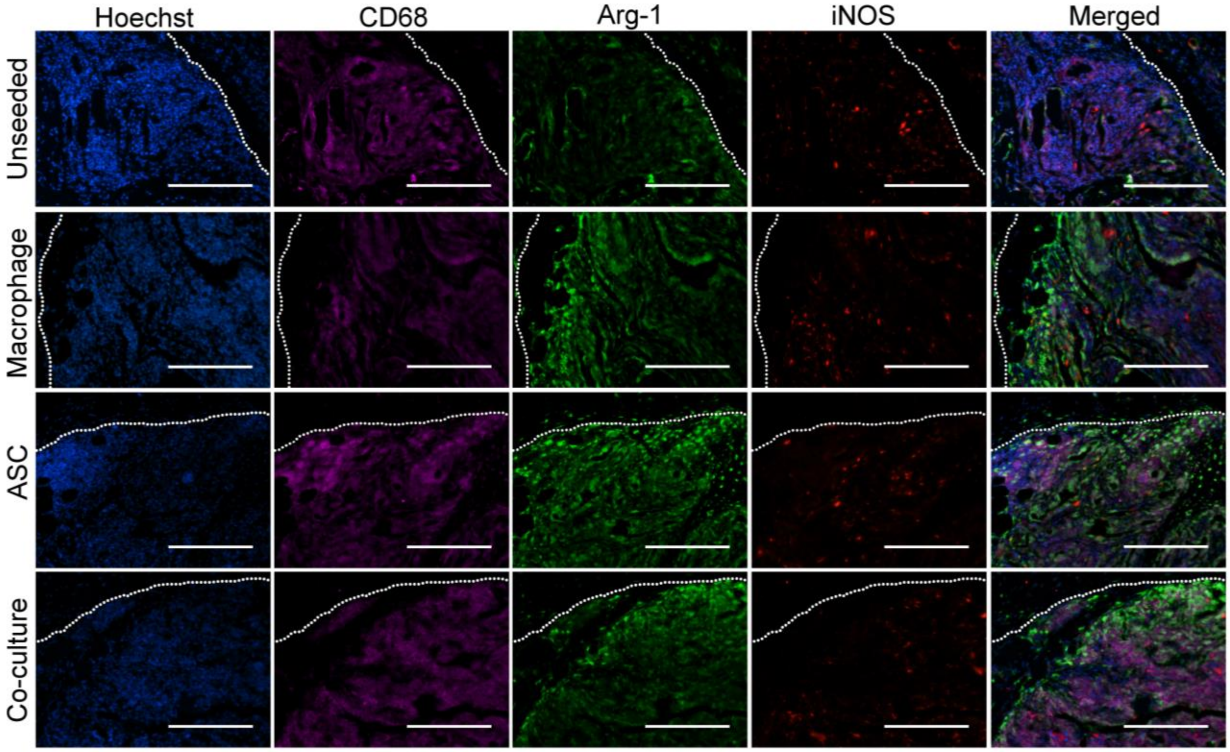
Hoechst
CD68
Arg-1
iNOS
Merged
Unseeded
Macrophage
ASC
Co-culture

Figure 3.16. Representative images of CD68, Arg-1, and iNOS, co-staining along the apical and basal borders from all seeding conditions after 2 weeks *in vivo*. When comparing implants with a mid-to-high cell infiltration response, the relative abundance of CD68$^+$ (second from the left panel), Arg-1$^+$ (middle), iNOS$^+$ (second from the right panel) cells was qualitatively similar across all implant conditions at 2 weeks. Dotted line: scaffold periphery. Blue: cell nuclei, purple: CD68, green: Arg-1, red: iNOS. Scale bar: 200 µm.

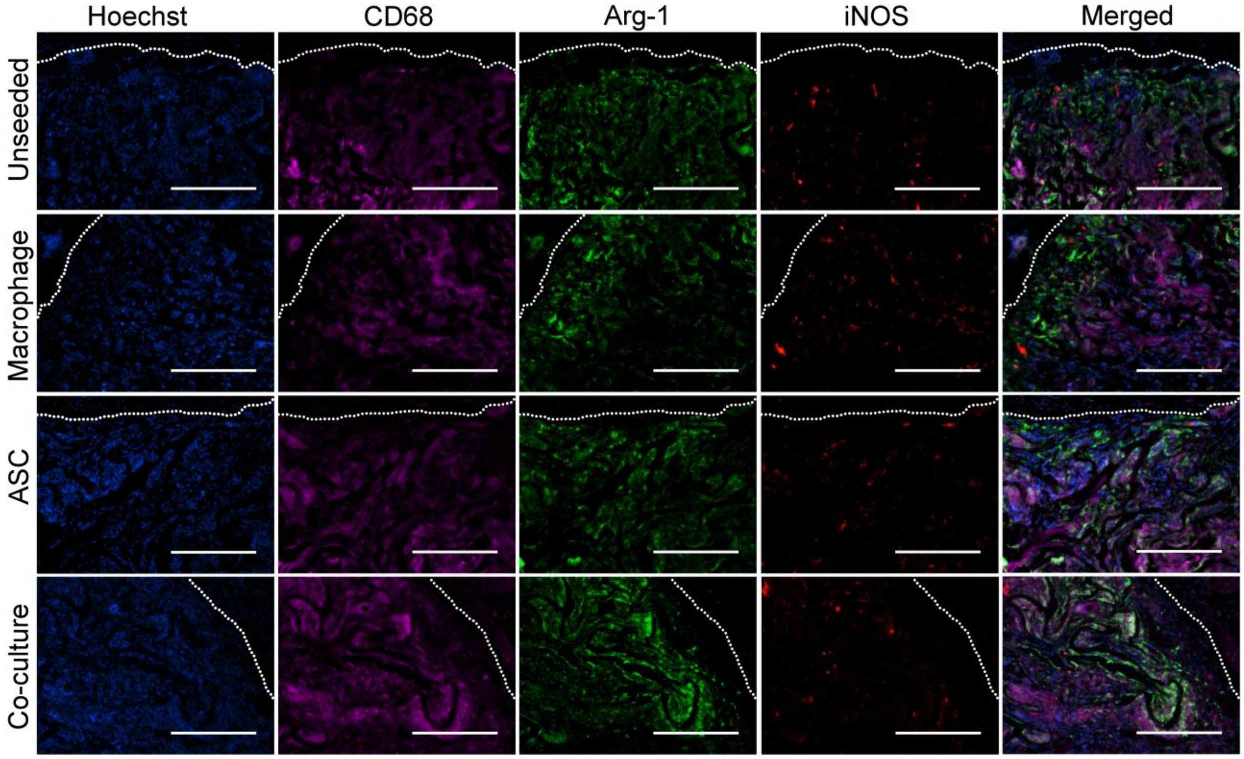
Hoechst
CD68
Arg-1
iNOS
Merged
Unseeded
Macrophage
ASC
Co-culture

Figure 3.17. Representative images of CD68, Arg-1, and iNOS co-staining along the apical and basal borders from all seeding conditions after 4 weeks *in vivo*. When comparing implants with a mid-to-high cell infiltration response, the relative abundance of CD68$^+$ (second from the left panel), Arg-1$^+$ (middle panel), iNOS$^+$ (second from the right panel) cells was qualitatively similar across all implant conditions at 4 weeks. Dotted line: scaffold periphery. Blue: cell nuclei, purple: CD68, green: Arg-1, red: iNOS. Scale bar: 200 µm.

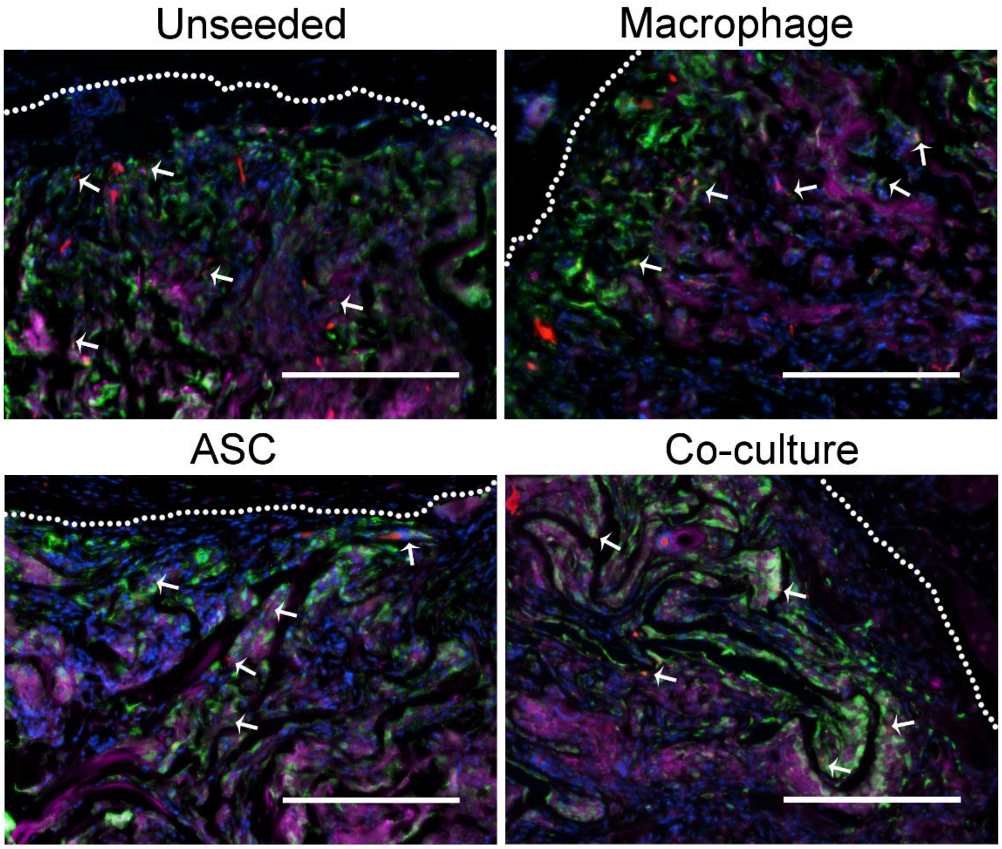

Figure 3.18. Implants from all seeding conditions contain and abundant subpopulation of CD68$^+$ Arg-1$^+$ iNOS$^-$ Hoechst$^+$ cells and a smaller population of CD68$^+$ Arg-1$^+$ iNOS$^+$ Hoechst$^+$ cells after 4 weeks *in vivo*. The representative merged images of the unseeded (top left panel), macrophage-seeded (top right panel), ASC-seeded (bottom left panel), and co-culture-seeded (bottom right panel) implants contained a high density of CD68$^+$ Arg-1$^+$ iNOS$^-$ Hoechst$^+$ cells and a smaller subpopulation of CD68$^+$ Arg-1$^+$ iNOS$^+$ Hoechst$^+$ cells, with no obvious differences found between the implant groups. Dotted line: scaffold periphery. White arrows: CD68$^+$ Arg-1$^+$ iNOS$^+$ Hoechst$^+$ cells. Blue: cell nuclei, purple: CD68, green: Arg-1, red: iNOS. Scale bar: 200 µm.

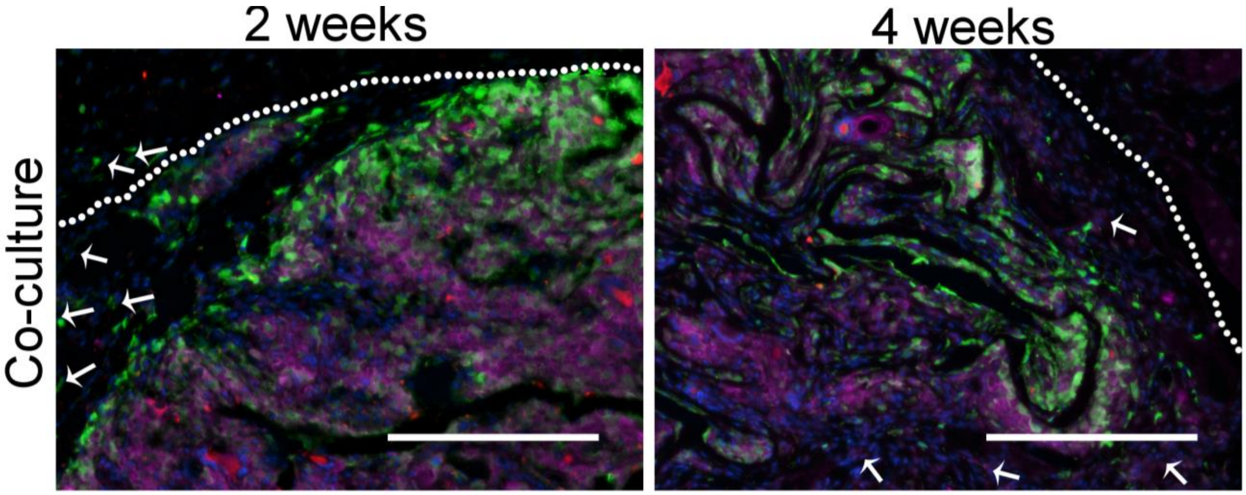

Figure 3.19. Subpopulations of CD68$^+$Arg-1$^-$ iNOS$^-$ Hoechst$^+$ cells and CD68$^-$ Arg-1$^+$ iNOS$^-$ Hoechst$^+$ cells were further identified in the DAT implants *in vivo*. Depicted is a representative merged image of co-culture DAT implants at 2 weeks (left panel) and 4 weeks (right panel). There have been no obvious differences found between the implant groups in the abundancy of either subpopulation of CD68$^+$ Arg-1$^-$ iNOS$^-$ Hoechst$^+$ cells or CD68$^+$ Arg-1$^-$ iNOS$^-$ Hoechst$^+$ cells. Dotted line: scaffold periphery. White arrows in the left panel: CD68$^-$ Arg-1$^+$ iNOS$^-$ Hoechst$^+$ cells. White arrows in the right panel: CD68$^+$ Arg-1$^-$ iNOS$^-$ Hoechst$^+$ cells. Blue: cell nuclei, purple: CD68, green: Arg-1, red: iNOS. Scale bar: 200 µm.

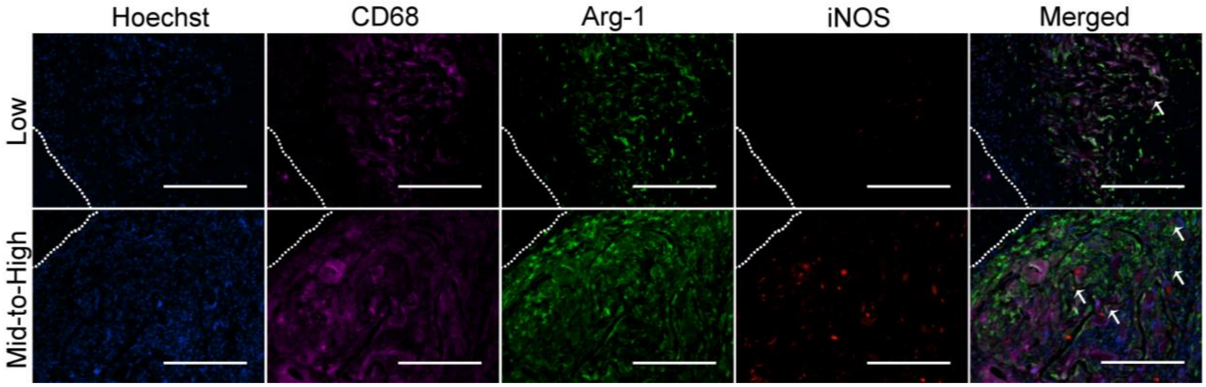

Figure 3.20. Representative images of the CD68, Arg-1, and iNOS co-staining from implants containing different levels of cell infiltration after 2 weeks *in vivo*. Sample images from ASC-seeded implants show how samples with a low (top panels) or mid-to-high (bottom panels) overall cellular infiltration response had a greater fraction of CD68$^+$Arg-1$^+$ iNOS$^+$ Hoechst$^+$ cells. However, iNOS expression was qualitatively enhanced in the implants containing higher levels of overall cellular infiltration, with a slightly higher qualitative abundance of CD68$^+$ Arg-1$^+$ iNOS$^+$ Hoechst$^+$ cells observed as compared to samples with low infiltration. Dotted line: scaffold periphery. White arrows: CD68$^+$ Arg-1$^+$ iNOS$^+$ Hoechst$^+$ cells. Blue: cell nuclei, purple: CD68, green: Arg-1, red: iNOS. Scale bar: 200 µm.

Chapter 4

4 Discussion

In the fields of plastic and reconstructive surgery, there has been growing interest in delivering pro-regenerative cell populations as a strategy to promote long-term, stable soft tissue regeneration[3,4]. As a result, there has been a large focus on designing cell-instructive biomaterials in order to improve the retention and therapeutic function of these populations *in vivo*. Adipose-derived stromal cells (ASCs) are a robust, abundant, and clinically-translatable population of cells that has the capacity to modulate *in vivo* adipose tissue regeneration through their paracrine secretions[124,138]. Macrophage-based therapies are also of emerging interest, building from the knowledge that various macrophage subtypes have been implicated in angiogenesis, as well as adipose tissue expansion and regeneration[167,258]. However, the potential of a macrophage-based strategy in the context of soft tissue regeneration has yet to be explored.

In order to provide a tissue-specific cell-delivery platform for adipose tissue-engineering applications, the Flynn lab has pioneered the design of decellularized adipose tissue (DAT) bioscaffolds[234]. When seeded in combination with ASCs, these constructs enhanced *in vivo* adipogenesis in both immunocompetent Wistar rat and MacGreen mouse models, and showed greater levels of cellular recruitment, neo-blood vessel formation, and a shift towards an M2-like, pro-regenerative macrophage phenotype as compared to unseeded controls[165,237,251]. The mechanisms behind ASC-mediated tissue regeneration have yet to be fully elucidated, including the interactions between ASCs, macrophages and the ECM.

In the present work, syngeneic donor macrophages and ASCs isolated from transgenic reporter mice were seeded onto DAT bioscaffolds and delivered subcutaneously into the inguinal region of immunocompetent C57Bl/6 mice. Over the course of 2 and 4 weeks, histological analysis of the scaffold explants was performed to evaluate cellular recruitment, angiogenesis and constructive implant remodeling into fat. Additional immunohistochemical analysis probing endothelial cell recruitment and macrophage phenotype was also performed. The results demonstrated that the DAT bioscaffolds and seeding regimen supported donor macrophage and ASC attachment *in vitro*. When unseeded, macrophage-seeded, ASC-seeded, and co-culture-seeded implants were delivered into the inguinal region, there was variation noted between implants belonging to the same group in terms of *in vivo* cellular infiltration, blood vessel density, and neo-fat formation at both time points. In general, higher levels of cellular infiltration in each seeding group correlated to enhanced blood vessel densities, CD31 expression, neo-fat formation, and inducible nitric oxide synthase (iNOS) expression, including the qualitatively enhanced presence of a $CD68^+$ $Arg\text{-}1^+$ $iNOS^+$ $Hoechst^+$ subpopulation within the implants. Overall, the variability in the findings suggests that variations in the scaffold positioning and local microenvironment may have affected cell infiltration into the implants, which subsequently influenced both neovascularization and macrophage phenotype.

The initial phase of this thesis focused on the development of an isolation, culture, and characterization protocol for murine bone marrow-derived macrophages, a cell type not previously studied in the Flynn laboratory. Due to their abundance, it is common practice to isolate primary macrophage precursor cells (i.e. monocytes) from murine bone marrow or human peripheral blood and subsequently differentiate these cells *in vitro* into macrophage populations[259,260]. Differentiation into macrophages requires the use of hematopoietic growth factors called colony stimulating factors (CSF), including granulocyte macrophage colony stimulating factor (GM-CSF), macrophage colony stimulating factor (M-CSF) and granulocyte colony stimulating factor (G-CSF)[159,160,261]. Other commonly-used macrophage sources include tissue-resident macrophages, such as murine peritoneal macrophages or splenic macrophages, or immortalized leukemic macrophage-like cells, including the RAW 264.7 (derived from mice) or THP-1 (derived from humans) cell lines[175]. When assessing macrophage-specific markers as well as polarization markers, there have been noted differences in the surface marker expression and gene expression profiles of macrophage populations due to cell sourcing, strain, gender, culture media formulation, CSF source (recombinant CSF or L929 conditioned media), tissue culture plastic, detachment methods, etc[259,262–266]. Incomplete reporting of the culture conditions and experimental design can impact the reproducibility of assays to assess differentiation and polarization[175], thus clear and transparent reporting is needed when using these cells for experiments.

There have been various protocols developed for isolating bone marrow-derived macrophage precursors from mice. While some protocols do not purify the bone marrow-derived cell population[12], the protocol utilized for these studies included additional steps to remove erythrocytes, T cells, and B cells in order to provide a more purified population. Cells harvested post-isolation were stored in liquid nitrogen and thawed for experiments as needed. In order to obtain sufficient numbers of cells for experiments, several variables were explored including different media formulations, types of culture flasks, and seeding densities. It was observed that seeding isolated cells at a density of 5 million cells/flask, using tissue culture-treated T75 flasks, and supplementing the RPMI 1640 with 4 mM l-glutamine and 20 ng/mL MCSF produced differentiated macrophage populations with a robust yield between 2-4 million cells/flask. However, the raw numbers of differentiated macrophages did vary from isolation-to-isolation, though it is also possible the cell banking and thawing process may need further refinement. After refining the *in vitro* culture conditions, the differentiated cell population was observed to spread out and to have cellular protrusions similar to what other groups have reported[267,268].

Murine ASCs were harvested from the inguinal depot of dsRed$^+$ mice following established methods in the Flynn lab[251]. Previous immunophenotype characterization of the isolated ASC population showed that these cells expressed stromal cell markers CD29, CD44, and CD90 and lacked the expression of for endothelial cell marker, CD31, and hematopoietic cell marker, CD45[251]. These cells also exhibited tri-lineage differentiation potential towards the adipogenic, osteogenic, and chondrogenic lineages[251]. In culture, it was observed that the ASCs had a spindle-shaped, fibroblast-like morphology in 2-D culture, which was distinct from the macrophage morphology. The growth of ASCs differed between isolations and passage number, as some ASC populations would be confluent after seeding within a few days, while other times, it would take 5 or more days.

When using flow cytometry to identify macrophage populations from other myeloid/lymphocyte subsets based on surface marker expression, the consensus has been to use multiple antibodies as many subsets share common expression patterns for myeloid specific markers[259,269]. The gating strategy utilized in the current studies examined several hematopoietic and macrophage/monocyte markers. As expected, the macrophages co-expressed CD45, CD11b, and F4/80 and showed negative expression for the neutrophil marker, Ly6G[269–274]. Taken together, this panel of myeloid/macrophage markers supports that most of the cells had differentiated into macrophages.

Since bone marrow-derived macrophages are believed to originate from circulating monocytes[275], the monocyte/macrophage marker, Ly6C, was also included in the analyses. It was found that on average, 94.9% of the CD45$^+$ CD11b$^+$ F4/80$^+$ Ly6G$^-$ subset did not express Ly6C. Some studies have suggested that Ly6C$^+$ or "classical" monocytes or monocyte-derived macrophage populations are recruited to tissues upon injury and develop pro-inflammatory macrophage characteristics *in vivo*[276]. In contrast, Ly6C$^-$ "non-classical" populations may play a role in patrolling the vasculature and have been associated with fibrosis and the resolution of inflammation[277]. However, other studies have shown that these cell populations do not necessarily follow this paradigm and their roles in wound repair differ based on the location they are isolated from and the pathophysiology of the animal model[275,278,161]. Therefore, the evaluation of an additional panel of surface markers in combination with flow cytometry is needed in order to confirm the expression of pro-inflammatory/"M1-like" markers, alternatively activated/"M2-like"markers, or a mixture thereof, as previous reports have demonstrated that media supplementation with MCSF may "pre-differentiate" monocyte-derived macrophages, enhancing the expression of M2-like markers[279,280].

Interestingly, Ly6C$^-$ and Ly6C$^+$ cells contained subpopulations with varying levels of GFP expression. GFP expression in the cells isolated from the MacGreen mice is under the control of the promoter for colony stimulating factor 1 receptor, CSF-1R (encoded by the *csf1r* or c *-fms* proto-oncogene), and FACS analysis has previously confirmed its expression in peritoneal, bone marrow-derived, and broncho/alveolar lavage macrophages, as well as Langerhans cells derived from MacGreen mice[281]. MCSF is a hemopoietic growth factor that regulates macrophage differentiation, proliferation and survival and exerts its effect by binding to CSF-1R[282]. Since the isolated cell population was cultured with MCSF, and they expressed other macrophage-specific markers such as F4/80 and Cd11b, greater GFP expression was expected. It could be that the method of cell culture, including the MCSF concentration, may have affected the *csf1r* and *gfp* expression in the cultured macrophages, and as a result, requires further refinement.

To confirm that these GFP subsets are not unique to bone marrow-derived macrophages, macrophages from other tissues could be similarly evaluated. Additionally, it could be that CSF-1R expression is naturally present in cultured macrophages at differing levels within subsets of macrophages. Though the *csf1r*-EGFP transgene has been detected in macrophages[283] and other myeloid cell populations like dendritic cells and neutrophils[281], the variation in the GFP expression between subsets of MacGreen mononuclear cells has been previously reported. One study examining peritoneal foreign body reactions observed different Ly6C subsets including $\text{EGFP}^{\text{low}}\ \text{Ly6C}^{\text{med-high}}$, $\text{EGFP}^{\text{high}}\ \text{Ly6C}^{\text{med}}$, and $\text{EGFP}^{\text{high}}\ \text{Ly6C}^{\text{high}}$ cells, as well as different Gr1 subsets including $\text{EGFP}^{\text{high}}\ \text{Gr1}^{\text{high}}$ and $\text{EGFP}^{\text{low}}\ \text{Gr1}^{\text{low}}$ cells[272]. Further, Kampfrath *et al.* reported a similar trend in a different mouse model, $\text{c-fms}^{\text{YFP+}}$, which expresses yellow fluorescent protein (YFP) under the control of the *csf1r* promoter[284]. They found that $\text{Ly6C}^{\text{high}}$ F4/80^{+} cells tended to be YFP^{high}, while Ly6C^{low} F4/80^{+} tended to be YFP^{low} [284]. In future experiments, donor macrophage populations could alternatively be derived from EGFP^{+} mice in which EGFP is under control of the human ubiqutin C promoter in all tissues to enable tracking of all subsets of donor macrophage populations *in vivo*.

In the second part of this thesis, protocols were established for seeding the macrophages both alone and in combination with the dsRed^{+} ASCs on DAT bioscaffolds. Porous scaffolds serve to support, instruct, and deliver pro-regenerative donor cell populations, but obtaining a homogenous spatial distribution and high cell density *in vitro* can be challenging with large scaffolds[285]. Current seeding procedures rely on static or dynamic seeding strategies. Static seeding involves adding a concentrated cell suspension over scaffolds and allowing the cells to passively adhere over time[286]. In pilot studies, static seeding was employed to seed ASCs and/or macrophages onto the DAT bioscaffolds, and histologically the cells were localized to the periphery of the scaffold, with limited infiltration within the inner portions. Other studies have shown that a dense layer of cells at the scaffold periphery can consume or prevent the diffusion of oxygen and nutrients into the inner portions of the scaffold, causing necrosis[287].

Consequently, a dynamic culture approach was applied to seed the macrophages both alone and in combination with the ASCs by gently rocking the cells with the scaffolds in 3 mL of media in a vented 15 mL conical tube for 24 hours. After seeding, the macrophages and ASCs were observed to be distributed along the periphery and the inner portions, except for areas with dense portions of the ECM. These findings highlight how physical properties such as the scaffold microarchitecture and porosity can further affect cell infiltration, as an open, permeable porous network can facilitate oxygen, nutrients, and waste transport in addition to providing migration tracks for the cells[285,287,288].

When assessing the cellularity of the scaffolds after the dynamic seeding period, there was variability observed in the quantitative assessment of dsDNA content and metabolic activity, which led to no significant differences between the implant groups. The variability may be attributed to donor differences in the cell populations and/or ECM-derived materials. In previous studies, DAT bioscaffolds have been demonstrated to promote the viability and proliferation of human, murine, and rat ASCs[131,234,237,239,249]. Moreover, native adipose tissue contains tissue-resident macrophage populations[24], and the accumulation of macrophages during inflammatory conditions such as in the case of obesity, is thought to be due to the migration of bone marrow-derived monocyte populations[289]. The aim of decellularization is to remove antigenic cellular components from the adipose tissue, while maintaining the biological activity and mechanical integrity of the ECM. The Flynn lab decellularization protocol utilizes detergent-free methods to process adipose tissue, as residual amounts of detergents are known to cause cytotoxicity, and their use can disrupt the ECM integrity in such a way that it can negatively impact bioscaffold repopulation[233,290]. Immunohistochemical and mass spectrometry analyses have identified ECM components that are conserved in DAT bioscaffolds including collagen types I and IV, laminin, and fibronectin[234,248], which promote cell adhesion, survival, and proliferation[15,68,78,81]. Thus, it was expected that both cell types would be able to attach to the DAT bioscaffold.

The current study did not, however, directly evaluate cell viability or proliferation, and instead focused on quantifying cell retention after seeding and evaluating cellular metabolism. Cellular metabolic activity is often tied to cellular proliferation, but it can be affected by several different factors. For example, cells at different densities can have different levels of metabolic activity, though this does not necessarily correlate linearly[291]. In the case of the direct co-culture of ASCs and macrophages, the cell-cell and cell-ECM interactions could stimulate a change in cellular metabolism such as proliferation or phagocytosis[292]. Future studies could include staining for Ki67, a nuclear marker of proliferation[293], or cell viability assays with additional time points. It may also be worth probing the secreted factors in the culture media for pro-angiogenic and anti-apoptotic factors. Overall, the combined qualitative and quantitative measures of cellular retention and metabolic activity suggest that while there may have been donor-to-donor viability, the total cell density within the DAT scaffolds was similar between the macrophage-seeded, ASC-seeded, and co-culture seeded groups within each trial.

Following the *in vitro* studies, unseeded, macrophage-seeded, ASC-seeded, and co-culture seeded DAT bioscaffolds were implanted subcutaneously into the inguinal region of immunocompetent C57Bl/6 mice. Previous animal studies in the Flynn lab utilizing Wistar rats and MacGreen mice involved subcutaneous implantation of ASC-seeded and unseeded DAT implants on the dorsa rather than in the inguinal region In the MacGreen mouse model, the previous studies showed that there was limited cell infiltration into the unseeded DAT implants on the back of the mice[251]. In contrast, more recent pilot studies in the Flynn lab indicated that implantation within the inguinal region may greatly enhance cell recruitment, possibly due to the localization of the DAT in proximity to the femoral artery and/or inguinal fat pad. Other animal studies in the context of fat grafting have either derived fat grafts from the inguinal pad or have used the inguinal region as the recipient site[294]. For these reasons, implantation in the inguinal region was selected for the current study.

Qualitative histological assessment of all implant groups at both 2 and 4 weeks through Masson's trichrome staining revealed a thin layer of fibrous connective tissue surrounding the seeded and unseeded implant groups, which has been observed in our previous animal studies[131,165,251]. Acellular fibrous capsule formation has long been associated with a negative foreign body response to *in vivo* biomaterial implantation, including silicone breast implants[295]. Moreover, its formation is thought to be mediated by macrophage-fibroblast interactions[296,297]. In the current study, the fibrous capsule formation may have been stimulated due to the human sourcing of DAT or its dense microarchitecture[298]. However, its presence is not alarming because the observed capsule is highly cellular, and in some cases, contains adipocytes and erythrocyte-filled blood vessels along the implant periphery. Additionally, the capsule integrated well with adjacent fat pads and previous studies have observed the fibrous capsule surrounding DAT implants to decrease in thickness and remodel over time[44].

Qualitative and quantitative assessment of cellular recruitment into the scaffolds in the present study revealed variation between implants belonging to the same seeding condition, which led to no detectable differences between groups at either time point. As expected, at 2 weeks a larger fraction of the cell-seeded implants showed higher levels of infiltration as compared to unseeded implants. At 4 weeks, the unseeded implants showed a greater range of cell infiltration responses and a greater fraction showed slightly higher levels of infiltration as compared to their 2-week counterparts, which was also expected. In contrast, at 4 weeks, infiltration into the cell-seeded scaffolds appeared to be less variable, although the levels of cell recruitment did not significantly change over time. In the previous study, subcutaneous dorsal implantation of both ASC-seeded and unseeded DAT implants into MacGreen mice also showed some degree of variability within implants from the same group, although not as much as the current study[251]. Within the dorsal implant model, the ASC-seeded implants showed greater levels of cell recruitment at 8 weeks as compared to unseeded implants, although the unseeded implants also showed greater recruitment over time[251]. The previous study was in agreement with other studies that have demonstrated that ASCs can augment cellular recruitment into biomaterial scaffolds in comparison to unseeded controls[128–131].

The variation found within each group, as well as the infiltration response in the cell-seeded groups at 4 weeks, could be explained by a few different factors. First, when comparing scaffolds with ASCs and/or macrophages sourced from the same donors that were implanted into different recipient mice, there were differences observed in the levels of cellular infiltration between individual mice. For example, some mice would show higher levels of cellular recruitment into both implanted scaffolds, no matter their seeding condition, while other mice would comparatively show less migration into implants derived some the same donor.

Secondly, there were differences noted when comparing the ASC-seeded or macrophage-seeded implants and co-culture implants derived seeded with cells sourced from the same donors and placed into the same recipient mice, pointing to possible differences due to implant positioning and the implantation method. The inguinal implant recipient site is closer to the leg, which could cause cyclical mechanical loading in the implant and thus increase variability. During the surgical procedure, the implants were placed into subcutaneous pockets made as close to the femoral artery as possible. As previously mentioned, adipose tissue growth is largely dependent on vascularization and the infiltration of immune cell populations[59]. The vasculature within the inguinal region includes the femoral artery and the capillary network feeding the local soft tissues including muscle and fat. In some cases, the lack of noticeable differences could be due to implants being situated closer or farther from the tissues that have greater access to the vasculature, thereby accelerating or delaying the influx of host cell populations and masking differences between conditions. Luttikhuizen *et al.* highlighted the fact that different implantation sites of collagen disks in C56Bl/6 mice led to differences in inflammatory cytokine signaling and downstream outcomes such as foreign body reaction propagation, implant degradation, immune cell recruitment, and angiogenesis[299]. In a different study, fat grafts derived from rabbit inguinal fat pads were grafted subcutaneously, supramuscularly, or submuscularly into the cheeks of New Zealand white rabbits[300]. Through magnetic resonance imaging (MRI) and histological analyses, the fat grafts placed in the supramuscular region was found to have retained a larger volume in comparison to the other areas[300]. Taken together, this highlights how the local microenvironment of the recipient area may affect the cell recruitment and remodeling response *in vivo*. Further refinement of the surgical procedure could aid in promoting a more consistent infiltration response. Alternatively, implantation on the dorsa could be performed since differences between ASC-seeded and unseeded implants were previously detected in this model. Notably, there were implants from the cell-seeded groups, especially in the ASC-seeded and co-culture-seeded groups, that showed relatively low levels of cell infiltration, which would be due to other factors such as issues with the seeding procedure or poor cell attachment. Further probing using immunohistochemical staining could be performed to see if ASC and/or macrophage populations were retained within implants and if their absence could explain these low responsive implants.

The variation observed in the levels of cellular infiltration was also reflected in the assessment of the blood vessel densities and neo-adipocyte formation within the scaffolds in the current study. The overall neo-adipocyte formation was low for both groups at both time points, which was expected at these early time points. While the blood vessel density was also found to be fairly low between all groups at both time points, when comparing implants within a seeding condition the implants that had higher levels of cell infiltration tended to have slightly higher blood vessel densities, which was expected. The quantitative assessment of $CD31^+$ cell recruitment within the implant boundary showed similar patterns. Further analysis of CD31 co-staining with the cell proliferation marker, EdU, or the pro-angiogenic cytokine, vascular endothelial growth factor (VEGF)-A, could provide a stronger indication of the pro-angiogenic response. The inclusion of additional later time points could also result in differences being detected in the blood vessel and/or endothelial cell recruitment. For example, in the previous study using immunocompetent Wistar rats, it was observed that ASC-seeded implants showed a significant increase in

CD31$^+$VEGF-A$^+$ cells at 4 weeks, which was followed by a significantly greater number of erythrocyte-filled blood vessels at 8 and 12 weeks[165].

Angiogenesis is a tightly-coupled spatiotemporal process that requires the degradation and remodeling of the surrounding ECM in order to propagate[130,301,302]. Initially, the basement membrane must be degraded to allow for capillary sprouting from an existing blood vessel to occur[301]. This is followed by further degradation of the ECM near the sprouting site to allow for endothelial invasion, and this continues in order to create a space for the sprouting blood vessel lumen[301]. It is possible that DAT, in its intact form, may be too dense for blood vessel sprouting to occur at early time points. Further refinement of the porosity of the DAT bioscaffold may be carried out during the fabrication process by freezing the scaffolds at lower temperatures, thus increasing freezing rate and promoting greater ice crystal formation[303]. Alternatively, other methods of delivery could be explored including injectable hydrogel systems[131]. The Flynn lab has previously developed composite methacrylated chondroitin sulphate-DAT hydrogels to deliver rat ASCs into Wistar rats[131]. It was demonstrated that these composite constructs contained tunable mechanical properties, promoted the homogenous distribution of ASCs within the hydrogel, and promoted *in vivo* cellular infiltration, blood vessel development and neo-fat formation[131].

Finally co-staining for the pan-macrophage marker, CD68, with the “M2-like” marker, Arginase (Arg)-1, and the M1-like marker, iNOS, revealed that when comparing groups with similar levels of infiltration there was a qualitatively greater proportion of cells that expressed CD68 and Arg-1, with a lower fraction expressing iNOS at both time points. The merged images portraying co-localization revealed an abundant CD68$^+$ Arg-1$^+$ iNOS$^-$ cell population, pointing to an abundant recruited macrophage population with a shift towards a more “M2-like”, pro-regenerative phenotype. The fact that there was a large influx of cells with CD68 expression among all groups at both time points is consistent with the previous study using Wistar rats, which observed that CD68$^+$ expression was similar between ASC and unseeded implants, but the ASC-seeded implants contained a greater fraction of CD68$^+$macrophages that expressed the pro-regenerative macrophage marker, CD163[165]. In contrast, the studies using MacGreen mice observed augmented levels of macrophages expressing the pan-macrophage marker Iba1 in ASC-seeded implants, which peaked after 3 weeks[251].

The present study also identified several different subpopulations of cells. For example, there was a subpopulation of CD68$^+$ Arg-1$^-$ iNOS$^-$ Hoechst$^+$ cells identified, which was also found in a different study by Agrawal *et al.*, which assessed the *in vivo* remodeling response of different commercially available acellular dermis matrices subcutaneously implanted into Sprague Dawley rats[304]. CD68 is a scavenger receptor associated with lysosomes that has been found in monocytes and macrophages, but it can also be expressed by subsets of CD34-positive hematopoietic stem cells, dendritic cells, neutrophils, basophils, and mast cells[257]. While some of these cells could be contributing to the subpopulation of CD68$^+$ Arg-1$^-$ iNOS$^-$ Hoechst$^+$ cells, Agrawal *et al.* posited that that these cells were newly recruited and might not have been stimulated to express pro-inflammatory or pro-regenerative markers[304]. A separate subpopulation of CD68$^-$ Arg-1$^+$ iNOS$^-$ Hoechst$^+$ cells was found, which may be attributed to other cells commonly recruited to biomaterial implants that can express Arg-1 including fibroblasts, dendritic cells, and neutrophils[305].

Due to the limitations in the available host antibodies, it is common in studies evaluating macrophage phenotype to co-stain for a pan-macrophage marker in combination with either Arg-1 or iNOS. However, the current study utilized a triple stain and identified a small population of CD68$^+$ Arg-1$^+$ iNOS$^+$ Hoechst$^+$ cells, although their role *in vivo* is still unknown. This macrophage subpopulation may represent cells that are in transition from a pro-inflammatory to a pro-regenerative phenotype, as other studies have immunohistochemically evaluated other combinations of pro-inflammatory and pro-regenerative macrophage markers and have found a similar mixed macrophage phenotype[182,304]. Interestingly, the current study also found that higher levels of infiltration correlated with greater levels of iNOS expression and a greater number of CD68$^+$ Arg-1$^+$ iNOS$^+$ Hoechst$^+$ cells. Future studies could examine other combinations of pan-macrophage markers (e.g. F4/80, Iba-1, CD11b), pro-inflammatory markers (e.g. CD80, C-C chemokine receptor type (CCR)7, tumor necrosis factor (TNF)-α), and pro-regenerative markers (e.g. CD163, CD206, Il-10) with additional time points in order to gain a deeper understanding of the spatiotemporal localization and phenotype of recruited macrophage populations. Taken together, the findings of this study support that in order for angiogenesis and constructive remodeling of implants into neo-adipose tissue to occur in this mouse model, there is a need to mobilize a diverse range of macrophage responses.

Chapter 5

5 Conclusions and future directions

5.1 Summary of findings and conclusions

In the first aim, methods were established to harvest, culture, and differentiate syngeneic, murine bone marrow-derived macrophages from MacGreen mice. Characterization of the immunophenotype of the differentiated cell population using flow cytometry revealed that the cells co-expressed the hematopoietic marker CD45, as well as the macrophage markers, CD11b and F4/80. Importantly, the cells did not express the neutrophil marker, Ly6G. Taken together, the results support that the majority of the cells had differentiated into macrophages. Further analysis revealed that the majority of the $CD45^+$ $CD11b^+$ $F4/80^+$ $Ly6G^-$ subset did not express the monocyte/macrophage marker, Ly6C, which may suggest that the cells had a more pro-regenerative phenotype. However, further assessment of additional pro-inflammatory and pro-regenerative markers would be needed to draw firm conclusions. Interestingly, both $Ly6C^-$ and $Ly6C^+$ cells contained subpopulations with varying levels of GFP expression, emphasizing the diversity of the differentiated cell population.

In the second aim, a dynamic culture seeding strategy was employed to seed the macrophages both alone and in combination with syngeneic $dsRed^+$ adipose-derived stromal cells (ASCs) onto decellularized adipose tissue (DAT) bioscaffolds over 24 hours. After seeding, qualitative visualization verified the attachment of both cell types along the periphery and the inner portions of the DAT bioscaffolds, with the exception of areas with dense regions of extracellular matrix (ECM). Additional quantitative measures of cellularity including double stranded DNA (dsDNA) content and metabolic activity showed no significant differences between the implant groups. While the data reflects donor-to-donor variability in the cell populations and/or ECM-derived materials, the total cell density within the DAT scaffolds was similar between the macrophage-seeded, ASC-seeded, and co-culture seeded groups within each trial, suggesting similar levels of attachment.

In the third aim, the unseeded, macrophage-seeded, ASC-seeded, and co-culture-seeded DAT bioscaffolds were implanted subcutaneously into the inguinal region of immunocompetent

C57Bl/6 mice. Qualitative histological assessment of all implant groups at both 2 and 4 weeks through Masson's trichrome staining revealed a thin layer of fibrous connective tissue surrounding the seeded and unseeded implant groups, which had integrated well with the surrounding fat pads and contained cells. Notably, newly formed adipocytes and erythrocyte-filled blood vessels were observed along the periphery of the DAT implants, within or near the fibrous capsule.

Further qualitative and quantitative analysis of cellular recruitment into the scaffolds revealed variation between implants belonging to the same seeding condition, which led to no detectable differences between groups at either time point. As expected, at 2 weeks a greater fraction of the cell-seeded implants showed higher levels of infiltration in comparison to unseeded implants. At 4 weeks, the unseeded implants showed a greater range of cell infiltration responses, with a greater fraction showing slightly higher levels of infiltration as compared to the 2-week unseeded samples. In contrast, at 4 weeks, the cell-seeded scaffolds showed less variability in terms of the infiltration response, although the overall levels of cell recruitment did not significantly change over time. The variation found within implants belonging to the same seeding condition could be explained in part by physiological differences between mice, implantation in a mechanically dynamic area of the mouse's body, or issues with the seeding procedure.

Quantitative assessment of blood vessel density and neo-adipocyte formation within the scaffolds in all groups at both time points showed variability similar to the cellular infiltration analyses. In general, neo-adipocyte formation was low for all groups, which was expected at these early time points. The blood vessel density was also found to be low between all groups at both time points. However, it was noted that the implants that had higher levels of total cell infiltration tended to have slightly higher blood vessel densities. This trend was further reflected in the qualitative and quantitative assessment of CD31$^+$ endothelial cell recruitment within the implant periphery.

Finally, co-staining was performed for the pan-macrophage marker, CD68, the M2-like marker, Arginase-1 (Arg-1), and the M1-like marker, inducible nitric oxide synthase (iNOS). Qualitative assessment at both time points revealed that when comparing groups with similar levels of infiltration, there were no observed differences between any of the groups. DAT implants contained a greater proportion of cells that expressed CD68 and Arg-1, with a lower fraction expressing iNOS. Merged images visualizing co-localization revealed an abundant CD68$^+$ Arg-1$^+$ iNOS$^-$ Hoechst$^+$ cell population, which pointed towards a recruited macrophage population with a shift towards a more pro-regenerative phenotype. The phenotypes of the recruited cell populations were diverse and included smaller subpopulations of CD68$^+$ Arg-1$^-$ iNOS$^-$ Hoechst$^+$ cells and CD68$^-$ Arg-1$^+$ iNOS$^-$ Hoechst$^+$ cells, as well as recruited macrophages with a CD68$^+$ Arg-1$^+$ iNOS$^+$ Hoechst$^+$ phenotype, suggesting the cells may be in transition. However, differences were noted between DAT implants with different infiltration levels. In general, higher levels of cell infiltration corresponded to qualitatively greater levels of iNOS expression, as well as qualitatively higher levels of macrophages containing a mixed phenotype.

Taken together, higher levels of cell infiltration correlated with higher levels of blood vessel formation, CD31$^+$ endothelial cell recruitment, and a greater diversity in macrophage phenotype. Though a diverse range of macrophage phenotypes was recruited into the DAT implants, a greater fraction expressed Arg-1, suggestive of a more pro-regenerative phenotype. Overall, the findings highlight the complexity of macrophage phenotypes required for blood vessel development and downstream neo-adipocyte formation to occur.

5.2 Future recommendations

The present thesis served as a basis for the proof-of-concept of delivering macrophages and ASCs using ECM-derived bioscaffolds for soft tissue regeneration or repair. Initial flow cytometry characterization of the surface marker profile of differentiated bone marrow-derived cells examined a combination of macrophage-associated markers including CD45, CD11b, F4/80, Ly6C, GFP as well as the neutrophil marker, Ly6G to confirm that the cells were macrophages, while also revealing subpopulations. Further assessment of additional lymphocyte markers (e.g. CD4 and CD8) could further confirm the purity and the differentiated cell population’s commitment down the myeloid lineage. Additionally, the inclusion of a dendritic cell marker (e.g. CD11c) could further confirm the differentiation of these cells into macrophages.

In order to probe whether the *in vitro* culture conditions may have influenced macrophage polarization into an M1-like or M2-like phenotype, the macrophages could be differentiated and then polarized with lipopolysaccharide and interferon (IFN)-γ to induce M1-like macrophage polarization, interleukin (IL)-4 and interleukin (IL)-13 to induce M2a-like polarization, and interleukin (IL)-10 to induce an M2c-like polarization[182,306–308]. The surface marker expression of these stimulated macrophages could then be compared with the immunophenotype of unstimulated macrophages using a panel of pro-inflammatory markers (e.g. CCR7 and CD80) and pro-regenerative markers (e.g. CD206 and CD163). This characterization could then be further supported by additional analyses using reverse-transcription quantitative PCR to measure "M1-like" markers (*tnfα and ccl5*) and "M2-like" markers (*arg1, fizz1*).

In MacGreen mice, all myeloid cells were thought to express EGFP under the control of the *csf1r* promoter, which encodes colony stimulating factor receptor 1 (CSF1R or CD115) found on macrophages[281,309]. Further examination of CD115 could be performed in combination with GFP and/or Ly6C to further support the notion of specific MacGreen macrophage subpopulations that exist that lack GFP expression. These findings could also be probed by isolating, culturing and characterizing primary splenic or peritoneal macrophages from MacGreen mice.

Future *in vitro* studies could also focus on improving the characterization, viability, and retention of seeded cells after dynamic seeding. Macrophage and ASC cell attachment to DAT bioscaffolds were found to be localized to the more peripheral regions of the DAT bioscaffolds. Denser regions of ECM prevented the cells from fully infiltrating the scaffold, which could point to how the physical properties of the DAT bioscaffold, such as porosity, could be further refined. Alternatively, a composite methacrylated chondroitin sulphate-DAT hydrogel could be employed to encapsulate and retain the cells[131].

Further assessment of cell proliferation through immunohistochemical staining for the proliferation marker, Ki-67, could be performed. Alternatively, the scaffolds could be enzymatically digested to release the cells, and staining of apoptotic markers, such as annexin V in combination with propidium iodide, could be performed using flow cytometry. In these assessments, additional time points such as 48 hours, 3 days, 7 days, and 14 days could be used to assess cell retention over a greater period of time. It would also be interesting to further assess the effects of the seeding conditions on macrophage phenotype alone or in co-culture with the ASCs. Immunohistochemical analyses could be performed to assess a range of pro-inflammatory markers (e.g. iNOS, CD80, tumor necrosis factor (TNF)-α) and pro-regenerative markers (e.g. Arg-1, CD206, CD163, interleukin (IL)-10) in combination with further probing of pro- and anti-inflammatory cytokines by using western blotting. In addition, analysis of the conditioned medium, including the macrophages in co-culture with the ASCs, could be performed using MultiPlex ELISA to assess whether detectable levels of pro-angiogenic and immunomodulatory factors are being secreted from the cells over time, with conditioned media from macrophages and ASCs cultured separately as a comparison. The abundance of these factors in normoxia could be compared to seeded DAT bioscaffolds cultured under *in vitro* hypoxic conditions (5% CO_2/2% O_2 in N_2). In a previous study performed in the Flynn lab, human ASCs were encapsulated in a composite poly(trimethylene carbonate)-b-poly(ethylene glycol)-b-poly(trimethylene carbonate) diacrylate and methacrylated glycol chitosan functionalized with an RGD-containing peptide (PEG-(PTMC-A)2 + MGC-RGD) hydrogel and subsequently cultured in hypoxia (5% CO_2/2% O_2 in N_2) [310]. After 14 days, the ASCs in hypoxia released significantly higher levels of pro-angiogenic, anti-apoptotic, and chemoattractant factors as compared to ASCs cultured in normoxic conditions including hepatocyte growth factor (HGF), platelet-derived growth factor (PDGF)-AA, stromal-derived growth factor (SDF)-1α, and monocyte chemoattractant protein (MCP)-1, leptin, Angiogenin, vascular endothelial growth factor (VEGF)-A, Angiopoietin-1, and placental growth factor (PlGF)-1[310].

In terms of future *in vivo* work, the variability found when comparing implants belonging to the same seeding condition may have masked differences in the cell recruitment, blood vessel formation, or neo-adipose formation between the groups. As an alternative approach, the cell-seeded and unseeded DAT implants could be implanted subcutaneously in the dorsa of C57Bl/6 mice, where differences have been reported between ASC-seeded and unseeded implants in terms of cell recruitment and implant remodeling in host-derived fat[251]. The further inclusion of additional time points (e.g. 1, 4, 8 weeks) may also reveal differences in the levels of cellular infiltration, blood vessel densities, and adipocyte formation.

Masson’s trichrome staining revealed that a few of the implants in the seeded conditions at both time points had relatively low levels of infiltration, which was not expected. Although, there may be inherent physiological differences between recipient mice, the histological analyses were performed along a single plane of the implant. By cutting and staining the DAT implants along a different plane, there may be additional clues as to the migration patterns of recruited cells within the implants. While this subset of samples may not be viewed as being highly infiltrated along one plane of the implant, assessing a different plane may reveal higher levels of infiltration. Moreover, immunohistochemical staining of dsRed$^+$ and/or GFP$^+$ cells could be performed to confirm the retention of donor ASCs and macrophages in the scaffolds over time and whether the low cell infiltration could be due to issues with the seeding method. Previously it was confirmed that the syngeneic donor ASCs were retained in the majority of seeded implants over the course of 8 weeks in the dorsal implantation site[251].

Deeper assessment of the phenotype of the infiltrating macrophages should be performed by staining for additional pan-macrophage markers (e.g. F4/80, Iba-1, CD11b), pro-inflammatory markers (e.g. CD80, CCR7, TNF-α), and pro-regenerative markers (e.g. CD163, CD206, Il-10) with the inclusion of additional time points. Further co-localization of the pro-inflammatory/regenerative markers with EGFP could reveal the phenotype of subpopulations of the donor macrophages over time *in vivo*.

Finally, as a step towards clinically translating these findings, future studies could explore human ASCs and human macrophages derived from peripheral blood monocytes in immunocompromised mouse models, as there have been differences noted in human and mouse macrophage function[175]. Also, our studies included the delivery of macrophages that had not been exogenously stimulated *in vitro* by cytokines. Since macrophage subtypes, such as M1, M2a, and M2c macrophages, have previously been implicated as playing different roles in wound healing[148] and angiogenesis[182], it is possible that delivering polarized macrophages may have an alternative *in vivo* effect with respect to unpolarized controls in terms of stimulating blood vessel formation and implant remodeling.

References

1. Choe, S. S., Huh, J. Y., Hwang, I. J., Kim, J. I. & Kim, J. B. Adipose tissue remodeling : its role in energy metabolism and metabolic disorders. *Front. Endocrinol. (Lausanne).* **7**, 1–16 (2016).

2. Berry, D. C., Stenesen, D., Zeve, D. & Graff, J. M. The developmental origins of adipose tissue. *Development* **140**, 3939–3949 (2013).

3. Choi, J. H. *et al.* Adipose tissue engineering for soft tissue regeneration. *Tissue Eng. Part B. Rev.* **16**, 413–26 (2010).

4. Mahoney, C. M., Imbarlina, C., Yates, C. C. & Marra, K. G. Current therapeutic strategies for adipose tissue defects/repair using engineered biomaterials and biomolecule formulations. *Front. Pharmacol.* **9**, 1–12 (2018).

5. Grunfeld, E. A. Satisfaction with outcome and attitudes towards scarring among women undergoing breast reconstructive surgery. *Patient Educ. Couns.* **66**, 243–249 (2007).

6. Heijer, M. Den *et al.* Body image and psychological distress after prophylactic mastectomy and breast reconstruction in genetically predisposed women : A prospective long-term follow-up study. *Eur. J. Cancer* **48**, 1263–1268 (2011).

7. Blasco, J. A. Satisfaction with psychological impact of immediate and deferred breast reconstruction. *Ann. Oncol.* **19**, 1430–1434 (2008).

8. Cordeiro, P. G. Breast reconstruction after surgery for breast cancer. *N. Engl. J. Med.* **359**, 1590–1601 (2008).

9. Pulagam, S. R., Poulton, T. & Eleftherios, P. Long-term clinical and radiologic results with autologous fat transplantation for breast augmentation: case reports and review of the literature. *Breast J.* **12**, 63–65 (2006).

10. Ikeda, K., Maretich, P. & Kajimura, S. The common and distinct features of brown and beige adipocytes. *Trends Endocrinol. Metab.* **29**, 191–200 (2018).

11. Sacks, H. & Symonds, M. E. Anatomical locations of human brown adipose tissue: functional relevance and implications in obesity and type 2 diabetes. *Perspect. Diabetes* **62**, 1783–1790 (2013).

12. Stock, M. J. & Cinti, S. Structure and function of brown adipose tissue. *Encycl. Food Sci. Nutr. (Second Ed.* 29–34 (2003).

13. Coelho, M., Oliveira, T. & Fernandes, R. Biochemistry of adipose tissue : an endocrine organ. *Arch. Med. Sci.* **9**, 191–200 (2013).

14. Wronska, A. & Kmiec, Z. Structural and biochemical characteristics of various white adipose tissue depots. *Acta Physiol.* **205**, 194–208 (2012).

15. Kubo, Y., Kaidzu, S., Nakajima, I., Takenouchi, K. & Nakamura, F. Organization of extracellular matrix components during differentiation of adipocytes in long-term culture. *Vitr. Cell. Dev. Biol. - Anim.* **36**, 38–44 (2000).

16. Giordano, A. *et al.* White adipose tissue lacks significant vagal innervation and immunohistochemical evidence of parasympathetic innervation. *Am. J. Physiol. Regul. Integr. Comp. Physiol.* **4010**, 1243–1255 (2019).

17. Yar, S., Chang, H. & Ardehali, H. The good neighbor: Coping with insulin resistance by modulating adipose tissue endothelial cell function. *Circ. Res.* **118**, 776–778 (2016).

18. Trayhurn, P. Endocrine and signalling role of adipose tissue : new perspectives on fat. *Acta Physiol. Scand.* **184**, 285–293 (2005).

19. Galic, S., Oakhill, J. S. & Steinberg, G. R. Adipose tissue as an endocrine organ. *Mol. Cell. Endocrinol.* **316**, 129–139 (2010).

20. Rosen, E. D. & Spiegelman, B. M. What we talk about when we talk about fat*. *Cell* **156**, 20–44 (2014).

21. Pope, B. D., Warren, C. R., Parker, K. K. & Cowan, C. A. Microenvironmental control of adipocyte fate and function. *Trends Cell Biol.* **26**, 745–755 (2016).

22. Christiaens, V. & Lijnen, H. R. Angiogenesis and development of adipose tissue. *Mol. Cell. Endocrinol.* **318**, 2–9 (2010).

23. Dubey, N. K. *et al.* Revisiting the advances in isolation, characterization and secretome of adipose-derived stromal/stem cells. *Int. J. Mol. Sci.* **19**, 1–23 (2018).

24. Ramakrishnan, V. M. & Boyd, N. L. The adipose stromal vascular fraction as a complex cellular source for tissue engineering applications. *Tissue Eng. - Part B Rev.* **24**, 289–299 (2018).

25. Ye, J. Adipose tissue vascularization: its role in chronic inflammation. *Curr. Diab. Rep.* **11**, 203–210 (2011).

26. Silva, H. M. *et al.* Vasculature-associated fat macrophages readily adapt to inflammatory and metabolic challenges. *J. Exp. Med.* **216**, 786–806 (2019).

27. Ferrante, A. W. The immune cells in adipose tissue. *Diabetes, Obes. Metab.* **15**, 34–38 (2013).

28. Joe, A. W. B., Lin, Y., Even, Y., Vogl, A. W. & Rossi, F. M. V. Depot-specific differences in adipogenic progenitor abundance and proliferative response to high-fat diet. *Stem Cells* **27**, 2563–2570 (2009).

29. Weisberg, S. P. *et al.* Obesity is associated with macrophage accumulation in adipose tissue Find the latest version : Obesity is associated with. *J Clin Invest.* **112**, 1796–1808 (2003).

30. Morange, P. E. *et al.* Influence of t-PA and u-PA on adipose tissue development in a murine model of diet-induced obesity. *Thromb. Haemost.* **87**, 306–310 (2002).

31. Martyniak, K. & Masternak, M. M. Changes in adipose tissue cellular composition during obesity and aging as a cause of metabolic dysregulation. *Exp. Gerentology* **94**, 59–63 (2018).

32. Miyamoto, Y., Ikeuchi, M., Noguchi, H., Yagi, T. & Hayashi, S. Enhanced adipogenic

differentiation of human adipose-derived stem cells in an in vitro microenvironment: the preparation of adipose-like microtissues using a three-dimensional culture. *Cell Med.* **9**, 35–44 (2017).

33. Sarantopoulos, C. N. *et al.* Elucidating the preadipocyte and its role in adipocyte formation: a comprehensive review. *Stem Cell Rev. Reports* **14**, 27–42 (2018).

34. Ong, W. K. *et al.* Identification of specific cell-surface markers of adipose-derived stem cells from subcutaneous and visceral fat depots. *Stem Cell Reports* **2**, 171–179 (2014).

35. Mitterberger, M. C., Lechner, S., Mattesich, M. & Zwerschke, W. Adipogenic differentiation is impaired in replicative senescent human subcutaneous adipose-derived stromal/progenitor cells. *Journals Gerontol. - Ser. A Biol. Sci. Med. Sci.* **69**, 13–24 (2014).

36. Durandt, C., Dessels, C., da Silva, C., Murdoch, C. & Pepper, M. S. The effect of early rounds of ex vivo expansion and cryopreservation on the adipogenic differentiation capacity of adipose-derived stromal/stem cells. *Sci. Rep.* **9**, 1–13 (2019).

37. Doi, K. *et al.* Differential contributions of graft-derived and host-derived cells in tissue regeneration/remodeling after fat grafting. *Plast. Reconstr. Surg.* **135**, 1607–1617 (2015).

38. Suga, H. *et al.* Adipose tissue remodeling under ischemia: Death of adipocytes and activation of stem/ progenitor cells. *Plast. Reconstr. Surg.* **126**, 1911–1923 (2010).

39. Frazier, T. P. *et al.* Serially transplanted nonpericytic CD146- adipose stromal/stem cells in silk bioscaffolds regenerate adipose tissue in vivo. *Stem Cells* **34**, 1097–1111 (2016).

40. Kroeze, R. J., Knippenberg, M. & Helder, M. N. *Osteogenic differentiation strategies for adipose-derived mesenchymal stem cells. Methods in molecular biology (Clifton, N.J.)* **702**, (2011).

41. Jiabing, F. *et al.* Enhanced osteogenesis of adipose-derived stem cells by regulating bone morphogenetic protein signaling antagonists and agonists. *Stem Cells Transl. Med.* **5**, 539–551 (2016).

42. Hung, B. P. *et al.* Platelet-derived growth factor BB enhances osteogenesis of adipose-derived but not bone marrow-derived mesenchyal stromal/stem cells. *Stem Cells* **33**, 2773–2784 (2015).

43. Rada, T., Reis, R. L. & Gomes, M. E. Distinct stem cells subpopulations isolated from human adipose tissue exhibit different chondrogenic and osteogenic differentiation potential. *Stem Cell Rev. Reports* **7**, 64–76 (2011).

44. Lu, C. H. *et al.* Improved chondrogenesis and engineered cartilage formation from TGF-β3-expressing adipose-derived stem cells cultured in the rotating-shaft bioreactor. *Tissue Eng. - Part A* **18**, 2114–2124 (2012).

45. Puetzer, J. L., Petitte, J. N. & Loboa, E. G. Comparative review of growth factors for induction of three-dimensional in vitro chondrogenesis in human mesenchymal stem cells isolated from bone marrow and adipose tissue. *Tissue Eng. - Part B Rev.* **16**, 435–444 (2010).

46. Eng, J. T. *et al.* In-depth physiological characterization of primary human hepatocytes in a 3D hollow-fiber bioreactor. *Stem Cell Rev. Reports* **7**, 570–578 (2011).

47. Fraser, J. K. *et al.* Plasticity of human adipose stem cells toward endothelial cells and cardiomyocytes. *Nat. Clin. Pract. Cardiovasc. Med.* **3**, 33–37 (2006).

48. Mitchell, J. B. *et al.* Immunophenotype of human adipose-derived cells: temporal changes in stromal-associated and stem cell-associated markers. *Stem Cells* **24**, 376–385 (2006).

49. Lin, G. *et al.* Defining stem and progenitor cells within adipose tissue. *Stem Cells Dev.* **17**, 1053–1063 (2008).

50. Hong, S. J., Traktuev, D. O. & March, K. L. Therapeutic potential of adipose-derived stem cells in vascular growth and tissue repair. *Curr. Opin. Organ Transplant.* **15**, 86–91 (2010).

51. Zimmerlin, L. *et al.* Stromal vascular progenitors in adult human adipose tissue. *Cytom. Part A* **77**, 22–30 (2010).

52. Crisan, M. *et al.* A perivascular origin for mesenchymal stem cells in multiple human organs. *Cell Stem Cell* **3**, 301–313 (2008).

53. Baer, P. C. & Geiger, H. Adipose-derived mesenchymal stromal/stem cells: Tissue localization, characterization, and heterogeneity. *Stem Cells Int.* **2012**, (2012).

54. Bourin, P. *et al.* Stromal cells from the adipose tissue-derived stromal vascular fraction and culture expanded adipose tissue-derived stromal/ stem cells: a joint statement of the International Federation for Adipose Therapeutics (IFATS) and Science and the International S. *Cytotherapy* **15**, 641–648 (2014).

55. Varma, M. J. O. *et al.* Phenotypical and functional characterization of freshly isolated adipose tissue-derived stem cells. *Stem Cells Dev.* **16**, 91–104 (2007).

56. Baer, P. C. Adipose-derived mesenchymal stromal/stem cells: An update on their phenotype in vivo and in vitro. *World J. Stem Cells* **6**, 256 (2014).

57. Cawthorn, W. P., Scheller, E. L. & MacDougald, O. A. Adipose tissue stem cells meet preadipocyte commitment: Going back to the future. *J. Lipid Res.* **53**, 227–246 (2012).

58. Tsekouras, A. *et al.* Comparison of the viability and yield of adipose-derived stem cells (ASCs) from different donor areas. *In Vivo (Brooklyn).* **31**, 1229–1234 (2017).

59. Cleal, L., Aldea, T. & Chau, Y. Y. Fifty shades of white: Understanding heterogeneity in white adipose stem cells. *Adipocyte* **6**, 205–216 (2017).

60. Bunnell, B. A., Flaat, M., Gagliardi, C., Patel, B. & Ripoll, C. Adipose-derived stem cells: isolation, expansion and differentiation. *Methods* **45**, 115–120 (2008).

61. Danoviz, M. E. *et al.* Adipose tissue-derived stem cells from humans and mice differ in proliferative capacity and genome stability in long-term cultures. *Stem Cells Dev.* **20**, 661–670 (2011).

62. Choi, E. W. *et al.* Characteristics of mouse adipose tissue-derived stem cells and therapeutic comparisons between syngeneic and allogeneic adipose tissue-derived stem

cell transplantation in experimental autoimmune thyroiditis. *Cell Transplant.* **23**, 873–887 (2014).

63. Zheng, B., Cao, B., Li, G. & Huard, J. Mouse adipose-derived stem cells undergo multilineage differentiation in vitro but primarily osteogenic and chondrogenic differentiation in vivo. *Tissue Eng.* **12**, 1891–1901 (2006).

64. Taha, M. F. & Hedayati, V. Isolation, identification and multipotential differentiation of mouse adipose tissue-derived stem cells. *Tissue Cell* **42**, 211–216 (2010).

65. Yamamoto, N. *et al.* Isolation of multipotent stem cells from mouse adipose tissue. *J. Dermatol. Sci.* **48**, 43–52 (2007).

66. Efimenko, A., Starostina, E., Kalinina, N. & Stolzing, A. Angiogenic properties of aged adipose derived mesenchymal stem cells after hypoxic conditioning. *J. Transl. Med.* **9**, 1–13 (2011).

67. Luna, A. C. L. *et al.* Characterization of adipose-derived stem cells of anatomical region from mice. *BMC Res. Notes* **7**, 1–12 (2014).

68. Daley, W. P., Peters, S. B. & Larsen, M. Extracellular matrix dynamics in development and regenerative medicine. *J. Cell Sci.* **121**, 255–264 (2008).

69. Yue, B. Biology of the extracellular matrix: An overview. *J. Glaucoma* **23**, S20–S23 (2014).

70. Mori, S., Kiuchi, S., Ouchi, A., Hase, T. & Murase, T. Characteristic expression of extracellular matrix in subcutaneous adipose tissue development and adipogenesis; Comparison with visceral adipose tissue. *Int. J. Biol. Sci.* **10**, 825–833 (2014).

71. Datta, R., Podolsky, M. J. & Atabai, K. Fat fibrosis: friend or foe? *JCI insight* **3**, 1–16 (2018).

72. Muiznieks, L. D. & Keeley, F. W. Molecular assembly and mechanical properties of the extracellular matrix: A fibrous protein perspective. *Biochim. Biophys. Acta - Mol. Basis*

Dis. **1832**, 866–875 (2013).

73. Lin, D., Chun, T.-H. & Kang, L. Adipose extracellular matrix remodelling in obesity and insulin resistance. *Biochem. Pharmacol.* **119**, 8–16 (2016).

74. Mariman, E. C. M. & Wang, P. Adipocyte extracellular matrix composition, dynamics and role in obesity. *Cell. Mol. Life Sci.* **67**, 1277–1292 (2010).

75. Reggio, S. *et al.* Increased basement membrane components in adipose tissue during obesity: Links with TGF- And metabolic phenotypes. *J. Clin. Endocrinol. Metab.* **101**, 2578–2587 (2016).

76. Oh, C.-D. & Chun, J.-S. Signaling mechanisms leading to the regulation of differentiation and apoptosis of articular chondrocytes by insulin-like growth factor-1. *J. Biol. Chem.* **278**, 36563–36571 (2003).

77. Martinez-Santibanez, G. *et al.* Obesity-induced remodeling of the adipose tissue elastin network is independent of the metalloelastase MMP-12. *Adipocyte* **4**, 264–272 (2015).

78. Jayadev, R. & Sherwood, D. R. Basement membranes. *Curr. Biol.* **27**, R207–R211 (2017).

79. Chun, T.-H. Peri-adipocyte ECM remodeling in obesity and adipose tissue fibrosis. *Adipocyte* **1**, 89–95 (2012).

80. Dai, J., Ma, M., Feng, Z. & Pastor-Pareja, J. C. Inter-adipocyte Adhesion and Signaling by Collagen IV Intercellular Concentrations in Drosophila. *Curr. Biol.* **27**, 2729-2740.e4 (2017).

81. Sillat, T. *et al.* Basement membrane collagen type IV expression by human mesenchymal stem cells during adipogenic differentiation. *J. Cell. Mol. Med.* **16**, 1485–1495 (2012).

82. Shoulders, M. D. & Raines, R. T. Collagen Structure and Stability. *Annu. Rev. Biochem.* **78**, 929–958 (2009).

83. Wenstrup, R. J. *et al.* Type V collagen controls the initiation of collagen fibril assembly. *J. Biol. Chem.* **279**, 53331–53337 (2004).

84. Divoux, A. *et al.* Fibrosis in human adipose tissue: Composition, distribution, and link with lipid metabolism and fat mass loss. *Diabetes* **59**, 2817–2825 (2010).

85. Rupnick, M. A. *et al.* From the Cover: Adipose tissue mass can be regulated through the vasculature. *Proc. Natl. Acad. Sci.* **99**, 10730–10735 (2002).

86. Barczyk, M. & Carracedo, S. Integrins. *Cell Tissue Res.* **339**, 269–280 (2010).

87. Bouloumié, A., Sengenès, C., Portolan, G., Galitzky, J. & Lafontan, M. Adipocyte produces matrix metalloproteinases 2 and 9 involvement in adipose differentiation. *Diabetes* **50**, 2080–2086 (2001).

88. Berg, G., Barchuk, M. & Miksztowicz, V. Behavior of metalloproteinases in adipose tissue, liver and arterial wall: an update of extracellular matrix remodeling. *Cells* **8**, 158 (2019).

89. Chavey, C. *et al.* Matrix metalloproteinases are differentially expressed in adipose tissue during obesity and modulate adipocyte differentiation. *J. Biol. Chem.* **278**, 11888–11896 (2003).

90. Maquoi, E., Munaut, C., Colige, A., Collen, D. & Roger Lijnen, H. Modulation of adipose tissue expression of murine MMP and their TIMP with obesity. *Diabetes* **51**, 1093–1101 (2002).

91. Patrick, C. W. Tissue engineering strategies for adipose tissue repair. *Anat. Rec.* **263**, 361–366 (2001).

92. Doornaert, M., Colle, J., De Maere, E., Declercq, H. & Blondeel, P. Autologous fat grafting: Latest insights. *Ann. Med. Surg.* **37**, 47–53 (2019).

93. Yoshimura, K. & Coleman, S. R. Complications of fat grafting: how they occur and how to find, avoid, and treat them. *Clin. Plast. Surg.* **42**, 383–388 (2015).

94. Bray, D., Hopkins, C. & Roberts, D. N. A review of dermal fillers in facial plastic surgery. *Curr. Opin. Otolaryngol. Head Neck Surg.* **18**, 295–302 (2010).

95. Vasei, N., Shishegar, A., Ghalkhani, F. & Darvishi, M. Fat necrosis in the breast: A systematic review of clinical. *Lipids Health Dis.* **18**, 1–9 (2019).

96. Zielins, E. R., Brett, E. A., Longaker, M. T. & Wan, D. C. Autologous fat grafting: the science behind the surgery. *Aesthetic Surg. J.* **36**, 488–496 (2016).

97. La Gatta, A., Schiraldi, C., Papa, A. & De Rosa, M. Comparative analysis of commercial dermal fillers based on crosslinked hyaluronan: Physical characterization and in vitro enzymatic degradation. *Polym. Degrad. Stab.* **96**, 630–636 (2011).

98. Allemann, I. B. & Baumann, L. Hyaluronic acid gel (Juvéderm^{TM}) preparations in the treatment of facial wrinkles and folds. *Clin. Interv. Aging* **3**, 629–634 (2008).

99. Tran, C., Carraux, P., Micheels, P., Kaya, G. & Salomon, D. In vivo bio-integration of three hyaluronic acid fillers in human skin: A histological study. *Dermatology* **228**, 47–54 (2014).

100. Rohrich, R. J., Ghavami, A. & Crosby, M. A. The role of hyaluronic acid fillers (Restylane) in facial cosmetic surgery: Review and technical considerations. *Plast. Reconstr. Surg.* **120**, 41–54 (2007).

101. Matarasso, S. L., Carruthers, J. D. & Jewell, M. L. Consensus recommendations for soft-tissue augmentation with nonanimal stabilized hyaluronic acid (Restylane). *Plast. Reconstr. Surg.* **117**, 3–34 (2006).

102. Salzberg, C. A., Ashikari, A. Y., Koch, R. M. & Chabner-Thompson, E. An 8-year experience of direct-to-implant immediate breast reconstruction using human acellular dermal matrix (AlloDerm). *Plast. Reconstr. Surg.* **127**, 514–524 (2011).

103. Nava, M. B., Rancati, A., Angrigiani, C., Catanuto, G. & Rocco, N. How to prevent complications in breast augmentation. *Gland Surg.* **6**, 210–217 (2017).

104. MacAdam, S. A., Bovill, E. S., Buchel, E. W. & Lennox, P. A. Evidence-based medicine: autologous breast reconstruction. *Plast. Reconstr. Surg.* **139**, 204e-229e (2017).

105. Vardanian, A. J. *et al.* Comparison of implant-based immediate breast reconstruction with and without acellular dermal matrix. *Plast. Reconstr. Surg.* **128**, 403–410 (2011).

106. Lijnen, H. R. Angiogenesis and obesity. *Cardiovasc. Res.* **78**, 286–293 (2008).

107. Han, J. *et al.* The spatiotemporal development of adipose tissue. *Development* **138**, 5027–5037 (2011).

108. Eto, H. *et al.* The fate of adipocytes after nonvascularized fat grafting: Evidence of early death and replacement of adipocytes. *Plast. Reconstr. Surg.* **129**, 1081–1092 (2012).

109. Brett, E. *et al.* A review of cell-based strategies for soft tissue reconstruction. *Tissue Eng. - Part B Rev.* **23**, 336–346 (2017).

110. Mitchell, A. C., Briquez, P. S., Hubbell, J. A. & Cochran, J. R. Engineering growth factors for regenerative medicine applications. *Acta Biomater.* **30**, 1–12 (2016).

111. Marquez, M. P. *et al.* The role of cellular proliferation in adipogenic differentiation of human adipose tissue-derived mesenchymal stem cells. *Stem Cells Dev.* **26**, 1578–1595 (2017).

112. Gorecka, J. *et al.* The potential and limitations of induced pluripotent stem cells to achieve wound healing. *Stem Cell Res. Ther.* **10**, 1–10 (2019).

113. Strioga, M., Viswanathan, S., Darinskas, A., Slaby, O. & Michalek, J. Same or not the same? Comparison of adipose tissue-derived versus bone marrow-derived mesenchymal stem and stromal cells. *Stem Cells Dev.* **21**, 2724–2752 (2012).

114. Ivanova-Todorova, E. *et al.* Adipose tissue-derived mesenchymal stem cells are more potent suppressors of dendritic cells differentiation compared to bone marrow-derived mesenchymal stem cells. *Immunol. Lett.* **126**, 37–42 (2009).

115. Ribeiro, A. *et al.* Mesenchymal stem cells from umbilical cord matrix, adipose tissue and bone marrow exhibit different capability to suppress peripheral blood B, natural killer and T cells. *Stem Cell Res. Ther.* **4**, (2013).

116. Mohamed-Ahmed, S. *et al.* Adipose-derived and bone marrow mesenchymal stem cells: A donor-matched comparison. *Stem Cell Res. Ther.* **9**, 1–15 (2018).

117. Bertozzi, N., Simonacci, F., Grieco, M. P., Grignaffini, E. & Raposio, E. The biological and clinical basis for the use of adipose-derived stem cells in the field of wound healing. *Ann. Med. Surg.* **20**, 41–48 (2017).

118. Dong, Z., Peng, Z., Chang, Q. & Lu, F. The survival condition and immunoregulatory function of adipose stromal vascular fraction (SVF) in the early stage of nonvascularized adipose transplantation. *PLoS One* **8**, 1–11 (2013).

119. Nyberg, E., Farris, A., O'Sullivan, A., Rodriguez, R. & Grayson, W. Comparison of stromal vascular fraction and passaged adipose-derived stromal/stem cells as point-of-care agents for bone regeneration. *Tissue Eng. Part A* **25**, 1459–1469 (2019).

120. Zhou, L. *et al.* Comparison of human adipose stromal vascular fraction and adipose-derived mesenchymal stem cells for the attenuation of acute renal ischemia/reperfusion injury. *Sci. Rep.* **7**, 1–9 (2017).

121. Sheu, J. J. *et al.* Therapeutic effects of adipose derived fresh stromal vascular fraction-containing stem cells versus cultured adipose derived mesenchymal stem cells on rescuing heart function in rat after acute myocardial infarction. *Am. J. Transl. Res.* **11**, 67–86 (2019).

122. You, D. *et al.* Comparative study of autologous stromal vascular fraction and adipose-derived stem cells for erectile function recovery in a rat model of cavernous nerve injury. *Stem Cells Transl. Med.* 351–358 (2014).

123. Minonzio, G. *et al.* Frozen adipose-derived mesenchymal stem cells maintain high capability to grow and differentiate. *Cryobiology* **69**, 211–216 (2014).

124. Bajek, A. *et al.* Adipose-derived stem cells as a tool in cell-based therapies. *Arch. Immunol. Ther. Exp. (Warsz).* **64**, 443–454 (2016).

125. Doornaert, M. *et al.* Human decellularized dermal matrix seeded with adipose-derived

stem cells enhances wound healing in a murine model: Experimental study. *Ann. Med. Surg.* **46**, 4–11 (2019).

126. Kallmeyer, K. *et al.* Fate of systemically and locally administered adipose-derived mesenchymal stromal cells and their effect on wound healing. *Stem Cells Transl. Med.* 1–14 (2019). doi:10.1002/sctm.19-0091

127. Robb, K. P., Shridhar, A. & Flynn, L. E. Decellularized matrices as cell-instructive scaffolds to guide tissue-specific regeneration. *ACS Biomater. Sci. Eng.* **4**, 3627–3643 (2018).

128. Wu, X., Black, L., Santacana-Laffitte, G. & Patrick Jr., C. W. Preparation and assessment of glutaraldehyde-crosslinked collagen-chitosan hydrogels for adipose tissue engineering. *J. Biomed. Mater. Res. A* 59–65 (2006). doi:10.1002/jbm.a

129. Iyyanki, T. S. *et al.* Adipose-derived stem-cell-seeded non-cross-linked porcine acellular dermal matrix increases cellular infiltration, vascular infiltration, and mechanical strength of ventral hernia repairs. *Tissue Eng. - Part A* **21**, 475–485 (2015).

130. Zhang, Q. *et al.* Engineering vascularized soft tissue flaps in an animal model using human adipose-derived stem cells and VEGF+PLGA/PEG microspheres on a collagen-chitosan scaffold with a flow-through vascular pedicle. *Biomaterials* **73**, 198–213 (2015).

131. Cheung, H. K. *et al.* Composite hydrogel scaffolds incorporating decellularized adipose tissue for soft tissue engineering with adipose-derived stem cells. *Biomaterials* **35**, 1914–1923 (2013).

132. Mizuno, H. *et al.* Adipose-Derived Stem Cells in Regenerative Medicine. *Princ. Gender-Specific Med. Gend. Genomic Era Third Ed.* 459–479 (2017). doi:10.1016/B978-0-12-803506-1.00050-4

133. Suga, H., Glotzbach, J. P., Sorkin, M., Longaker, M. T. & Gurtner, G. C. Paracrine mechanism of angiogenesis in adipose-derived stem cell transplantation. *Ann. Plast. Surg.* **72**, 234–41 (2014).

134. Garza, R. M. *et al.* Adipose-derived stromal cell gene expression in cell-assisted lipotransfer. *Plast. Reconstr. Surg.* **135**, 1045–1055 (2015).

135. Matsuda, K. *et al.* Adipose-derived stem cells promote angiogenesis and tissue formation for in vivo tissue engineering. *Tissue Eng. - Part A* **19**, 1327–1335 (2013).

136. Ding, D. *et al.* Precise and long-term tracking of adipose-derived stem cells and their regenerative capacity via superb bright and stable organic nanodots. *ACS Nano* **8**, 12620–12631 (2014).

137. Fukumura, D. *et al.* Paracrine regulation of angiogenesis and adipocyte differentiation during in vivo adipogenesis. *Circ Res* **93**, 1–20 (2009).

138. Kapur, S. K. & Katz, A. J. Review of the adipose derived stem cell secretome. *Biochimie* **95**, 2222–2228 (2013).

139. Miranville, A. *et al.* Improvement of postnatal neovascularization by human adipose tissue-derived stem cells. *Circulation* **110**, 349–355 (2004).

140. Rehman, J. *et al.* Secretion of angiogenic and antiapoptotic factors by human adipose stromal cells. *Circulation* **109**, 1292–1298 (2004).

141. Rohringer, S. *et al.* Mechanisms of vasculogenesis in 3D fibrin matrices mediated by the interaction of adipose-derived stem cells and endothelial cells. *Angiogenesis* **17**, 921–933 (2014).

142. Merfeld-Clauss, S., Gollahalli, N., March, K. L. & Traktuev, D. O. Adipose tissue progenitor cells directly interact with endothelial cells to induce vascular network formation. *Tissue Eng. - Part A* **16**, 2953–2966 (2010).

143. Grainger, S. J. & Putnam, A. J. Assessing the permeability of engineered capillary networks in a 3D culture. *PLoS One* **6**, (2011).

144. Yañez, R. *et al.* Adipose tissue-derived mesenchymal stem cells have in vivo immunosuppressive properties applicable for the control of the Graft-Versus-Host disease.

Stem Cells **24**, 2582–2591 (2006).

145. Wang, Y. C., Chen, R. F., Brandacher, G., Lee, W. P. A. & Kuo, Y. R. The suppression effect of dendritic cells maturation by adipose-derived stem cells through TGF-β1 related pathway. *Exp. Cell Res.* **370**, 708–717 (2018).

146. Anderson, P. *et al.* Adipose-derived mesenchymal stromal cells induce immunomodulatory macrophages which protect from experimental colitis and sepsis. *Gut* **62**, 1131–1141 (2013).

147. Manning, C. N. *et al.* Adipose-derived mesenchymal stromal cells modulate tendon fibroblast responses to macrophage-induced inflammation in vitro. *Stem Cell Res. Ther.* **6**, 74 (2015).

148. Wynn, T. A. & Vannella, K. M. Macrophages in tissue repair, regeneration, and fibrosis. *Immunity* **44**, 450–462 (2016).

149. Hattori, H. *et al.* Angiogenesis following cell injection is induced by an excess inflammatory response coordinated by bone marrow cells. *Cell Transplant.* **22**, 2381–2392 (2013).

150. Hattori, H. & Ishihara, M. Altered protein secretions during interactions between adipose tissue- or bone marrow-derived stromal cells and inflammatory cells. *Stem Cell Res. Ther.* **6**, 1–10 (2015).

151. Li, Z. *et al.* Macrophages undergo M1-to-M2 transition in adipose tissue regeneration in a rat tissue engineering model. *Artif. Organs* **40**, E167–E178 (2016).

152. Adutler-Lieber, S. *et al.* Human macrophage regulation via interaction with cardiac adipose tissue-derived mesenchymal stromal cells. *J. Cardiovasc. Pharmacol. Ther.* **18**, 78–86 (2013).

153. Freytes, D. O., Kang, J. W., Marcos-Campos, I. & Vunjak-Novakovic, G. Macrophages modulate the viability and growth of human mesenchymal stem cells. *J. Cell. Biochem.* **114**, 220–229 (2013).

154. Kim, J. *et al.* Proteomic analysis of Tumor Necrosis Factor-α-induced secretome of human adipose tissue-derived mesenchymal stem cells. *J. Proteome Res.* **9**, 1754–1762 (2010).

155. Murray, P. J. & Wynn, T. A. Protective and pathogenic functions of macrophage subsets. *Nat. Rev. Immunol.* **11**, 723–737 (2011).

156. Novak, M. L. & Koh, T. J. Phenotypic transitions of macrophages orchestrate tissue repair. *Am. J. Pathol.* **183**, 1352–1363 (2013).

157. Epelman, S., Lavine, K. J. & Randolph, G. J. Origin and function of tissue macrophages. *Immunity* **41**, 21–35 (2014).

158. Röszer, T. Understanding the biology of self-renewing macrophages. *Cells* **7**, 103 (2018).

159. Pittet, M. J., Nahrendorf, M. & Swirski, F. K. The journey from stem cell to macrophage. *Ann. N. Y. Acad. Sci.* **1319**, 1–18 (2014).

160. Hamilton, T. A., Zhao, C., Pavicic, P. G. & Datta, S. Myeloid colony-stimulating factors as regulators of macrophage polarization. *Front. Immunol.* **5**, 1–6 (2014).

161. Misharin, A. V. *et al.* Nonclassical Ly6C- monocytes drive the development of inflammatory arthritis in mice. *Cell Rep.* **9**, 591–604 (2014).

162. Gordon, S., Plüddemann, A. & Martinez Estrada, F. Macrophage heterogeneity in tissues: Phenotypic diversity and functions. *Immunol. Rev.* **262**, 36–55 (2014).

163. Ruytinx, P., Proost, P., Van Damme, J. & Struyf, S. Chemokine-induced macrophage polarization in inflammatory conditions. *Front. Immunol.* **9**, 1–12 (2018).

164. Mosser, D. M. & Edwards, J. P. Exploring the full spectrum of macrophage activation. *Nat. Rev. Immunol.* **8**, 958–69 (2008).

165. Han, T. T. Y., Toutounji, S., Amsden, B. G. & Flynn, L. E. Adipose-derived stromal cells mediate in vivo adipogenesis, angiogenesis and inflammation in decellularized adipose tissue bioscaffolds. *Biomaterials* **72**, 125–137 (2015).

166. Brown, B. N., Valentin, J. E., Stewart-Akers, A. M., McCabe, G. P. & Badylak, S. F. Macrophage phenotype and remodeling outcomes in response to biologic scaffolds with and without a cellular component. *Biomaterials* **30**, 1482–1491 (2009).

167. Spiller, K. L. & Koh, T. J. Macrophage-based therapeutic strategies in regenerative medicine. *Adv. Drug Deliv. Rev.* **122**, 74–83 (2017).

168. Morris, A. H., Stamer, D. K. & Kyriakides, T. R. The host response to naturally-derived extracellular matrix biomaterials. *Semin. Immunol.* **29**, 72–91 (2017).

169. Boscá, L., Zeini, M., Través, P. G. & Hortelano, S. Nitric oxide and cell viability in inflammatory cells: A role for NO in macrophage function and fate. *Toxicology* **208**, 249–258 (2005).

170. Rath, M., Müller, I., Kropf, P., Closs, E. I. & Munder, M. Metabolism via arginase or nitric oxide synthase : two competing arginine pathways in macrophages. **5**, 1–10 (2014).

171. Novak, M. L., Weinheimer-Haus, E. M. & Koh, T. J. Macrophage activation and skeletal muscle healing following traumatic injury. *J. Pathol.* **232**, 344–55 (2014).

172. Anderson, J. M., Rodriguez, A. & Chang, D. T. Foreign body reaction to biomaterials. *Semin. Immunol.* **20**, 86–100 (2008).

173. Lin, Y. W. & Wei, L. N. Innate immunity orchestrates adipose tissue homeostasis. *Horm. Mol. Biol. Clin. Investig.* **31**, 5–12 (2017).

174. Mosser, D. M. & Edwards, J. P. Exploring the full spectrum of macrophage polarization. *Nat Rev Immunol.* **8**, 958–969 (2009).

175. Saeij, J. P. *et al.* Macrophage activation and polarization: nomenclature and experimental guidelines. *Immunity* **41**, 14–20 (2014).

176. Mantovani, A. *et al.* The chemokine system in diverse forms of macrophage activation and polarization. *Trends Immunol.* **25**, 677–686 (2004).

177. Avdic, S. *et al.* Human cytomegalovirus interleukin-10 polarizes monocytes toward a

deactivated M2c phenotype to repress host immune responses. *J. Virol.* **87**, 10273–82 (2013).

178. Cho, C. H. *et al.* Angiogenic role of LYVE-1-positive macrophages in adipose tissue. *Circ. Res.* **100**, (2007).

179. Cai, J., Feng, J., Liu, K., Zhou, S. & Lu, F. Early macrophage infiltration improves fat graft survival by inducing angiogenesis and hematopoietic stem cell recruitment. *Plast. Reconstr. Surg.* **141**, 376–386 (2018).

180. Lilja, H. E. *et al.* An adipoinductive role of inflammation in adipose tissue engineering: key factors in the early development of engineered soft tissues. *Stem Cells Dev.* **22**, 1602–13 (2013).

181. Debels, H. *et al.* Macrophages play a key role in angiogenesis and adipogenesis in a mouse tissue engineering model. *Tissue Eng. Part A* **19**, 2615–25 (2013).

182. Spiller, K. L. *et al.* The role of macrophage phenotype in vascularization of tissue engineering scaffolds. *Biomaterials* **35**, 4477–4488 (2014).

183. Haque, M. A., Kurokawa, T. & Gong, J. P. Super tough double network hydrogels and their application as biomaterials. *Polymer (Guildf).* **53**, 1805–1822 (2012).

184. Kim, J. S., Choi, J. S. & Cho, Y. W. Cell-Free Hydrogel System Based on a Tissue-Specific Extracellular Matrix for In Situ Adipose Tissue Regeneration. *ACS Appl. Mater. Interfaces* **9**, 8581–8588 (2017).

185. Phipps, K. D. *et al.* Alternatively activated M2 macrophages improve autologous fat graft survival in a mouse model through induction of angiogenesis. *Plast. Reconstr. Surg.* **135**, 140–149 (2015).

186. Samani, A., Zubovits, J. & Plewes, D. Elastic moduli of normal and pathological human breast tissues: An inversion-technique-based investigation of 169 samples. *Phys. Med. Biol.* **52**, 1565–1576 (2007).

187. Young, D. A., Choi, Y. S., Engler, A. J. & Christman, K. L. Stimulation of adipogenesis of adult adipose-derived stem cells using substrates that mimic the stiffness of adipose tissue. *Biomaterials* **34**, 8581–8588 (2013).

188. Lee, J., Abdeen, A. A., Tang, X., Saif, T. A. & Kilian, K. A. Matrix directed adipogenesis and neurogenesis of mesenchymal stem cells derived from adipose tissue and bone marrow. *Acta Biomater.* **42**, 46–55 (2016).

189. Zhang, T. *et al.* Regulating osteogenesis and adipogenesis in adipose-derived stem cells by controlling underlying substrate stiffness. *J. Cell. Physiol.* **233**, 3418–3428 (2018).

190. Benayahu, D., Wiesenfeld, Y. & Sapir-Koren, R. How is mechanobiology involved in mesenchymal stem cell differentiation toward the osteoblastic or adipogenic fate? *J. Cell. Physiol.* **234**, 12133–12141 (2019).

191. Marra, K. G. *et al.* FGF-2 enhances vascularization for adipose tissue engineering. *Plast. Reconstr. Surg.* **121**, 1153–1164 (2008).

192. Choi, Y. S. *et al.* Adipogenic differentiation of adipose tissue derived adult stem cells in nude mouse. *Biochem. Biophys. Res. Commun.* **345**, 631–637 (2006).

193. Cho, S. W. *et al.* Engineered adipose tissue formation enhanced by basic fibroblast growth factor and a mechanically stable environment. *Cell Transplant.* **16**, 421–434 (2007).

194. Shanti, R. M. *et al.* In vitro adipose tissue engineering using an electrospun nanofibrous scaffold. *Ann. Plast. Surg.* **61**, 566–571 (2008).

195. Wang, W., Cao, B., Cui, L., Cai, J. & Yin, J. Adipose tissue engineering with human adipose tissue-derived adult stem cells and a novel porous scaffold. *J. Biomed. Mater. Res. - Part B Appl. Biomater.* **101 B**, 68–75 (2013).

196. Xu, J., Chen, Y., Yue, Y., Sun, J. & Cui, L. Reconstruction of epidural fat with engineered adipose tissue from adipose derived stem cells and PLGA in the rabbit dorsal laminectomy model. *Biomaterials* **33**, 6965–6973 (2012).

197. Cho, S. W. *et al.* Enhancement of adipose tissue formation by implantation of adipogenic-differentiated preadipocytes. *Biochem. Biophys. Res. Commun.* **345**, 588–594 (2006).

198. Patrick, C. W., Zheng, B., Johnston, C. & Reece, G. P. Long-term implantation of preadipocyte-seeded PLGA scaffolds. *Tissue Eng.* **8**, 283–293 (2002).

199. Gentile, P., Chiono, V., Carmagnola, I. & Hatton, P. V. An overview of poly(lactic-co-glycolic) Acid (PLGA)-based biomaterials for bone tissue engineering. *Int. J. Mol. Sci.* **15**, 3640–3659 (2014).

200. Place, E. S., George, J. H., Williams, C. K. & Stevens, M. M. Synthetic polymer scaffolds for tissue engineering. *Chem. Soc. Rev.* **38**, 1139–1151 (2009).

201. Chew, S. A., Arriaga, M. A. & Hinojosa, V. A. Effects of surface area to volume ratio of PLGA scaffolds with different architectures on scaffold degradation characteristics and drug release kinetics. *J. Biomed. Mater. Res. - Part A* **104**, 1202–1211 (2016).

202. Lu, L. *et al.* In vitro and in vivo degradation of porous poly(DL-lactic-co-glycolic acid) foams. *Biomaterials* **21**, 1837–1845 (2000).

203. Pan, Z. & Ding, J. Poly(lactide-co-glycolide) porous scaffolds for tissue engineering and regenerative medicine. *Interface Focus* **2**, 366–377 (2012).

204. Lee, S., Tong, X. & Yang, F. The effects of varying poly(ethylene glycol) hydrogel crosslinking density and the crosslinking mechanism on protein accumulation in three-dimensional hydrogels. *Acta Biomater.* **10**, 4167–4174 (2014).

205. Liu, Y. & Chan-Park, M. B. Hydrogel based on interpenetrating polymer networks of dextran and gelatin for vascular tissue engineering. *Biomaterials* **30**, 196–207 (2009).

206. Lin, C. C. & Anseth, K. S. PEG hydrogels for the controlled release of biomolecules in regenerative medicine. *Pharm. Res.* **26**, 631–643 (2009).

207. Wade, R. J. & Burdick, J. A. Engineering ECM signals into biomaterials. *Mater. Today* **15**, 454–459 (2012).

208. Sreejalekshmi, K. G. & Nair, P. D. Biomimeticity in tissue engineering scaffolds through synthetic peptide modifications-Altering chemistry for enhanced biological response. *J. Biomed. Mater. Res. - Part A* **96 A**, 477–491 (2011).

209. Ali, S., Saik, J. E., Gould, D. J., Dickinson, M. E. & West, J. L. Immobilization of cell-adhesive laminin peptides in degradable PEGDA hydrogels influences endothelial cell tubulogenesis. *Biores. Open Access* **2**, 241–249 (2013).

210. Brandl, F. P., Seitz, A. K., Teßmar, J. K. V., Blunk, T. & Göpferich, A. M. Enzymatically degradable poly(ethylene glycol) based hydrogels for adipose tissue engineering. *Biomaterials* **31**, 3957–3966 (2010).

211. Bellas, E. *et al.* Injectable silk foams for soft tissue regeneration. *Adv. Healthc. Mater.* **4**, 452–459 (2015).

212. Sang, Y. *et al.* Biomimetic silk scaffolds with an amorphous structure for soft tissue engineering. *ACS Appl. Mater. Interfaces* **10**, 9290–9300 (2018).

213. Han, H. *et al.* Silk biomaterials with vascularization capacity. *Adv. Funct. Mater.* **26**, 421–432 (2016).

214. Rodríguez-Vázquez, M., Vega-Ruiz, B., Ramos-Zúñiga, R., Saldaña-Koppel, D. A. & Quiñones-Olvera, L. F. Chitosan and its potential use as a scaffold for tissue engineering in regenerative medicine. *Biomed Res. Int.* **2015**, (2015).

215. Croisier, F. & Jérôme, C. Chitosan-based biomaterials for tissue engineering. *Eur. Polym. J.* **49**, 780–792 (2013).

216. Debnath, T. *et al.* Proliferation and differentiation potential of human adipose-derived stem cells grown on chitosan hydrogel. *PLoS One* **10**, 1–14 (2015).

217. Kang, S. W. *et al.* The effect of conjugating RGD into 3D alginate hydrogels on adipogenic differentiation of human adipose-derived stromal cells. *Macromol. Biosci.* **11**, 673–679 (2011).

218. Guneta, V., Loh, Q. L. & Choong, C. Cell-secreted extracellular matrix formation and differentiation of adipose-derived stem cells in 3D alginate scaffolds with tunable properties. *J. Biomed. Mater. Res. - Part A* **104**, 1090–1101 (2016).

219. Jing, W. *et al.* Ectopic adipogenesis of preconditioned adipose-derived stromal cells in an alginate system. *Cell Tissue Res.* **330**, 567–572 (2007).

220. Chuang, C.-H., Lin, R.-Z., Melero-Martin, J. M. & Chen, Y.-C. Comparison of covalently and physically cross-linked collagen hydrogels on mediating vascular network formation for engineering adipose tissue. *Artif. Cells, Nanomedicine, Biotechnol.* **46**, 434–447 (2018).

221. Itoi, Y., Takatori, M., Hyakusoku, H. & Mizuno, H. Comparison of readily available scaffolds for adipose tissue engineering using adipose-derived stem cells. *J. Plast. Reconstr. Aesthetic Surg.* **63**, 858–864 (2010).

222. Tedeschi, A. *et al.* Human adipose-derived stem cells promote vascularization of collagen-based scaffolds transplanted into nude mice. *Regen. Med.* **11**, 261–271 (2016).

223. Davidenko, N., Campbell, J. J., Thian, E. S., Watson, C. J. & Cameron, R. E. Collagen-hyaluronic acid scaffolds for adipose tissue engineering. *Acta Biomater.* **6**, 3957–3968 (2010).

224. Chang, K. H., Liao, H. T. & Chen, J. P. Preparation and characterization of gelatin/hyaluronic acid cryogels for adipose tissue engineering: In vitro and in vivo studies. *Acta Biomater.* **9**, 9012–9026 (2013).

225. Spearman, B. S. *et al.* Tunable methacrylated hyaluronic acid-based hydrogels as scaffolds for soft tissue engineering applications. *J. Biomed. Mater. Res. - Part A* (2019). doi:10.1002/jbm.a.36814

226. Song, Y. H., Shon, S. H., Shan, M., Stroock, A. & Fischbach, C. Adipose-derived stem cells increase angiogenesis through matrix metalloproteinase-dependent collagen remodeling. *Integr. Biol.* **15**, 205–215 (2016).

227. Zöller, N. *et al.* Collagen I promotes adipocytogenesis in adipose-derived stem cells in vitro. *Cells* **8**, 302 (2019).

228. Mccoy, M. G., Seo, B. R., Choi, S. & Fischbach, C. Collagen I hydrogel microarchitechture and composition conjointly regulate vascular network formation. *Acta Biomater.* **44**, 200–208 (2016).

229. Mauney, J. R. *et al.* Engineering adipose-like tissue in vitro and in vivo utilizing human bone marrow and adipose-derived mesenchymal stem cells with silk fibroin 3D scaffolds. *Biomaterials* **28**, 5280–5290 (2007).

230. Charulatha, V. & Rajaram, A. Influence of different crosslinking treatments on the physical properties of collagen membranes. *Biomaterials* **24**, 759–767 (2003).

231. Mi, S., Chen, B., Wright, B. & Connon, C. J. Plastic compression of a collagen gel forms a much improved scaffold for ocular surface tissue engineering over conventional collagen gels. *J. Biomed. Mater. Res. - Part A* **95 A**, 447–453 (2010).

232. Klingman, A. M. & Armstrong, R. C. Histologic response to intradermal Zyderm and Zyplast (glutaraldehyde cross-linked) collagen in Humans. *J. Dermatologic Surg. Oncol.* 351–357 (1986).

233. Gilpin, A. & Yang, Y. Decellularization strategies for regenerative medicine: from processing techniques to applications. *Biomed Res. Int.* **2017**, (2017).

234. Flynn, L. E. The use of decellularized adipose tissue to provide an inductive microenvironment for the adipogenic differentiation of human adipose-derived stem cells. *Biomaterials* **31**, 4715–4724 (2010).

235. Flynn, L., Prestwich, G. D., Semple, J. L. & Woodhouse, K. A. Adipose tissue engineering in vivo with adipose-derived stem cells on naturally derived scaffolds. *J. Biomed. Mater. Res. - Part A* **89**, 929–941 (2009).

236. Choi, J. S. *et al.* Decellularized extracellular matrix derived from human adipose tissue as a potential scaffold for allograft tissue engineering. *J. Biomed. Mater. Res. - Part A* **97 A**,

292–299 (2011).

237. Yu, C. *et al.* Porous decellularized adipose tissue foams for soft tissue regeneration. *Biomaterials* **34**, 3290–3302 (2013).

238. Russo, V., Omidi, E., Samani, A., Hamilton, A. & Flynn, L. E. Porous, ventricular extracellular matrix-derived foams as a platform for cardiac cell culture. *Biores. Open Access* **4**, 374–388 (2015).

239. Flynn, L. E., Brown, C., Kornmuller, A., Hoare, T. & Yu, C. Decellularized adipose tissue microcarriers as a dynamic culture platform for human adipose-derived stem/stromal cell expansion. *Biomaterials* **120**, 66–80 (2016).

240. Xing, Q. *et al.* Decellularization of fibroblast cell sheets for natural extracellular matrix scaffold preparation. *Tissue Eng. - Part C Methods* **21**, 77–87 (2015).

241. Wang, Z. *et al.* Cartilaginous extracellular matrix derived from decellularized chondrocyte sheets for the reconstruction of osteochondral defects in rabbits. *Acta Biomater.* **81**, 129–145 (2018).

242. Aamodt, J. M. & Grainger, D. W. Extracellular matrix-based biomaterial scaffolds and the host response. *Biomaterials* **86**, 68–82 (2016).

243. Altman, A. M. *et al.* Dermal matrix as a carrier for in vivo delivery of human adipose-derived stem cells. *Biomaterials* **29**, 1431–1442 (2008).

244. Doornaert, M. *et al.* Human decellularized dermal matrix seeded with adipose-derived stem cells enhances wound healing in a murine model: Experimental study. *Ann. Med. Surg.* **46**, 4–11 (2019).

245. Orbay, H., Takami, Y., Hyakusoku, H. & Mizuno, H. Acellular dermal matrix seeded with adipose-derived stem cells as a subcutaneous implant. *Aesthetic Plast. Surg.* **35**, 756–763 (2011).

246. Zhang, Q. *et al.* Decellularized skin/adipose tissue flap matrix for engineering

vascularized composite soft tissue flaps. *Acta Biomater.* **35**, 166–184 (2016).

247. Wang, J. Q., Fan, J., Gao, J. H., Zhang, C. & Bai, S. L. Comparison of in vivo adipogenic capabilities of two different extracellular matrix microparticle scaffolds. *Plast. Reconstr. Surg.* **131**, 174–187 (2013).

248. Kuljanin, M., Brown, C. F. C., Raleigh, M. J., Lajoie, G. A. & Flynn, L. E. Collagenase treatment enhances proteomic coverage of low-abundance proteins in decellularized matrix bioscaffolds. *Biomaterials* **144**, 130–143 (2017).

249. Shridhar, A. *et al.* Culture on tissue-specific coatings derived from α-amylase-digested decellularized adipose tissue enhances the proliferation and adipogenic differentiation of human adipose-derived stromal cells. *Biotechnol. J.* 1–31 (2019). doi:10.1002/pmic.201400614.This

250. Wang, L., Johnson, J. A., Zhang, Q. & Beahm, E. K. Combining decellularized human adipose tissue extracellular matrix and adipose-derived stem cells for adipose tissue engineering Lina. *Acta Biomater.* **9**, 8921–8931 (2013).

251. Robb, K. P. Syngenic adipose-derived stem/stromal cells delivered in Decellularized Adipose Tissue scaffolds enhance in vivo tissue regeneration through host cell recruitment. (University of Western Ontario, 2017).

252. Yu, G. *et al. Isolation of Murine Adipose-Derived Stem Cells*. **702**,

253. Sasmono, R. T. *et al.* A macrophage colony-stimulating factor receptor – green fluorescent protein transgene is expressed throughout the mononuclear phagocyte system of the mouse. *Blood* **101**, 1155–1163 (2003).

254. Marim, F. M., Silveira, T. N., Lima, D. S. & Zamboni, D. S. A method for generation of bone marrow-derived macrophages from cryopreserved mouse bone marrow cells. *PLoS One* **5**, 1–8 (2010).

255. Lertkiatmongkol, P., Liao, D., Mei, H., Hu, Y. & Newman, P. J. Endothelial functions of PECAM-1 (CD31). *Curr. Opin. Hematol.* **23**, 253–259 (2017).

256. Janda, E., Boi, L. & Carta, A. R. Microglial phagocytosis and its regulation: A therapeutic target in parkinson's disease? *Front. Mol. Neurosci.* **11**, 1–8 (2018).

257. Naeim, F. Principles of immunophenotyping. *Hematopathology* 27–55 (2008). doi:10.1016/B978-0-12-370607-2.00002-8

258. Chan, M. W. Y. & Viswanathan, S. Recent progress on developing exogenous monocyte/macrophage-based therapies for inflammatory and degenerative diseases. *Cytotherapy* **21**, 393–415 (2019).

259. Murray, P. J., Allen, J. E., Fisher, E. A. & Lawrence, T. Macrophage activation and polarization: nomenclature and experimental guidelines. *Immunity* **41**, 14–20 (2015).

260. Manzanero, S. *Leucocytes methods and protocols*. *Methods in Molecular Biology* **844**, (2012).

261. Jones, C. V. & Ricardo, S. D. Macrophages and CSF-1: Implications for development and beyond. *Organogenesis* **9**, 249–260 (2013).

262. Bhasin, J. M. *et al.* Sex specific gene regulation and expression QTLs in mouse macrophages from a strain intercross. *PLoS One* **3**, (2008).

263. Lee, C. M. & Hu, J. Cell density during differentiation can alter the phenotype of bone marrow-derived macrophages. *Cell Biosci.* **3**, 3–7 (2013).

264. Chamberlain, L. M., Holt-Casper, D., Gonzalez-Juarrero, M. & Grainger, D. W. Extended culture of macrophages from different sources and maturation results in a common M2 phenotype. *J. Biomed. Mater. Res. - Part A* **103**, 2864–2874 (2015).

265. Warren, M. K. & Vogel, S. N. Bone marrow-derived macrophages: development and regulation of differentiation markers by colony-stimulating factor and interferons. *J. Immunol.* **134**, 982–9 (1985).

266. Yakhteh, C. J. *et al.* Comparative study of the effect of LPS on the function of BALB/c and C57BL/6 peritoneal macrophages. *Cell* **15**, 45–54 (2013).

267. McWhorter, F. Y., Wang, T., Nguyen, P., Chung, T. & Liu, W. F. Modulation of macrophage phenotype by cell shape. *Proc. Natl. Acad. Sci. U. S. A.* **110**, 17253–17258 (2013).

268. Wang, C. *et al.* Characterization of murine macrophages from bone marrow, spleen and peritoneum. *BMC Immunol.* **14**, 1–10 (2013).

269. Liyanage, S. E. *et al.* Flow cytometric analysis of inflammatory and resident myeloid populations in mouse ocular inflammatory models. *Exp. Eye Res.* **151**, 160–170 (2016).

270. Yu, Y. R. A. *et al.* A protocol for the comprehensive flow cytometric analysis of immune cells in normal and inflamed murine non-lymphoid tissues. *PLoS One* **11**, 1–23 (2016).

271. Misharin, A. V., Morales-Nebreda, L., Mutlu, G. M., Budinger, G. R. S. & Perlman, H. Flow cytometric analysis of macrophages and dendritic cell subsets in the mouse lung. *Am. J. Respir. Cell Mol. Biol.* **49**, 503–510 (2013).

272. Mooney, J. E. *et al.* Cellular plasticity of inflammatory myeloid cells in the peritoneal foreign body response. *Am. J. Pathol.* **176**, 369–380 (2010).

273. Rahman, K. *et al.* Inflammatory Ly6Chi monocytes and their conversion to M2 macrophages drive atherosclerosis regression. *J. Clin. Invest.* **127**, 2904–2915 (2017).

274. Francke, A., Herold, J., Weinert, S., Strasser, R. H. & Braun-Dullaeus, R. C. Generation of mature murine monocytes from heterogeneous bone marrow and description of their properties. *J. Histochem. Cytochem.* **59**, 813–825 (2011).

275. Ramachandran, P. *et al.* Differential Ly-6C expression identifies the recruited macrophage phenotype, which orchestrates the regression of murine liver fibrosis. *Proc. Natl. Acad. Sci.* **109**, E3186–E3195 (2012).

276. Gordon, S. & Taylor, P. R. Monocyte and macrophage heterogeneity. *Nat. Rev. Immunol.* **5**, 953–964 (2005).

277. Nahrendorf, M. *et al.* The healing myocardium sequentially mobilizes two monocyte

subsets with divergent and complementary functions. *J. Exp. Med.* **204**, 3037–3047 (2007).

278. Lin, S. L., Castaño, A. P., Nowlin, B. T., Lupher, M. L. & Duffield, J. S. Bone marrow Ly6C high monocytes are selectively recruited to injured kidney and differentiate into functionally distinct populations. *J. Immunol.* **183**, 6733–6743 (2009).

279. Mia, S., Warnecke, A., Zhang, X. M., Malmström, V. & Harris, R. A. An optimized protocol for human M2 macrophages using M-CSF and IL-4/IL-10/TGF-β yields a dominant immunosuppressive phenotype. *Scand. J. Immunol.* **79**, 305–314 (2014).

280. Jaguin, M., Houlbert, N., Fardel, O. & Lecureur, V. Polarization profiles of human M-CSF-generated macrophages and comparison of M1-markers in classically activated macrophages from GM-CSF and M-CSF origin. *Cell. Immunol.* **281**, 51–61 (2013).

281. Hume, D. A. Applications of myeloid-specific promoters in transgenic mice support in vivo imaging and functional genomics but do not support the concept of distinct macrophage and dendritic cell lineages or roles in immunity. *J. Leukoc. Biol.* **89**, 525–538 (2011).

282. Stanley, E. R. & Chitu, V. CSF-1 receptor signaling in myeloid cells. *Cold Spring Harb. Perspect. Biol.* **6**, (2014).

283. Hume, D. A. Applications of myeloid-specific promoters in transgenic mice support in vivo imaging and functional genomics but do not support the concept of distinct macrophage and dendritic cell lineages or roles in immunity. *J. Leukoc. Biol.* **89**, 525–538 (2010).

284. Kampfrath, T. *et al.* A mouse model of yellow fluorescent protein (YFP) expression in hematopoietic cells to assess leukocyte–endothelial interactions in the microcirculation. *Microvasc. Res.* **73**, 294–300 (2009).

285. Olivares, A. L. & Lacroix, D. Simulation of cell seeding within a three-dimensional porous scaffold: A fluid-particle analysis. *Tissue Eng. - Part C Methods* **18**, 624–631 (2012).

286. Kim, B. S., Putnam, A. J., Kulik, T. J. & Mooney, D. J. Optimizing seeding and culture methods to engineer smooth muscle tissue on biodegradable polymer matrices. *Biotechnol. Bioeng.* **57**, 46–54 (1998).

287. Melchels, F. P. W. *et al.* Effects of the architecture of tissue engineering scaffolds on cell seeding and culturing. *Acta Biomater.* **6**, 4208–4217 (2010).

288. Melchels, F. P. W. *et al.* The influence of the scaffold design on the distribution of adhering cells after perfusion cell seeding. *Biomaterials* **32**, 2878–2884 (2011).

289. Hill, D. A. *et al.* Distinct macrophage populations direct inflammatory versus physiological changes in adipose tissue. *Proc. Natl. Acad. Sci. U. S. A.* **115**, E5096–E5105 (2018).

290. Saldin, L. T., Cramer, M. C., Velankar, S. S., White, L. J. & Badylak, S. F. Extracellular matrix hydrogels from decellularized tissues: Structure and function. *Acta Biomater.* **49**, 1–15 (2017).

291. Ng, K. W., Leong, D. T. W. & Hutmacher, D. W. The challenge to measure cell proliferation in two and three dimensions. *Tissue Eng.* **11**, 182–191 (2005).

292. Kalucka, J. *et al.* Metabolic control of the cell cycle. *Cell Cycle* **14**, 3379–3388 (2015).

293. Scholzen, T. & Gerdes, J. The Ki-67 protein: From the known and the unknown. *J. Cell. Physiol.* **182**, 311–322 (2000).

294. Lujan-Hernandez, J., Appasani, R., Sullivan, K., Siegel-Reamer, L. & Lalikos, J. F. Experimental in-vivo models used in fat grafting research for volume augmentation in soft tissue reconstruction. *Arch. Plast. Surg.* **44**, 361–369 (2017).

295. Bui, J. M. *et al.* Histological characterization of human breast implant capsules. *Aesthetic Plast. Surg.* **39**, 306–315 (2015).

296. Witherel, C. E., Abebayehu, D., Barker, T. H. & Spiller, K. L. Macrophage and Fibroblast Interactions in Biomaterial-Mediated Fibrosis. *Adv. Healthc. Mater.* **1801451**, 1–16

(2019).

297. Zhan, W. & Lu, F. Activated macrophages as key mediators of capsule formation on adipose constructs in tissue engineering chamber models. *Cell Biol. Int.* **41**, 354–360 (2017).

298. Witherel, C. E., Abebayehu, D., Barker, T. H. & Spiller, K. L. Macrophage and fibroblast interactions in biomaterial-mediated fibrosis. *Adv. Healthc. Mater.* **8**, 1–16 (2019).

299. Luttikhuizen, D. T. *et al.* The correlation between difference in foreign body reaction between implant locations and cytokine and MMP expression. *Biomaterials* **27**, 5763–5770 (2006).

300. Karacaoglu, E. *et al.* The role of recipient sites in fat-graft survival: Experimental study. *Ann. Plast. Surg.* **55**, 63–68 (2005).

301. Crosby, C. O. & Zoldan, J. Mimicking the physical cues of the ECM in angiogenic biomaterials. *Regen. Biomater.* **6**, 61–73 (2019).

302. Hanjaya-Putra, D. *et al.* Spatial control of cell-mediated degradation to regulate vasculogenesis and angiogenesis in hyaluronan hydrogels. *Biomaterials* **33**, 6123–6131 (2012).

303. Kono, S., Kon, M., Araki, T. & Sagara, Y. Effects of relationships among freezing rate, ice crystal size and color on surface color of frozen salmon fillet. *J. Food Eng.* **214**, 158–165 (2017).

304. Agrawal, H., Tholpady, S. S., Capito, A. E., Drake, D. B. & Katz, A. J. Macrophage phenotypes correspond with remodeling outcomes of various acellular dermal matrices. *Open J. Regen. Med.* **01**, 51–59 (2012).

305. Suwanpradid, J. *et al.* Arginase1 deficiency in monocytes/macrophages upregulates inducible nitric oxide synthase to promote cutaneous contact hypersensitivity. *J. Immunol.* **199**, 1827–1834 (2017).

306. Dalby, E. *Activating murine macrophages in vitro*. *Methods in Molecular Biology* (2018).

307. Knipper, J. A. *et al.* Interleukin-4 Receptor α signaling in myeloid cells controls collagen fibril assembly in skin repair. *Immunity* **43**, 803–816 (2015).

308. Wilbers, R. H. P. *et al.* Re-evaluation of IL-10 signaling reveals novel insights on the contribution of the intracellular domain of the IL-10R2 chain. *PLoS One* **12**, 1–17 (2017).

309. Sester, D. P., Hume, D. A., Ovchinnikov, D. A., DeBats, C. E. E. & Sweet, M. J. A conserved distal segment of the mouse CSF-1 receptor promoter is required for maximal expression of a reporter gene in macrophages and osteoclasts of transgenic mice. *J. Leukoc. Biol.* **87**, 815–822 (2010).

310. Young, S. A. Mechanically robust injectable hydrogel scaffolds for the intramuscular delivery of adipose-derived stem/stromal cells. (Queen's University, 2017).

Appendix 1

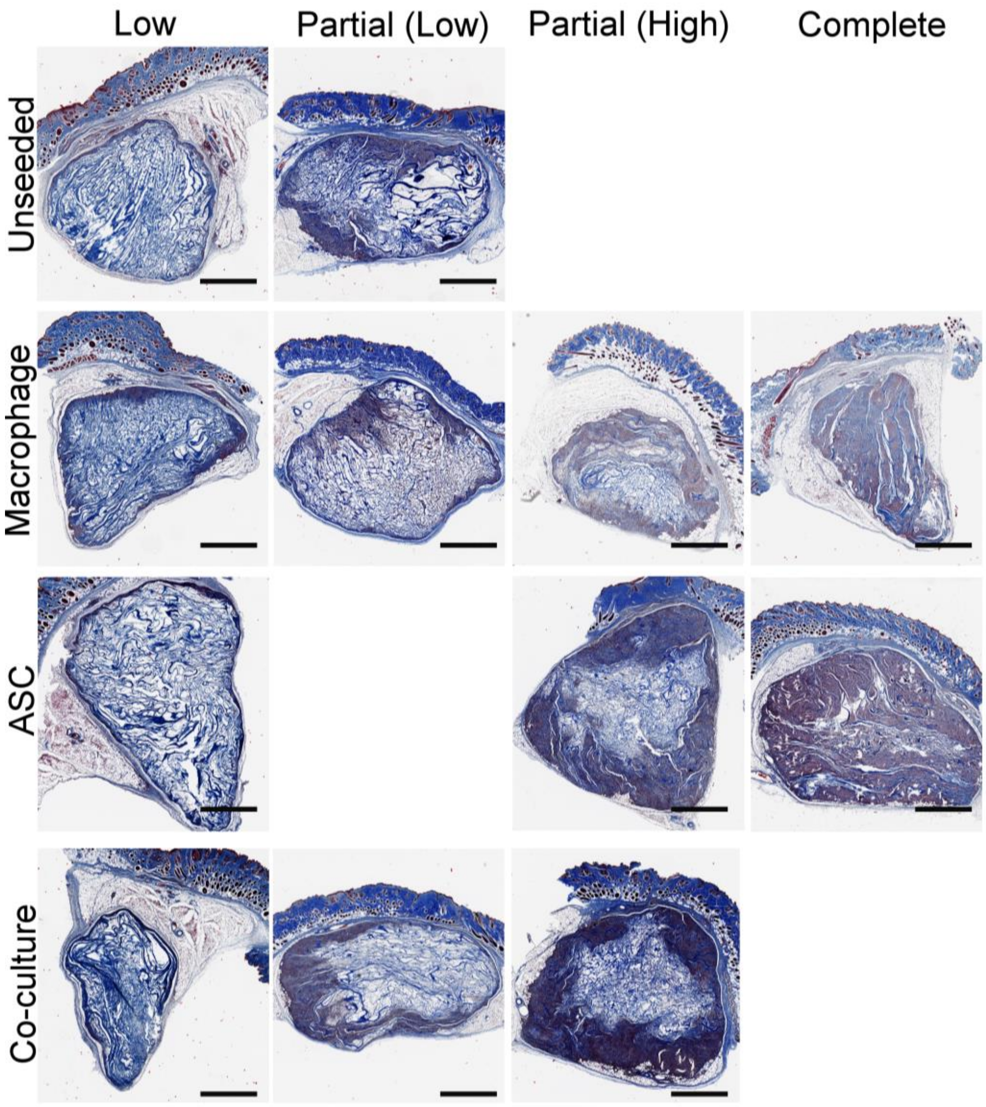

Supplementary Figure 1: Implants within each seeding condition showed a range of *in vivo* cell recruitment responses at 2 weeks post-implantation in C57Bl/6 mice. Representative images of Masson's trichrome stained cross-sections from unseeded, macrophage, ASC, and co-culture seeded implants revealed variability in the *in vivo* response between implants belonging the same group. The unseeded implants showed a smaller range of infiltration responses, with a tendency towards low levels of infiltration. The macrophage, ASC, and co-culture seeded implants exhibited a greater range of *in vivo* responses including low, partial (low), partial (high), or complete levels of cellular infiltration. Scale bars = 1 mm.

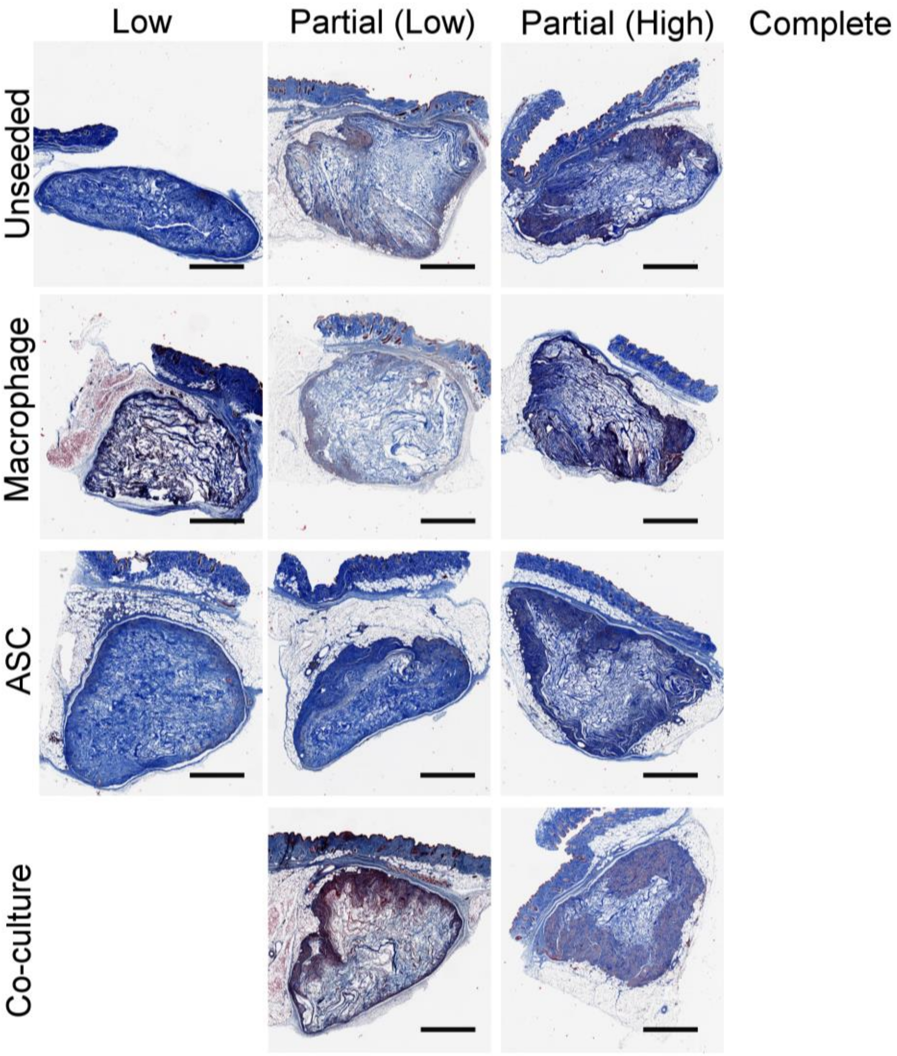

Supplementary Figure 2. Implants within each seeding condition showed a range of *in vivo* cell recruitment responses at 4 weeks post-implantation in C57Bl/6 mice. Representative images of Masson's trichrome stained cross-sections from unseeded, macrophage, ASC, and co-culture seeded implants revealed variability in the *in vivo* response between implants belonging the same group. At 4 weeks, the unseeded implants showed a greater range of cellular infiltration as compared to 2 weeks post-implantation. The macrophage, ASC, and co-culture seeded implants exhibited a similar range of *in vivo* responses as compared to implants at 2 weeks post-implantation, though none of the implants exhibited complete cellular infiltration. Scale bars = 1 mm.

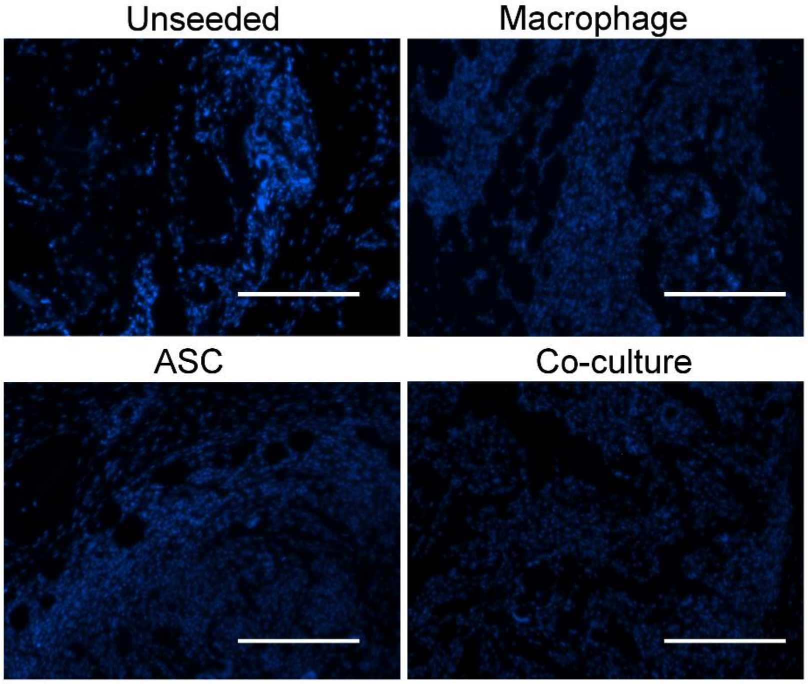
Unseeded
Macrophage
ASC
Co-culture

Supplementary Figure 3: Immunohistochemistry of no primary controls for CD31 staining. Representative images of no primary control are shown for unseeded (top left), macrophage-seeded (top right), ASC-seeded (bottom left) and co-culture-seeded (bottom right) implants. Blue: cell nuclei. Scale: 200 μm.

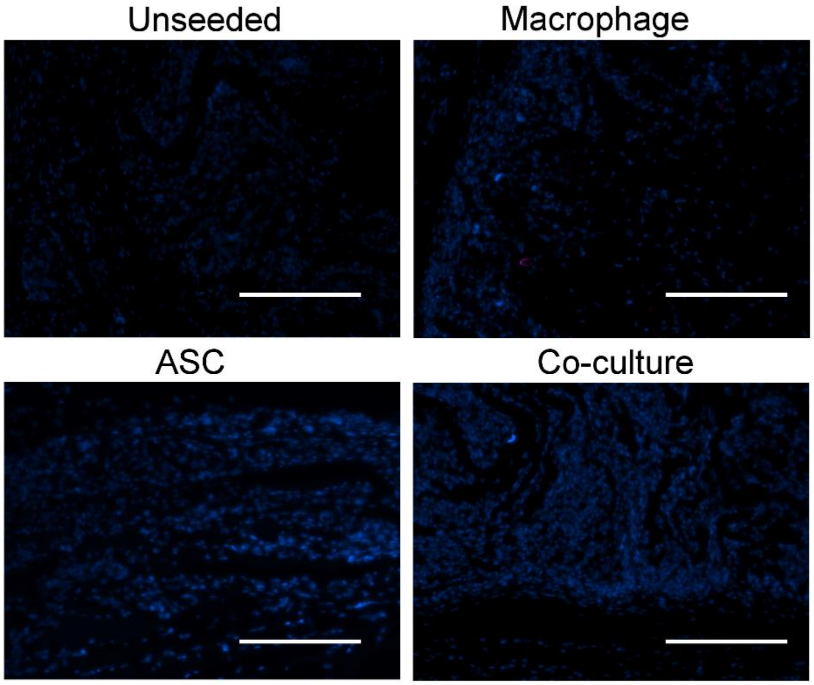
Unseeded
Macrophage
ASC
Co-culture

Supplementary Figure 4. Immunohistochemistry of no primary controls for CD68, Arg-1, and iNOS staining. Representative images of no primary control are shown for unseeded (top left), macrophage-seeded (top right), ASC-seeded (bottom left) and co-culture-seeded (bottom right) implants. Blue: cell nuclei. Scale: 200 μm.

Curriculum Vitae

Name:	Hisham Kamoun
Post-secondary Education and Degrees:	Virginia Commonwealth University Richmond, VA 2011-2015 B.S. Biomedical Engineering, *magna cum laude* The University of Western Ontario London, Ontario, Canada 2016-2019 MESc Candidate
Honours and Awards:	Canadian Biomaterials Society Travel Award ($600) 2018 CONNECT! NSERC CREATE Travel Award ($500) 2018 CONNECT! NSERC CREATE Program in Soft Connective Tissue Regeneration/Therapy Training Award ($12,000/annum) 2016-2018 CMHR Transdisciplinary Bone and Joint Training Award ($10,000/annum) 2016-2018 Western Graduate Research Scholarship 2016-2019
Related Work Experience	Teaching Assistant, University of Western Ontario CBE 2290A (Fall 2016, 2017) ES 2211 (Winter 2017) Intern Octane Orthobiologics Inc. Kingston, ON, Canada May 2018
Oral/Poster Presentation	(Poster) **Kamoun, H.,** Barreira, C., Dekaban, G. & Flynn, L. E. (2019) The co-delivery of syngeneic adipose-derived stem/stromal cells and macrophages on decellularized adipose tissue bioscaffolds for *in vivo* soft tissue regeneration. Centre for Advanced Materials and

Biomaterials Research Day (London, ON).

(Poster) **Kamoun, H.,** Barreira, C., Dekaban, G. & Flynn, L. E. (2019) The co-delivery of syngeneic adipose-derived stem/stromal cells and macrophages on decellularized adipose tissue bioscaffolds for *in vivo* soft tissue regeneration. London Health Research Day (London, ON).

(Oral Presentation) **Kamoun, H.,** Barreira, C., Dekaban, G. & Flynn, L. E. (2018) The co-delivery of syngeneic adipose-derived stem/stromal cells and macrophages on decellularized adipose tissue bioscaffolds for *in vivo* soft tissue regeneration. Canadian Biomaterials Society Conference (Victoria, BC).

(Poster) **Kamoun, H.,** Barreira, C., Dekaban, G. & Flynn, L. E. (2019) The co-delivery of syngeneic adipose-derived stem/stromal cells and macrophages on decellularized adipose tissue bioscaffolds for *in vivo* soft tissue regeneration. Bone and Joint Conference, Western University (London, ON).